

2008

Development of New Stimuli-Responsive Vesicles Using A Novel Surfactant

Yuming Yang

Louisiana State University and Agricultural and Mechanical College

Follow this and additional works at: https://digitalcommons.lsu.edu/gradschool_dissertations



Part of the [Chemistry Commons](#)

Recommended Citation

Yang, Yuming, "Development of New Stimuli-Responsive Vesicles Using A Novel Surfactant" (2008). *LSU Doctoral Dissertations*. 4011.

https://digitalcommons.lsu.edu/gradschool_dissertations/4011

This Dissertation is brought to you for free and open access by the Graduate School at LSU Digital Commons. It has been accepted for inclusion in LSU Doctoral Dissertations by an authorized graduate school editor of LSU Digital Commons. For more information, please contact gradetd@lsu.edu.

**DEVELOPMENT OF NEW STIMULI-RESPONSIVE VESICLES USING A NOVEL
SURFACTANT**

A Dissertation

Submitted to the Graduate Faculty of the
Louisiana State University and
Agricultural and Mechanical College
in partial fulfillment of the
requirements for the degree of
Doctor of Philosophy

In

The Department of Chemistry

by

Yuming Yang

B.E., Southwest Petroleum Institute, 1994

M.S., Louisiana Tech University, 2003

May, 2008

DEDICATION

This dissertation is dedicated to:

My father Guowei Yang

My mother Cheng He

My brother Yutong Yang

ACKNOWLEDGEMENTS

I would like to thank my advisor, Dr. Robin McCarley, for giving me the intelligent guidance during my PhD study. This project would have been impossible without his patient and support. His broad knowledge in chemistry gives me great help on the preparing for a chemistry profession.

Thanks to my parents Guowei Yang and Cheng He, you always care about me and encourage me. Your love is one of the most important things in my life. Thanks to my brother Yutong Yang, it is a wonderful childhood time to grow up with you. To my grandpa Xingye Yang and Weifa He: I always remind me that how many difficulties you have ever faced when you came alone to study in the United States at your young age, and you still can go through it successfully. Thank you for giving me the invaluable encouragement. To my grandma Shuzhen Yang and Zhixing He: thank you for taking care of me in the summer time when I was a child. Thanks to all my uncles, aunts, cousins and nieces, we always have so many funs together.

I would like to thank Dr. Paul Russo, for teaching me in a memorable macromolecule class, for giving me chances to learn to use a variety of instruments, and for advising me on the research. I would like to acknowledge Dr. Doug Gilman and Dr. Robert Hammer to work on my research committee and give me advices during my PhD study. My special thanks go to Dr. Rafael Cueto for helping me on a variety of experiments which include light scattering, HPLC and AF4. I want to thank Dr. Isiah Warner for allowing me to conduct the tensiometry measurements in his laboratory. I thank Dr. Ioan Negulescu helping me on the DSC measurement. I thank Dr. Dale Treleaven for helping me on NMR experiments. I thank Cindy Henk in biological department for her help on TEM experiments. I also would like to thank Angela Cruciano at NCMI for her help on CryoEM experiments. I grateful acknowledge NSF, Electrochemical Society, Charles E. Coates Memorial Fund for funding this work.

I would like to thank many friends I met when I studied at Louisiana State University, as well as the friends back in china; whose friendship helps me go through these years. I have learned so many things from you, not only on the academic, but also, on the spirit and humanities. There is an old Chinese proverb: “Ocean is wide because it receives hundreds of rivers.” Except to be friends of you and learning from you, I can not image how limited mind I would be.

I also would like to thank every McCarley group colleague for helping me throughout these years. It is a memorable experience to be group member with you. I wish everybody have a success in the future.

TABLE OF CONTENTS

DEDICATION	ii
ACKNOWLEDGEMENTS	iii
LIST OF TABLES	viii
LIST OF FIGURES	ix
LIST OF SCHEMES	xii
LIST OF SPECTRUMS	xiii
LIST OF ABBREVIATIONS AND SYMBOLS	xiv
ABSTRACT	xvi
CHAPTER 1. INTRODUCTION	1
1.1 Research Goals.....	1
1.2 Research Synopsis.....	2
1.2.1 Synthesis of Novel Redox Stimuli-responsive Amphiphilic Molecules.....	2
1.2.2 Structural Characterization.....	3
1.2.3 Study of the Properties of Novel Redox Stimuli-Responsive Amphiphilic Molecules	4
1.2.4 Development of New Vesicles through Aggregation.....	4
1.2.5 Encapsulation Experiment.....	5
1.3 Background.....	5
1.3.1 Vesicle Aggregation.....	5
1.3.2 Redox-responsive Aggregates.....	11
1.3.3 Quinonoid Compounds.....	13
1.3.4 “Tri-methyl Lock” Mechanism of The Quinone Compound.....	15
1.4 References.....	18
CHAPTER 2. MATERIALS AND METHODS	22
2.1 Chemicals	22
2.2 Methodologies.....	22
2.2.1 Extrusion Technique for Development of Vesicles Aggregates.....	22
2.2.2 Preparation of Samples for Light Scattering.....	23
2.2.3 Dynamic Light Scattering.....	24
2.2.4 Surface Tension Measurement.....	24
2.2.5 Theory of Critical Aggregation Concentration.....	25
2.2.6 Mechanism of Asymmetrical Flow Field Flow Fractionation (AF4).....	26
2.2.7 AF4 Studies on Extruded Q9 Sample.....	27
2.2.8 Preparative Size Exclusive Chromatography.....	28
2.2.9 Dye Encapsulation and Release Experiment.....	29
2.2.10 Preparation of Samples for Transmission Electron Microscopy.....	29

2.3 Instrumentation.....	30
2.3.1 Nuclear Magnetic Resonance Spectroscopy (NMR).....	30
2.3.2 Gas Chromatography Mass Spectrometry (GC-MS).....	31
2.3.3 Electrospray Ionization Mass Spectrometry (ESI-MS).....	31
2.3.4 Cryogenic Electron Microscopy (CryoEM).....	31
2.3.5 Ultraviolet-visible (UV-vis) Spectroscopy.....	32
2.3.6 Fluorescence Spectrometry.....	32
2.4 References.....	33
CHAPTER 3. SYNTHESIS OF A NOVEL SURFACTANT.....	35
3.1 Introduction.....	35
3.2 Synthesis Discussion.....	36
3.2.1 Synthesis of Lactone Product 2.....	38
3.2.2 Synthesis Quinone Acid 3.....	40
3.2.3 Synthesis and Separation of NHS Substitute Quinone 4.....	41
3.2.4 Synthesis of tert-butyl 6-(benzyloxycarbonylamino) Hexanoate 6.....	42
3.2.5 Synthesis of t-Butyl Protected 6-aminohexanoic Acid 7.....	43
3.2.6 Synthesis of Molecule 8.....	43
3.2.7 Remove the Protecting Group of Compound 8 to Achieve the Final Product 9.....	44
3.3 References.....	48
CHAPTER 4. PROPERTIES OF THE NOVEL SURFACTANT Q9.....	50
4.1 The pH Sensitivity of Q9 Molecule.....	50
4.2 Redox Stimuli-responsive Property of Q9.....	53
4.2.1 Confirmation of the Cleavage of Q9 Structure Upon Redox Stimulation.....	53
4.2.2 Kinetic Study of Lactonization Reaction.....	55
4.3 Critical Aggregation Concentration Study.....	59
4.4 References.....	63
CHAPTER 5. Q9 VESICLES FORMATION AND CHARACTERIZATION.....	64
5.1 Formation of Q9 Vesicles by Extrusion Treatment.....	64
5.2 TEM Experiment on Q9 Vesicles With Stained Materials.....	64
5.3 Light Scattering Measurement on Q9 Vesicles Sample.....	66
5.3.1 Light Scattering Experiments on a Home-Built Instrument.....	66
5.3.2 Dynamic Light Scattering Experiment on Zetasizer Nano Instrument.....	68
5.4 CryoEM Experiment on Q9 Vesicles.....	70
5.5 Study of the Q9 Vesicles Distribution by Asymmetrical Flow Field Flow Fractionation (AF4) Technology.....	71
5.6 Conclusion from Different Characterization Methods.....	74
5.7 References.....	75
CHAPTER 6. STUDY OF THE ENCAPSULATION AND CONTROLLABLE RELEASE PROPERTIES OF Q9 VESICLES.....	77
6.1 DLS Experiments on Q9 Vesicles.....	77
6.2 Encapsulation of Water-soluble Dye Calcein in Q9 Vesicles.....	80
6.3 Study of the Controllable Release Property of Q9 Vesicles.....	83
6.4 References.....	85

CHAPTER 7. SUMMARY OF CONCLUSIONS AND FUTURE STUDIES.....	86
7.1 Summary of Conclusions.....	86
7.2 Future Work.....	88
7.3 References.....	92
APPENDIX 1. PRODUCTS MINIMUM PURITY CALCULATION.....	93
APPENDIX 2. PERMISSION OF REPRINT.....	100
VITA.....	102

LIST OF TABLES

Table 4.1 Integrated ^1H NMR signals for peak e and peak a of Q9 as a function of time after addition of $\text{Na}_2\text{S}_2\text{O}_4$ to 5 mM Q9 in pD 7.8 D_2O	58
Table 5.1 Light scattering experiments on Q9 vesicle PBS solutions (50 mM with 50 mM NaCl).....	67

LIST OF FIGURES

Figure 1.1 Release of reagents from the core of a vesicle.....	1
Figure 1.2 Tri-methyl lock reactions.....	3
Figure 1.3 Structure of Q9.....	4
Figure 1.4 Bilayer planner structure.....	6
Figure 1.5 Titration experiments on (decanoate + decanoic acid) and (acetate + acetic acid) system. Adapted from Ref 21.....	8
Figure 1.6 TEM image of decanoic acid/decanoate (a) vesicles and (b) micelles. Adapted from Ref 25.....	9
Figure 1.7 Proposed scheme of dynamic processes occurring between micelle aggregation and fatty acid vesicles. Adapted from Ref 16.....	10
Figure 1.8 Structure of ubiquinone.....	14
Figure 1.9 “Tri-methyl lock” mechanism.....	15
Figure 1.10 Mechanisms for utilizing “tri-methyl lock” mechanism for prodrug.....	16
Figure 1.11 A quinone propionic ester with a bi-functional group.....	17
Figure 2.1 Extrusion apparatus preparation.....	23
Figure 2.2 Surface tension measurement by du Nuoy ring method.....	25
Figure 2.3 The mechanism of AF4 separation based on the particle sizes. Adapted from Reference 7.....	27
Figure 3.1 Structure of Q9.....	35
Figure 3.2 Q9 reduction and intramolecular cyclization/elimination event.....	36
Figure 3.3 GC-MS result on product 2.....	39
Figure 3.4 High resolution ESI-MS of product Q9.....	45
Figure 4.1 UV-vis spectra of Q9 samples prepared in 0.1M pH 7.0 PBS, 0.1M pH10.2 PBS, 0.1 M pH 11 PBS, 0.1 M pH 14 NaOH and PBS solution.....	51
Figure 4.2 ¹ H NMR spectra (300 MHz) of 8 mM Q9 in pD 8.0 D ₂ O (NaD ₂ PO ₄) immediately (a) and 72 hours (b) after sample preparations.....	52

Figure 4.3 Proposed cleavage of Q9 structure triggered by the reducing agent.....	54
Figure 4.4 Location of proton e and a in the reactant and products.....	54
Figure 4.5 ¹ H NMR spectra after Na ₂ S ₂ O ₄ addition at 3 and 300 mins.....	56
Figure 4.6 Spectrum of Q9 and ¹ H NMR assignments.....	57
Figure 4.7 NMR kinetic experiments from 2 mM Q9 in pH 7.8 D ₂ O exposed to solid sodium dithionite.....	59
Figure 4.8 UV-vis absorbance change after Na ₂ S ₂ O ₄ addition of Q9 pH 7.8 PBS solution.....	60
Figure 4.9 Surface tension measurements of Q9 in 40 mM pH 7.8 PBS solution as a function of Q9 concentration.....	61
Figure 4.10 Surface tension measurements on 6-aminohexanoic acid in 40 mM pH 7.8 PBS solution.....	62
Figure 5.1 Representative TEM experimental results for Q9 vesicles stained with 2% uranyl acetate.....	65
Figure 5.2 DLS experimental results for DOPC vesicle sample (1 mg/mL DOPC in 50 mM pH 7.8 PBS).....	69
Figure 5.3 DLS experimental results for Q9 vesicle sample (12 mM Q9 in 50 mM pH 7.8 PBS).....	70
Figure 5.4 Q9 vesicles developed by extrusion treatment with a variety of sizes. Experiments were conducted under conditions described in Section 2.3.4 in Chapter 2.....	72
Figure 5.5 Light scattering intensity (recorded at 90°) of 12 mM Q9 sample in pH 7.8 PBS (50 mM) during the AF4 separation process; peak at 9 min and 70 min are generated by the flow condition change.....	73
Figure 5.6 <i>R_g</i> size distribution calculated from AF4 experiment on Q9 sample. The data value changed after 50 minutes due to the change of flow condition.....	73
Figure 6.1 DLS experiment on the redox-stimulation results (a) 12 mM Q9 vesicle sample in 50 mM pH 7.8 PBS (b) 12 mM Q9 vesicle sample in 50 mM pH 7.8 PBS after Na ₂ S ₂ O ₄ treatment.....	78
Figure 6.2 Particle's sizes of 12 mM Q9 vesicle sample in 50 mM PBS monitored by DLS after Na ₂ S ₂ O ₄ addition.....	79

Figure 6.3 Illustration of the color change during the preparative size-exclusion chromatography separation. (a) mixed free calcein and vesicle samples with self-quenching concentration; (b) particles separated based on size. Q9 vesicles (large) containing calcein move faster through the column and diluted free calcein (small) moves slower.....82

Figure 6.4 UV-vis absorbance experiment on the preparative size-exclusion chromatography separated Q9 vesicle sample with calcein encapsulated; and UV-vis absorbance experiment on 1 mM Q9 molecule in 100 mM pH 7.8 PBS.....82

Figure 6.5 Fluorescence intensity increases upon the addition of Na₂S₂O₄ to Q9 vesicle sample containing calcein.....84

Figure 7.1 Microfluidic channel with temperature gradient.....90

LIST OF SCHEMES

Scheme 3.1 Synthetic scheme for the NHS-substituted quinone.....	37
Scheme 3.2 Synthetic route for the t-butyl protected 6-aminohexanoic acid (7).....	38
Scheme 3.3 Synthetic route for the amphiphilic molecule Q9 with the quinone stimuli-responsive group.....	40

LIST OF SPECTRUMS

Spectrum 3.1 ^1H NMR spectrum of product 2.....	39
Spectrum 3.2 ^1H NMR spectrum of quinone acid 3.....	41
Spectrum 3.3 ^1H NMR spectrum of the NHS substitute structure 4.....	42
Spectrum 3.4 Comparison of ^1H NMR spectra of reactant 5 and product 6.....	44
Spectrum 3.5 Comparison of ^1H NMR spectra of <i>tert</i> -butyl group protected 6-aminohexanoic acid (7) and (6).....	46
Spectrum 3.6 (a) Proton-labeled molecule 7, 3 and 8 (b) Comparison of ^1H NMR spectra of product 8, 3 and 7.....	47
Spectrum 3.7 Labeled ^1H NMR of final product 9.....	48

LIST OF ABBREVIATIONS AND SYMBOLS

^1H NMR	proton nuclear magnetic resonance
AF4	asymmetrical flow field-flow fractionation
ATP	adenosine triphosphate
CAC	critical aggregation concentration
CBZ	carbobenzyloxy
CDCl_3	<i>deuterated</i> -chloroform
CryoEM	cryo-electron Microscopy
D	diffusion coefficient
DCC	dicyclohexylcarbodiimide
DCM	dichloromethane
DLS	dynamic light scattering
DOPC	dioleoylphosphatidylcholine
ESI-MS	electrospray ionization mass spectrometry
FRET	fluorescence resonance energy transfer
GC-MS	gas chromatography-mass spectrometry
HPLC	high performance liquid chromatography
mg	milligram
min	minute (s)
mL	milliliter
mM	millimolar
mN	millinewton
NBS	<i>N</i> -bromosuccinimide

NHS	<i>N</i> -hydroxysuccinimide
NIST	National Institute of Standards and Technology
nm	nanometer
PBS	phosphate buffered saline
PDMS	polydimethylsiloxane
PFS	polyferrocenylsilane
ppm	parts per million
RBF	round bottom flask
R_g	radius of gyration
R_h	hydrodynamic radius
RMS	root mean squared
SAMs	self-assembled monolayers
SLS	static light scattering
TEA	triethanolamine
TEM	transmission electron microscopy
THF	tetrahydrofuran
TLC	thin-layer chromatography
TMS	tetramethylsilane
UV-Vis	ultraviolet-visible spectroscopy
δ	chemical shift
μM	micromolar

ABSTRACT

Many amphiphilic molecules (surfactants) possess the ability to aggregate in aqueous solution to form thermodynamically stable aggregates that have potential for use as molecule containers and delivery systems in analytical or pharmaceutical applications. However, it is difficult to release the encapsulated molecules from these aggregates under a controllable manner, and this problem has dramatically limited the application of these aggregated systems. This study addresses this problem through fundamental structure modification by development of a novel redox stimuli-responsive amphiphile capable of forming vesicle aggregates. Aggregate structure can be adjusted through redox stimulation. The release of agents from the core of the aggregates containers can be controlled by the same mechanism.

The novel surfactant molecule, Q9 (Figure 1.3), containing a redox stimuli-responsive moiety was synthesized through seven synthetic steps for this purpose (Chapter 3). The molecular structures were characterized by ^1H NMR and mass spectrometry analysis methods. Properties of Q9 in aqueous solution were studied (Chapter 4). The pH sensitivity of Q9 was explored in a variety of phosphate-buffered saline (PBS) solutions with UV-vis measurements and ^1H NMR experiments; from these studies, suitable pH value was determined for Q9 vesicle formation. The stimuli-responsive mechanism of Q9 was confirmed by ^1H NMR kinetic studies. The critical aggregation concentration (CAC) was determined by surface tension measurements. Q9 vesicles were formed by the extrusion technique (Chapter 5). Vesicle characterizations were evaluated using transmission electron microscopy, light scattering, cryo-electron microscopy and asymmetrical flow field-flow fractionation. Q9 vesicles were used to encapsulate the model guest calcein (Chapter 6). Size-exclusion chromatography was used to isolate Q9 vesicles containing dye calcein. The successful release of calcein from Q9 vesicles was triggered by use of a chemical reducing agent as observed by the time-dependent increase in calcein fluorescence.

Based on the data, it appears that the loading volume and number density of Q9 vesicles dictates their capabilities as an efficient molecule delivery system.

CHAPTER 1. INTRODUCTION

1.1 Research Goals

The goal of this research is to develop a novel molecular container and delivery system based on the aggregation of surfactants that can be controlled and adjusted by redox stimulation. This new stimuli-responsive system has potential for application in drug delivery systems or for dispensing reagents in microfluidic analysis devices.¹⁻⁴

Amphiphilic (surfactant) molecules contain both a hydrophobic and a hydrophilic domain within its molecular structure and can assemble together to form various morphologies.⁵ Research has confirmed that these aggregates make excellent agent containers or delivery systems; however, the ability to release the encapsulated agents from these aggregates in a controllable manner presents a technical barrier. This problem has dramatically limited the real application of these systems. The study in this dissertation addresses this problem through fundamental structure modification: by use of a redox stimuli-responsive moiety as part of an amphiphilic molecule that is capable of forming aggregates. Aggregate structure and morphology can then be adjusted by changing structure of the amphiphilic molecule by redox stimulus, and the release of reagents from the aggregate core can be controlled (Figure 1.1).

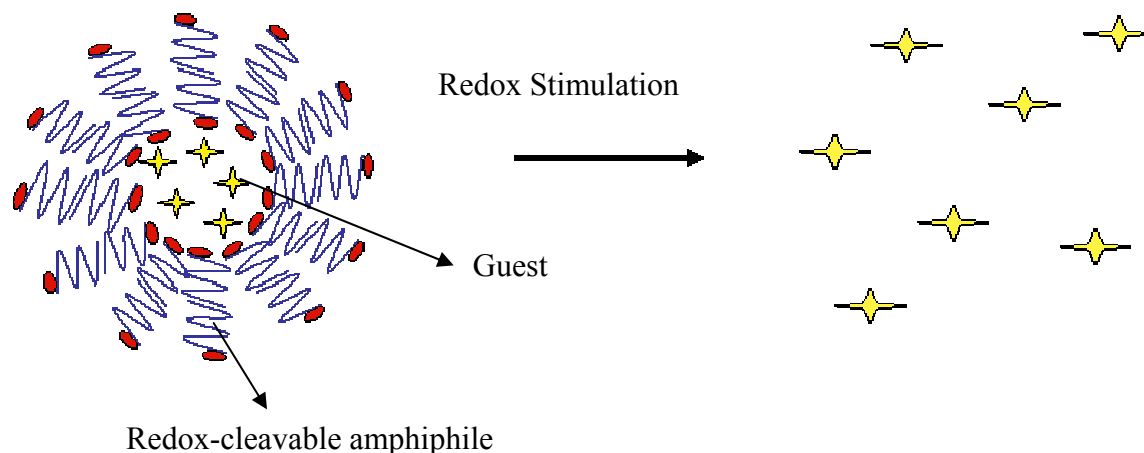


Figure 1.1 Release of reagents from the core of a vesicle.

Novel amphiphilic molecules containing redox stimuli-responsive functional group were synthesized for this purpose. The new molecules were characterized and determined to be the desired structures. Upon confirmation of the redox stimuli response of these molecules, aggregates were formed in aqueous environment, and their properties were studied by advanced analytical methods. Encapsulation and controllable release properties have also been studied by monitoring the leakage of a fluorescent, hydrophilic dye.

1.2 Research Synopsis

1.2.1 Synthesis of Novel Redox Stimuli-responsive Amphiphilic Molecules

Quinone molecules have been studied for decades to reveal their important role as electron acceptors in cell membrane and light-induced biological charge separation processes.⁶⁻⁹ These studies have established them as one of the well-known redox systems. Recently, these redox properties have been used for the construction of advanced redox stimuli-responsive materials.¹⁰⁻¹² Different redox-sensitive kinetic processes can be achieved through different quinone structures.

Borchard and Cohen discovered the “tri-methyl lock” mechanism based on a quinone carboxylic structure with three methyl groups.^{13, 14} From this mechanism, if a reducing agent is introduced, the quinone structure will be reduced to the corresponding hydroquinone. The three methyl groups (“tri-methyl lock”) of the hydroquinone structure make it conformationally unstable; thus, a spontaneous intramolecular cyclization/elimination reaction occurs to produce a lactone product (Figure 1.2). This mechanism will be utilized in this study to facilitate the release of encapsulated reagents.

A hydrocarbon chain that contains both a hydrophobic and a hydrophilic moiety is needed to make the surfactant molecule aggregate in aqueous solution. Considering both requirements for redox stimuli-responsiveness and aggregation of amphiphilic chain structures,

the novel surfactant molecules were designed with specific structures (Figure 1.3): A “tri-methyl lock” quinone moiety was introduced on one side of the surfactant structure to give the whole structure redox sensitivity, and it also served as the hydrophobic part in the amphiphilic structure. 6-Aminocarboxylic acid was used as the carbon chain in the structure, and it was covalently bonded with the redox-sensitive moiety through the carboxylic group on the tri-methyl quinone. The carboxylic group on the end of the aminocarboxylic acid molecule provided the hydrophilic side to the new surfactant. In total, seven steps of synthesis were conducted to achieve the final surfactant molecule, which was named Q9 (6-(3-methyl-3-(2,4,5-trimethyl-3,6-dioxocyclohexa-1,4-dienyl)butanamido)hexanoic acid) in this study. The structure of Q9 is shown in Figure 1.3. Synthesis of Q9 will be discussed in detail in Chapter 3.

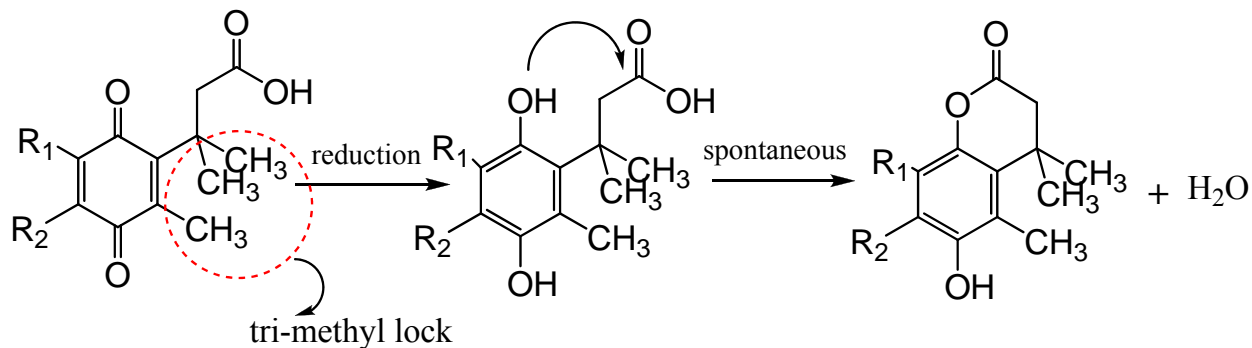
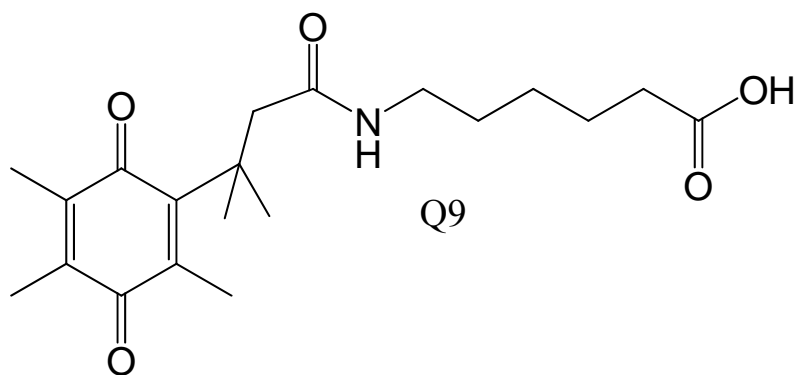


Figure 1.2 Tri-methyl lock reactions.

1.2.2 Structural Characterization

Confirmation of the desired product from each synthesis step was obtained from ^1H NMR. GC-MS, ESI-MS, and HPLC were also used for their characterization. Once Q9 was purified, NMR kinetic experiments were conducted to characterize the stimuli-responsive mechanism. The changes in the selected proton signal intensity were monitored after redox stimulation. Those intensity changes were caused by the chemical structure changes that were triggered by the redox stimulation, and can be used to confirm the reaction mechanism. Furthermore, the reaction rate can also be calculated using this method.



6-(3-methyl-3-(2,4,5-trimethyl-3,6-dioxocyclohexa-1,4-dienyl)butanamido)hexanoic acid

Figure 1.3 Structure of Q9.

1.2.3 Study of the Properties of Novel Redox Stimuli-responsive Amphiphilic Molecules

The unique properties of the newly synthesized surfactants were studied. The pH sensitivity was analyzed for future application in an aqueous environment. NMR, and UV-vis experiments were conducted to explore any potential changes in molecular structures and/or properties, which are affected by different pH environments. A suitable pH value was chosen for the following research.

Surface tension experiments were used to measure the critical aggregation concentration (CAC) of the new surfactant. This concentration is then used as the standard for the following aggregation development studies.

1.2.4 Development of New Vesicles through Aggregation

The newly synthesized surfactant structure is similar to that of n-alkanoic acid surfactants. Previous studies have shown that those molecules can aggregate into vesicles under certain conditions.¹⁵⁻¹⁷ The traditional phospholipids-based vesicle generation methodology was adopted to create vesicles with Q9,¹⁸ and employs mechanical extrusion. The experimental conditions were controlled at a suitable pH value and surfactant concentration. After their formation, vesicle size was obtained with light scattering. Advanced microscopy methods were

also used to study the lamellarity of the vesicles. The disassembly of the vesicles was triggered by a reducing agent and monitored by dynamic light scattering and TEM. Asymmetrical flow field-flow fractionation (AF4) was used to explore the size distribution of the Q9 vesicles.

1.2.5 Encapsulation Experiment

A water-soluble dye (calcein) was used as the reagent to be encapsulated inside the Q9 vesicles. Calcein is a self-quenching dye whose fluorescence is quenched when encapsulated inside the vesicles at a high initial concentration. In order to encapsulate the calcein, a solution of the Q9 surfactant and calcein at a concentration higher than the self-quenching concentration was extruded. A preparative size-exclusive chromatography column was then used to separate the vesicles from the free calcein. Salt concentration and pH were controlled carefully during this separation process. Fluorescence kinetic experiments were then set up to monitor the time-dependent fluorescence signal upon application of redox stimulation. Based on the expected redox-stimuli responsive mechanism, the introduction of a reducing agent should cause a disconnection in the surfactant and subsequent disassembly of the vesicles. Thus, calcein is released, it is diluted to a value less than its self-quenching concentration, and the increase in calcein fluorescence can then be observed.

1.3 Background

1.3.1 Vesicle Aggregation

Surfactant molecules, also called amphiphilics, contain both a hydrophobic part and a hydrophilic head group. When these molecules are dissolved in an aqueous solution, the hydrophobic part tries to minimize the contact area with water molecules. This phenomenon is called the hydrophobic effect and can cause the formation of different aggregates.¹⁹ Inside the structure of aggregates, a concentrated hydrophobic part is surrounded by the hydrophilic moiety

that contacts water molecules directly. This construction produces macro-homogenous systems (solution) with many “different” micro-phase structures (aggregates) inside.

Based on the variety of molecule structures, solution systems, and treatment methods, amphiphilic molecules can aggregate into different morphologies that include ordinary and inverse micelles, liquid crystals, bilayers, vesicles, and microemulsions.²⁰ Among them, research on vesicle structures has become increasingly important, because these aggregates possess potential for use as water-soluble reagent containers and delivery systems.

A bilayer structure formed by amphiphilic molecules is the basic construction unit for vesicles (Figure 1.4). The amphiphilic molecules are well organized inside the vesicles: the hydrophilic polar heads face the aqueous surroundings, and the hydrophobic parts constitute the interior of the bilayer. In the simplest case, the bilayer just forms planar structures (Figure 1.4); however, it is possible that the bilayer can be curved to form closed, spherical objects called vesicles. Vesicles can be many different sizes, such as small unilamellar vesicles (SUV, radius 4 – 20 nm), large unilamellar vesicles (LUV, radius 50 nm – 10 μ m), and multilamellar vesicles (MLV). Generally, unilamellar vesicles are more likely to be observed in dilute systems, while MLVs are typically found in concentrated systems.

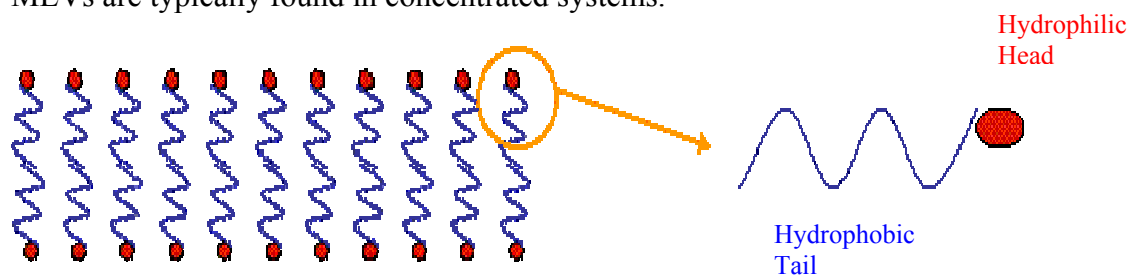


Figure 1.4 Bilayer planar structure.

The formation of vesicles from surfactants can be achieved through dispersion of lamellar bilayer, by dilution, input of external force, or spontaneously depending on amphiphile molecular structure. The detailed mechanism for each condition is still under investigation. Traditionally, three classic techniques are used to cause formation of phospholipid vesicles:

sonication, thin-film hydration, and extrusion.¹⁸ Among them, the extrusion technique is the most widely used. Using this technique, multilamellar surfactant is pushed through an extruder; the strong shear force reorganizes the lamellar sheet structure into vesicles. A membrane filter with a given pore size will cause phospholipids to form vesicles of approximately same size as the membrane pores.²¹

Phospholipid vesicles have been studied for a long time as classic vesicle models. These particular vesicles are formed by phospholipid molecules that usually possess two hydrophobic chains as the “tail” structure. Recent research has confirmed that vesicles can also be generated by single-chain surfactants.^{15, 22, 23} It has been suggested that these single-chain vesicle aggregates performed an important role in the early stages of life.²⁴ Szostak pointed out that these vesicles can provide a spatial microenvironment for photo-metabolic reactions, or a mechanism for the spatial confinement of genetic polymers.¹⁷

Walde studied single-chain vesicles formed by decanoic acid,²² whose structure is such that micelle aggregates form in aqueous solution. Based on Walde’s study, the ionization status of decanoic acid affects aggregate formation. Highly deprotonated decanoic acid (decanonate) easily forms micelles; however, when the ratio of unionized decanoic acid is increased in solution, vesicles can be formed. Walde mixed decanoic acid and the corresponding decanonate salt together under a variety of concentrations, and applied the titration method to adjust the pH of these solution systems (Figure 1.5).

The experiment results showed that these solutions undergo similar changes even though the concentrations are different. The solutions remained transparent if the pH was greater than 8.1, which indicated predominately micelle-style aggregates in the solution when decanoic acid was highly deprotonated. When the pH was decreased to 8.1, the solution started becoming turbid, indicating a change in aggregate formation. Using microscopy, the cause of these

changes has been confirmed to be the result of vesicle formation. To confirm this result, a mixed solution of acetic acid and the corresponding acetate salt has been used to perform the same titration experiment. No phase change can be observed during the pH adjustment because no aggregates were formed using this system. Walde pointed out that when the pH was decreased into the range of 6.5 to 8.1, a well-balanced solution of protonated and deprotonated decanoic acid was achieved, and this balanced condition was key to form the vesicles.

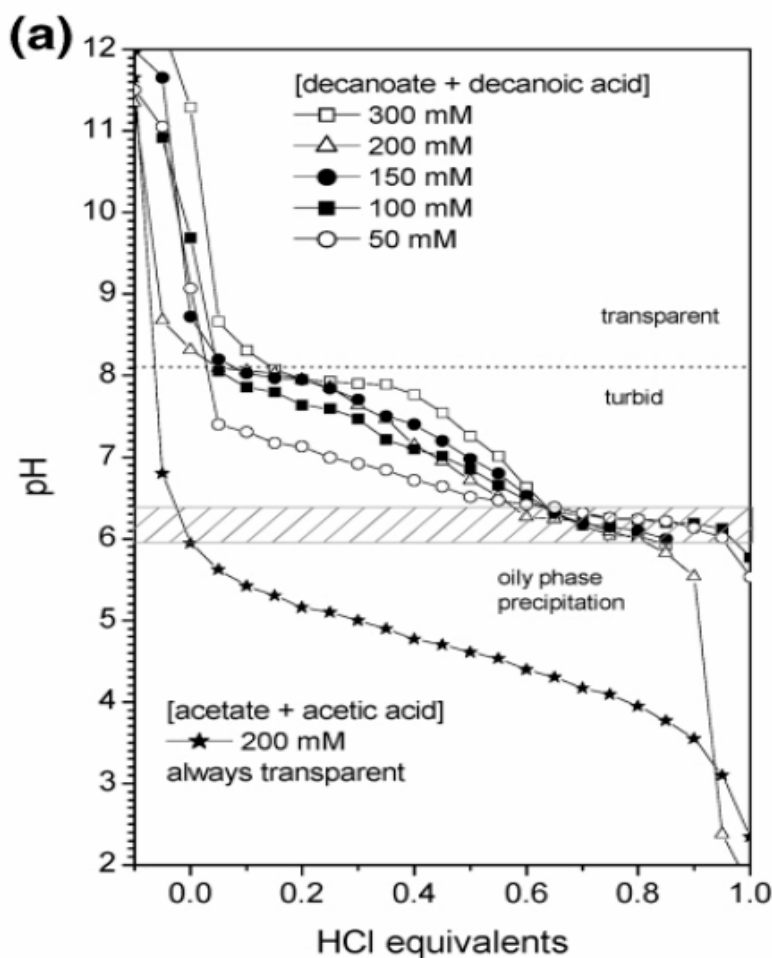


Figure 1.5 Titration experiments on (decanoate + decanoic acid) and (acetate + acetic acid) system. Adapted from Ref 22.

Blanchard also studied this decanoic acid solution system²⁵ and clearly confirmed that vesicles form from this single-chain amphiphile between pH 6.5 and 8.1 at concentration 100mM. The formation of micelles and vesicles could be observed from this single-chain surfactant

solution by TEM studies (Figure 1.6). These research results indicate that ionization plays an important role in aggregate formation from these single-chain fatty acid surfactants, and pH can be adjusted to control the aggregate type so as to generate vesicles.

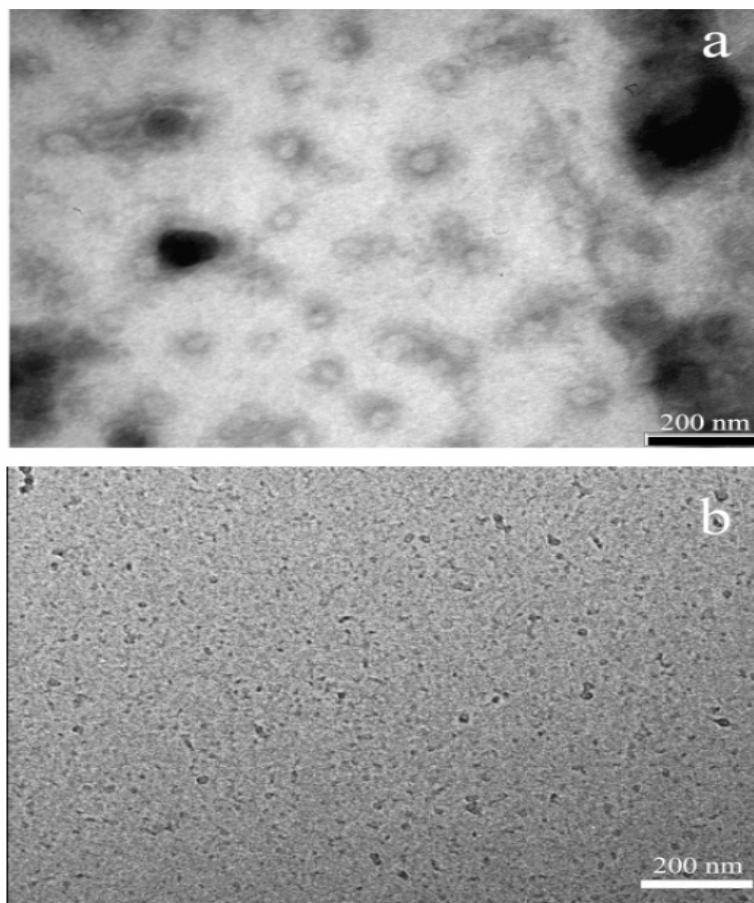


Figure 1.6 TEM image of decanoic acid/decanoate (a) vesicles and (b) micelles. Adapted from Ref 25.

Szostak studied the growth of this kind of vesicle from another point-of-view: transforming the micelles into vesicles.¹⁶ It was pointed out that these fatty acid vesicles possess different properties in comparison to those phospholipid vesicle counterparts. One difference is that although these vesicles still exist as stable supramolecular structures, their molecular components are in a rapid, dynamic exchange process with the surrounding solution and with each other. It has also been suggested that the spontaneous assembly of fatty acid vesicles from

alkaline micelles is an autocatalytic process. A certain sized oleate vesicle was used as a seed to initiate growth of the vesicles by incorporating additional oleates supplied by oleate micelles. Fluorescence was used to follow fatty acid vesicle growth. A non-exchanging, membrane-localized fluorescence resonance energy transfer (FRET) dye was applied here to measure the increase in vesicle surface area as the micelles transfer into vesicles. The experimental results showed that there are two mechanisms for vesicle size increase (Figure 1.7). In one mechanism oleates were transferred from micelles into vesicle directly by coating the preformed vesicles. In another mechanism, oleates formed aggregated intermediates first, then transferred into vesicles.

The vesicle formation process is hard to control and monitor. This study provides a novel way to observe how single-chain fatty acid vesicle size can be changed by adopting micelles surrounded in the solution. This finding will be useful on the monitoring of vesicles size change in the future vesicle studies.

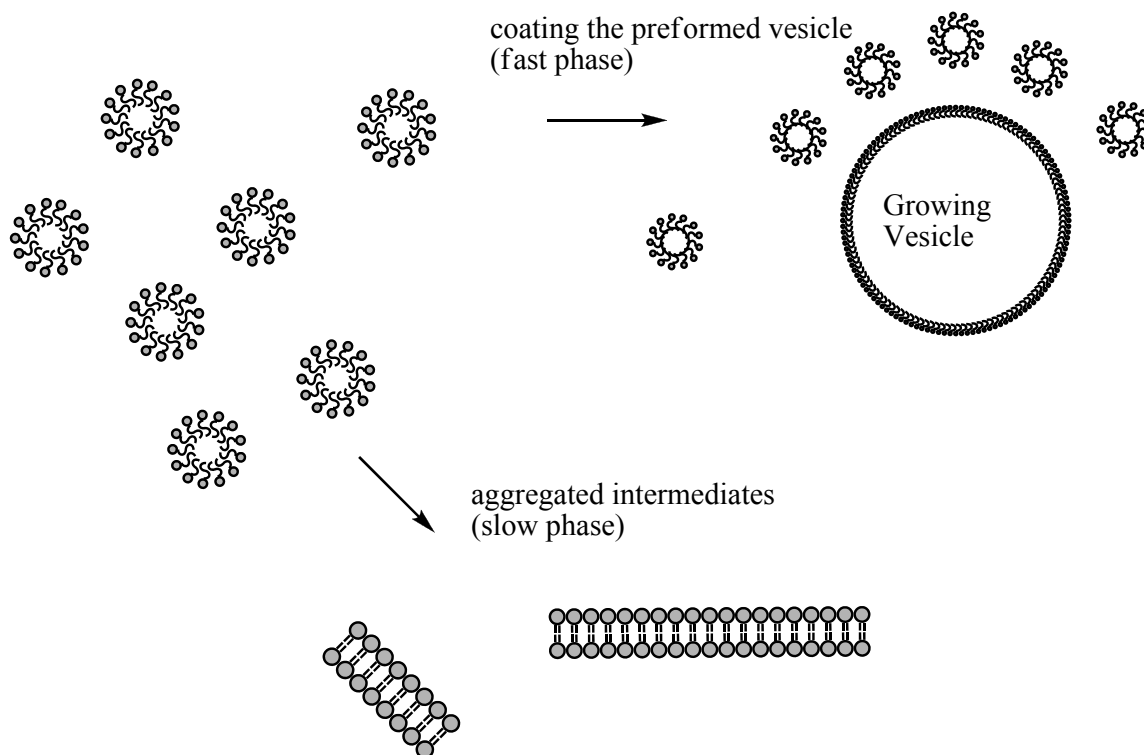


Figure 1.7 Proposed scheme of dynamic processes occurring between fatty acid micelles and vesicles.

In another article published by William R. Hargreaves and David W. Deamer, C₈-C₁₈ single-chain carboxylic acid amphiphiles were studied to understand the physicochemical conditions for the formation of membrane structures.¹⁵ A variety of characterization techniques were applied in this research to image vesicles, such as trapping of ionic dyes, negative-stain microscopy, and freeze-fracture electron microscopy. One interesting new method, phase-contrast microscopy, was utilized to image the vesicles wherein some solutes such as sucrose were added into the vesicle solution, which then creates differences in the refractive index to make vesicles appear brighter in the microscope.

1.3.2 Redox-responsive Aggregates

The stable chemical environment inside the aggregates, their nanometer size, and their long-term storage stability have enabled vesicles to be used in many different areas. For example, vesicles can be used as drug delivery systems to transport drugs to target position and protect those drugs from elimination by the body's immune system.^{26, 27} Vesicles can also be used as reagent-dispensing systems to delivery reagents in microfluidic analysis devices to enable advanced lab-on-a-chip technology.¹

Although vesicles have many advantages for a variety of applications, there does exist a technical barrier to overcome in order to utilize vesicles system: the controlled release of the encapsulated reagents from the vesicles. Researchers have tried different methods to achieve this control. Many of those works have focused on solving this problem from a fundamental structure point of view: to modify the surfactant structures to give them specific stimuli-responsive properties.^{4, 28-30} The aggregates formed from these surfactants are easily controlled by the same stimulation mechanism. Although some systems have been developed using this idea, their structure and properties are not well-defined. More studies still need to be conducted in order to develop new systems.

Redox-responsive surfactants are good candidates for stimuli-responsive structures by providing precise control over the disassembly of vesicles (through a reducing agent or an applied potential). Generally, these structures have a redox-sensitive functional group within the molecular structure. Upon a redox-stimulation, the structure of those sensitive groups changes and initiates the disassembly of the vesicles.

Many scientists have tried to synthesize these redox-responsive surfactants with different functional groups. For example, the Manners group has synthesized a new redox-sensitive amphiphilic structure,⁴ a diblock copolymer that employs polydimethylsiloxane (PDMS) as a hydrophobic block and polyferrocenylsilane (PFS) as a hydrophilic block. Based on their experiments, this newly synthesized amphiphilic structure can self-assemble into vesicles in water and has been confirmed by TEM experiments. PFS is an electroactive block that is controlled by redox stimulations. The previous study has shown that the redox reaction of the ferrocenyl group causes the change in the hydrophilic property of the surfactant.^{31, 32} It is predicted that vesicles generated by this diblock copolymer can be controlled by redox-stimulations; however, the goal of this project has yet to be demonstrated. Although the structure is well-designed and vesicles are formed, no evidence has been shown that vesicles morphology can be adjusted by redox stimulation. No reasons were cited for this, which indicates more research is still needed on this system.

Bhattacharya's group³⁰ has also developed three new surfactant structures that use an anthraquinone moiety as the redox-sensitive group. A hydrocarbon chain structure is covalently attached onto the anthraquinone. Based on their study, vesicles can be formed by sonicating these surfactants for several minutes in water. Anthraquinone is a redox-sensitive group that can be reduced into the corresponding hydroquinone upon introduction of a reducing agent or application of a reducing potential. Once it is reduced, the polarity of the group dramatically

changes; thus, vesicle morphology can be adjusted. UV-vis experiments have clearly shown the production of the hydroquinone product after introduction of dithionite ($S_2O_4^{2-}$), confirming that the designed mechanism is working. However, no guest release studies have been demonstrated to date.

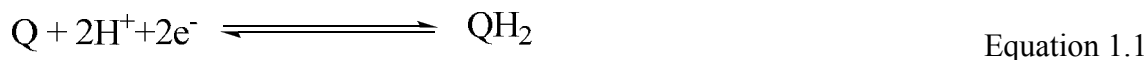
Some strategies to develop new redox-responsive surfactants can be derived from these examples discussed above: choose a redox-sensitive moiety as the polar group and attach a hydrocarbon chain covalently-bonded to a hydrophilic head group. Previous works confirmed that these kinds of amphiphilic structures can aggregate into vesicles.^{4,30} Meanwhile, the polarity change caused by redox-stimulation is capable of changing the amphiphilic nature of molecules and disassembling the vesicles to controllably release the payload. Studies have shown some progresses in developing redox-responsive aggregates, but the properties of those developed systems are still not well-defined.^{4,30}

Although ferrocenyl has been confirmed as a redox-sensitive structure in previous studies, it can not be shown if this redox reaction will actually drive the change in vesicle morphology that is described in Manner's paper. The work from Bhattacharya's group is encouraging, but their vesicles can only remain stable in storage for several hours based on light scattering data (suspected that the anthraquinone group photo-decompose), which will limit their application. Clearly, the development of new redox-responsive aggregates is very challenging work due to the difficulties with new surfactant syntheses, the complex mechanism of vesicle formation, and the limited methods for disassembling vesicles.

1.3.3 Quinonoid Compounds

Quinonoid compounds have been studied over many decades as the prototypical example of organic redox systems.³³ Usually, they are ring structures containing a cross-conjugated system. Quinone compounds can undergo electrochemical reactions, and the reduced

hydroquinone product will have a different polarity from the initial quinone structure. The half-reaction is a reversible reaction:



A particular quinone compound has been found to play a very important role in biological activity for most living systems during the synthesis of adenosine triphosphate (ATP).^{34,35} In the 1960s, people already knew that ATP was the energy source for most of life, but it was still unclear how ATP was generated until Nobel Laureate Peter Mitchell illustrated his chemiosmotic theory. Based on this theory, it is an electrochemical gradient generated in the cell membrane that drives the synthesis of ATP.^{34,36} A series of redox processes generate the electrochemical gradient in the cell membrane, and a quinone compound called ubiquinone performs a very important role to make these processes work normally.

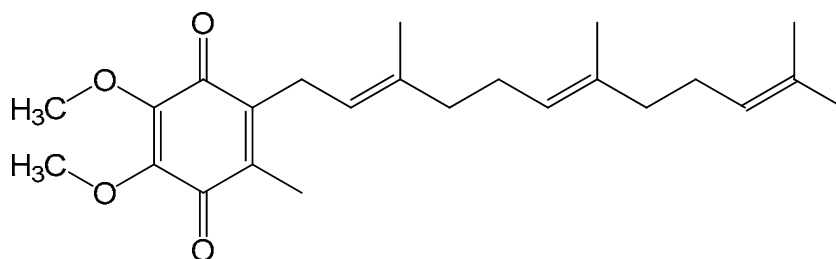


Figure 1.8 Structure of ubiquinone.

Ubiquinone is a lipid-soluble structure and is able to move freely inside the cell membrane, enabling ubiquinone molecules to shuttle electrons between immobile, larger complexes that are imbedded inside the cell membrane. The redox reactions of ubiquinone are similar to the redox reactions of other quinone structures. It is very interesting to see that even nature has utilized quinone redox properties for one of the most important processes in life. Furthermore, cell membranes resemble a vesicle structure; the presence of ubiquinone in this environment indicates the possibility for future incorporation of quinones in “artificial” vesicles.

Recent studies have shown that quinone compounds can also work as bioactive drug candidates for tumor cell treatment.^{10, 37-39} DT-diaphorase is a quinone oxidoreductase enzyme that exists in a wide variety of cells,⁴⁰ and it can reduce quinone compounds to the corresponding hydroquinone. Researchers at the National Cancer Institute have screened a variety of tumor cell lines to check their specific enzyme activities.³⁸ Three different enzymes were chosen for these studies, and the results showed that for every scanned tumor cell line, DT-diaphorase presented an obviously higher enzyme activity compared to the other two enzymes included in the study.³⁸ This extremely high enzyme activity for DT-diaphorase in cancer cells could be used as the trigger for the stimuli-response reaction mechanism, the reduction of quinone-based bioactive compounds will cause the degradation of the vesicle and release of the anti-cancer drug.

1.3.4 “Tri-methyl lock” Mechanism of the Quinone Compound

In 1972, Cohen and Borchard published their research concerning a series of quinone compounds that contained a 3-methylene carboxylic acid, a compound capable of undergoing a ring cyclization/lactonization reaction upon reduction to the hydroquinone.^{13, 41, 42} These structures and the corresponding ring cyclization/lactonization reactions have been studied in the following years; new stimuli-responsive molecules were designed from these studies.¹²

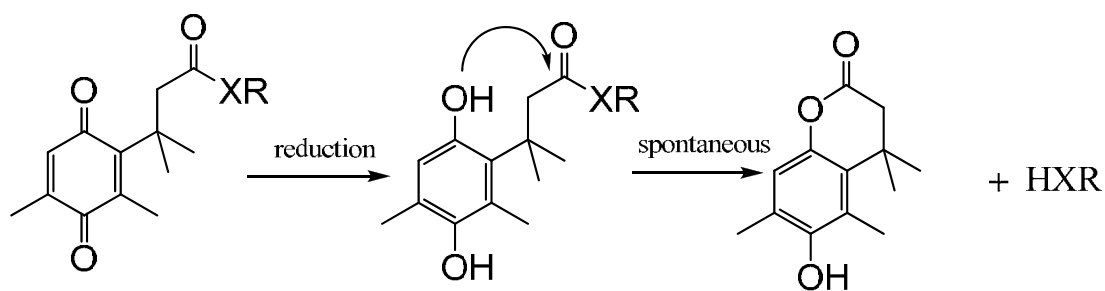


Figure 1.9 “Tri-methyl lock” mechanism.

Research has shown that molecular structures containing two methyl groups at the benzylic position together with a proximal methyl group on the ring, referred to as the “tri-methyl lock”, will exhibit enhanced lactonization rates. Upon reduction, an intramolecular

cyclization/elimination reaction occurs automatically following the formation of the hydroquinone; hence, the “tri-methyl lock” mechanism. The spontaneous lactonization reaction occurs because the three methyl groups create increased strain energy on the ring structure, which facilitates nucleophilic attack at the carbonyl carbon. The “tri-methyl lock” mechanism and the structures of the compounds involved in this process are shown in Figure 1.9.¹²

By varying the functional group (XR) adjacent to the carbonyl, the “tri-methyl lock” mechanism can be extended to other applications that also utilize this cyclization/elimination event. For example, researchers have used these “tri-methyl lock” quinone structures to develop prodrugs as delivery systems wherein HXR is some kind of drug. In particular, Borchardt and coworkers have reported that hydroxyl amide lactonization can be used as a potential esterase-sensitive amide prodrug.³⁷⁻³⁹ The mechanism for the redox-sensitive and esterase-sensitive system is shown in Figure 1.10.³⁹

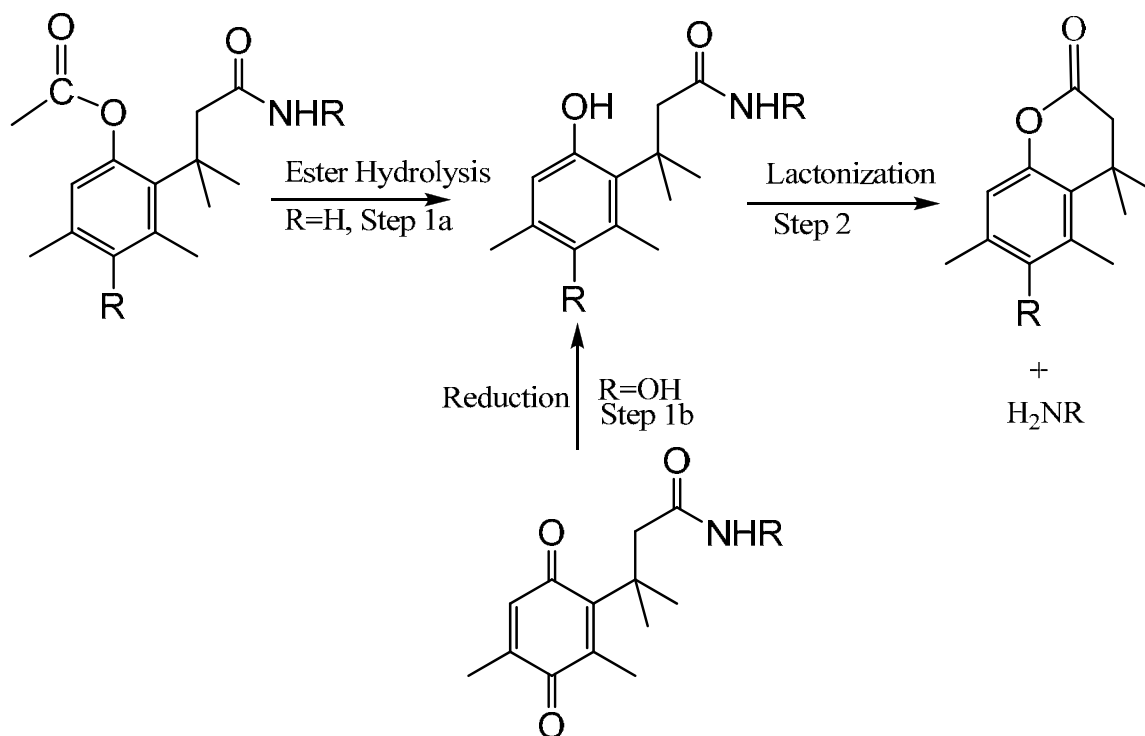


Figure 1.10 Mechanisms for utilizing “tri-methyl lock” mechanism for prodrug release.

In this application, the quinone moiety can be reduced under certain chemical conditions (step 1b), and then the following intermediate undergoes lactonization to release the potential drug compound (step 2). If an ester moiety is present on the hydroquinone, then the rate of lactonization depends on the rate of enzymatic or chemical hydrolysis of the initial structure (step 1a).³⁹ These structural designs helped to develop a prodrug system that is triggered by either an esterase or reducing agent.

Another paper, published by Mrksich's group, described a double side-chain structure that is also based on a "tri-methyl lock" quinonoid compound.⁴³ The purpose was to develop a new class of dynamic electroactive monolayers on surfaces that can selectively release immobilized ligands, which is very important to bio-interfacial science studies. The monomer structure of this double chain structure is illustrated in Figure 1.11.

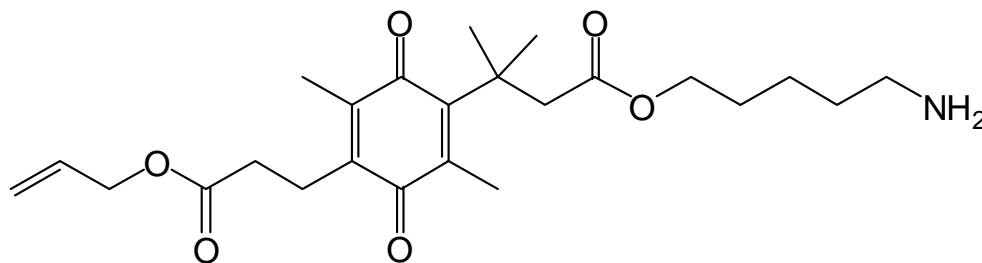


Figure 1.11 A quinone propionic ester with a bi-functional group.

The side chain containing the double bond in Figure 1.11 was used to connect the self-assembled monolayers (SAMs) of alkanethiolates onto gold surfaces while the other side with a terminal amine was used to capture biotin ligands. When a reduction potential was applied through gold, the quinones convert into the corresponding hydroquinones, which then undergo the cyclization/elimination reaction and release the biotin ligand. The "tri-methyl lock" in this structure serves to increase the rate of biotin release. This study combines self-assembly monolayer, the redox property of quinone structures, and biotechnology to demonstrate the great potential for mechanistic studies in cell biology.

1.4 References

1. Vreeland, W. N.; Locascio, L. E., Using Bioinspired Thermally Triggered Liposomes for High-Efficiency Mixing and Reagent Delivery in Microfluidic Devices. *Analytical Chemistry* 2003, 75, (24), 6906-6911.
2. Tan, Y. C.; Hettiarachchi, K.; Siu, M.; Pan, Y. P., Controlled Microfluidic Encapsulation of Cells, Proteins, and Microbeads in Lipid Vesicles. *Journal of the American Chemical Society* 2006, 128, (17), 5656-5658.
3. Leamon, C. P.; Low, P. S., Delivery of Macromolecules into Living Cells: A Method That Exploits Folate Receptor Endocytosis. *Proceedings of the National Academy of Sciences of the United States of America* 1991, 88, (13), 5572-5576.
4. Power-Billard, K. N.; Spontak, R. J.; Manners, I., Redox-Active Organometallic Vesicles: Aqueous Self-Assembly of a Diblock Copolymer with a Hydrophilic Polyferrocenylsilane Polyelectrolyte Block. *Angewandte Chemie, International Edition* 2004, 43, (10), 1260-1264.
5. Paul C. Hiemenz, R. R., *Principles of Colloid and Surface Chemistry*. 3 ed.; Marcel Dekker: 1997; p 15.
6. Lenaz, G.; Genova, M. L., *Encyclopedia of Biological Chemistry*. Elsevier: 2004; p 621-627.
7. Beyer, R. E.; Segura-Aguilar, J.; DiBernardo, S.; Cavazzoni, M.; Fato, R.; Fiorentini, D.; Galli, M. C.; Setti, M.; Landi, L.; Lenaz, G., The Role of D₁-Diaphorase in the Maintenance of the Reduced Antioxidant Form of Coenzyme Q in Membrane Systems. *Proceedings of the National Academy of Sciences of the United States of America* 1996, 93, (6), 2528-2532.
8. Crane, F. L.; Hatefi, Y.; Lester, R. L.; Widmer, C., Isolation of a Quinone from Beef Heart Mitochondria. *Biochimica Et Biophysica Acta* 1957, 25, (1), 220-221.
9. Mitchell, P., Protonmotive Redox Mechanism of Cytochrome-B-C₁ Complex in Respiratory-Chain - Protonmotive Ubiquinone Cycle. *Febs Letters* 1975, 56, (1), 1-6.
10. Naylor, M. A.; Thomson, P., Recent Advances in Bioreductive Drug Targeting. *Mini-Reviews in Medicinal Chemistry* 2001, 1, (1), 17-29.
11. Zheng, A.; Shan, D.; Wang, B., A Redox-Sensitive Resin Linker for the Solid Phase Synthesis of C-Terminal Modified Peptides. *Journal of Organic Chemistry* 1999, 64, (1), 156-161.
12. Wang, B. H.; Liu, S. M.; Borchardt, R. T., Development of a Novel Redox-Sensitive Protecting Group for Amines Which Utilizes a Facilitated Lactonization Reaction. *Journal of Organic Chemistry* 1995, 60, (3), 539-543.

13. Borchard, R. T.; Cohen, L. A., Stereopopulation Control .2. Rate Enhancement of Intramolecular Nucleophilic Displacement. *Journal of the American Chemical Society* 1972, 94, (26), 9166-9174.
14. Borchard, R. T.; Cohen, L. A., Stereopopulation Control .5. Conformational Selection of Alternative Oxidation Pathways. *Journal of the American Chemical Society* 1973, 95, (25), 8319-8326.
15. Hargreaves, W. R.; Deamer, D. W., Liposomes from Ionic, Single-Chain Amphiphiles. *Biochemistry* 1978, 17, (18), 3759-3768.
16. Chen, I. A.; Szostak, J. W., A Kinetic Study of the Growth of Fatty Acid Vesicles. *Biophysical Journal* 2004, 87, (2), 988-998.
17. Szostak, J. W.; Bartel, D. P.; Luisi, P. L., Synthesizing Life. *Nature* 2001, 409, (6818), 387-390.
18. New, R. R. C., *Liposomes : A Practical Approach*. IRL Press ; Oxford University Press: New York, 1990; p 301.
19. Hiemenz, P. C.; Rajagopalan, R., *Principles of Colloid and Surface Chemistry*. 3rd ed.; Marcel Dekker, Inc.: New York, 1997; p 371.
20. D. Fennell Evans, H. W., *The Colloidal Domanin Where Physics, Chemistry, Biology, and Technology Meet*. VCH Publishers: 1994; p 8.
21. Mui, B.; Chow, L.; Hope, M. J., Extrusion Technique to Generate Liposomes of Defined Size. In *Liposomes, Pt A*, 2003; Vol. 367, pp 3-14.
22. Namani, T.; Walde, P., From Decanoate Micelles to Decanoic Acid/Dodecylbenzenesulfonate Vesicles. *Langmuir* 2005, 21 (14), 6210-6219.
23. Namani, T.; Ishikawa, T.; Morigaki, K.; Walde, P., Vesicles from Docosahexaenoic Acid. *Colloids and Surfaces B: Biointerfaces* 2007, 54, 118-123.
24. Chakrabarti, A. C.; Breaker, R. R.; Joyce, G. F.; Deamer, D. W., Production of Rna by a Polymerase Protein Encapsulated within Phospholipid-Vesicles. *Journal of Molecular Evolution* 1994, 39, (6), 555-559.
25. Stevenson, S. A.; Blanchard, G. J., Investigating Internal Structural Differences between Micelles and Unilamellar Vesicles of Decanoic Acid/Sodium Decanoate. *Journal of Physical Chemistry B* 2006, 110, (26), 13005-13010.
26. Cevc, G., Lipid Vesicles and Other Colloids as Drug Carriers on the Skin. *Advanced Drug Delivery Reviews* 2004, 56, (5), 675-711.
27. Langer, R., Drug Delivery and Targeting. *Nature* 1998, 392, (6679), 5-10.

28. Checot, F.; Brulet, A.; Oberdisse, J.; Gnanou, Y.; Mondain-Monval, O.; Lecommandoux, S., Structure of Polypeptide-Based Diblock Copolymers in Solution: Stimuli-Responsive Vesicles and Micelles. *Langmuir* 2005, 21, (10), 4308-4315.
29. Saji, T.; Hoshino, K.; Aoyagui, S., Reversible Formation and Disruption of Micelles by Control of the Redox State of the Head Group. *Journal of the American Chemical Society* 1985, 107, (24), 6865-6868.
30. Bhattacharya, S.; Subramanian, M., Synthesis, Redox, and Electrochemical Properties of Anthraquinone-Attached Micelle- and Vesicle-Forming Cationic Amphiphiles. *Journal of the Chemical Society, Perkin Transactions 2: Physical Organic Chemistry* 1996, (9), 2027-2034.
31. Kakizawa, Y.; Sakai, H.; Saji, T.; Yoshino, N.; Kondo, Y.; Abe, M., Effect of Ferrocenyl Group Oxidation on Micelle Formation and Benzene Derivatives Solubilization of a Cationic Ferrocenylated Surfactant. *Shikizai Kyokaiishi* 1999, 72, (2), 78-87.
32. Kakizawa, Y.; Sakai, H.; Yamaguchi, A.; Kondo, Y.; Yoshino, N.; Abe, M., Electrochemical Control of Vesicle Formation with a Double-Tailed Cationic Surfactant Bearing Ferrocenyl Moieties. *Langmuir* 2001, 17, (26), 8044-8048.
33. Patai, S.; Rappoport, Z.; Editors, *The Chemistry of the Quinonoid Compounds*. 1988; Vol. 2, p 1711.
34. Mitchell Peter, D., *Foundations of Vectorial Metabolism and Osmochemistry*. *Bioscience reports* 2004, 24, (4-5), 386-434; discussion 434-5.
35. Quagliariello, E.; Papa, S.; Palmieri, F.; Slater, E. C.; Siliprandi, N.; Editors, *Electron Transfer Chains and Oxidative Phosphorylation*. [Proceedings of the International Symposium Held in Selva Di Fasano, Italy, September 15-18, 1975]. 1975; p 452.
36. Rich, P. R.; Moore, A. L., The Involvement of the Protonmotive Ubiquinone Cycle in the Respiratory Chain of Higher Plants and Its Relation to the Branchpoint of the Alternate Pathway. *Febs Letters* 1976, 65, (3), 339-44.
37. Amsberry, K. L.; Borchardt, R. T., Amine Prodrugs Which Utilize Hydroxy Amide Lactonization .1. A Potential Redox-Sensitive Amide Prodrug. *Pharmaceutical Research* 1991, 8, (3), 323-330.
38. Fitzsimmons, S. A.; Workman, P.; Grever, M.; Paull, K.; Camalier, R.; Lewis, A. D., Reductase Enzyme Expression across the National Cancer Institute Tumor Cell Line Panel: Correlation with Sensitivity to Mitomycin C and Eo9. *Journal of the National Cancer Institute* 1996, 88, (5), 259-269.
39. Amsberry, K. L.; Gerstenberger, A. E.; Borchardt, R. T., Amine Prodrugs Which Utilize Hydroxy Amide Lactonization .2. A Potential Esterase-Sensitive Amide Prodrug. *Pharmaceutical Research* 1991, 8, (4), 455-461.

40. Landi, L.; Fiorentini, D.; Galli, M. C.; Segura-Aguilar, J.; Beyer, R. E., Dt-Diaphorase Maintains the Reduced State of Ubiquinones in Lipid Vesicles Thereby Promoting Their Antioxidant Function. *Free Radical Biology & Medicine* 1996, 22, (1/2), 329-335.
41. Borchard, R.; Cohen, L. A., Stereopopulation Control .3. Facilitation of Intramolecular Conjugate Addition of Carboxyl Group. *Journal of the American Chemical Society* 1972, 94, (26), 9175-9182.
42. Milstien, S.; Cohen, L. A., Stereopopulation Control .1. Rate Enhancement in Lactonizations of Ortho-Hydroxyhydrocinnamic Acids. *Journal of the American Chemical Society* 1972, 94, (26), 9158-9165.
43. Hodneland, C. D.; Mrksich, M., Biomolecular Surfaces That Release Ligands under Electrochemical Control. *Journal of the American Chemical Society* 2000, 122, (17), 4235-4236.

CHAPTER 2. MATERIALS AND METHODS

2.1 Chemicals

The following chemicals were purchased from Sigma-Aldrich and used as received: trimethylhydroquinone (97%), methanesulfonic acid (99.5%), dimethylacrylic acid (97%), ethyl acetate (99.5%), sodium bicarbonate (99.5%), sodium chloride (99.5%), magnesium sulfate (99.9%), deuterated chloroform (99.9 atom%), anhydrous tetrahydrofuran (99.9%), triethylamine (99.9%), anhydrous dichloromethane (99.9%), potassium carbonate (99%), hexane (99%), anhydrous chloroform (99.9%), *N*-bromosuccinimide (99%), 1,3-dicyclohexylcarbodiimide (99%), acetonitrile (99.9%), acetone (99.9%), 10% palladium on carbon catalyst powder, ethanol (99.9%), fuming sulfuric acid (18M), formic acid (96%), sodium dithionite (85%), calcein (93%), sodium phosphate dibasic (99%), sodium phosphate monobasic (99%), sodium phosphate (96%), isobutylene (99%). *N*-hydroxysuccinimide (Aldrich 97%) was purified by recrystallization prior to experiments. Additionally, *N*-benzyloxycarbonyl-6-aminohexanoic acid (Novabiochem, 90%), sephadex G25 gel (GE healthcare), sodium hydroxide (Fisher, 98.6%), 32-63 μm neutral silica gel having 6 nm pore size (Alltech), silica gel TLC plate (Alltech), were also used in these experiments. Water for these experiments was purified and deionized (18 M Ω -cm) through the use of a Barnstead-Nanopure water filtration system.

2.2 Methodologies

2.2.1 Extrusion Technique for Development of Vesicle Aggregates

Solid Q9 (2.1 mg) was dissolved in 10 mL dichloromethane (DCM), and the solvent was evaporated under vacuum in a round bottom flask (RBF) to form a dried homogenous Q9 thin film. Phosphate buffered saline (PBS) solution (50 mM with NaCl 50 mM, 0.7 mL, pH 7.8) solution was filtered through a sterile Anotop filter (Whatman, 0.02 μm pore size/10 mm

diameter), and added into the RBF to hydrate the Q9 dried film for 2 hours. The flask was then vortexed for 15 mins. A hand-held, mini-extruder from Avanti Polar Lipids with 100 nm pore size Nuclepore polycarbonate track-etched membrane (6-11 μm thickness) was used to extrude 21 repetitions the Q9 molecules for forming vesicles, Figure 2.1.

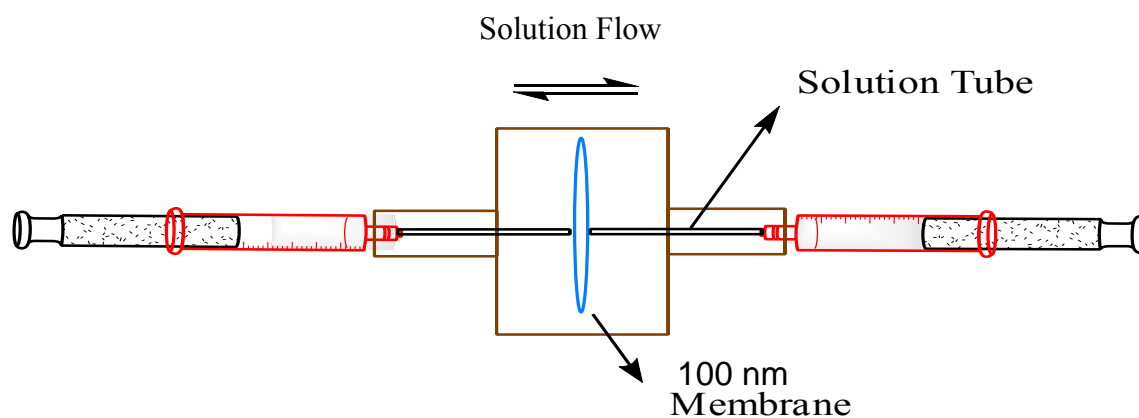


Figure 2.1 Extrusion.

Before the experiment, one polycarbonate track-etched membrane (Nuclepore, 100 nm, 6-11 μm thickness) was fitted in the middle part of extruder across the internal solution channel. Two Gas-Tight syringes were connected on each side of the solution tube. One syringe was filled with vortexed 10 mM Q9 in pH 7.8 PBS. This syringe was pushed by hand to force the solution through the membrane into the opposing syringe. Then it was pushed back to the original syringe. This process was repeated 20.5 times. The strong shear force generated as the solution is pushed through the membrane promotes vesicle formation.¹⁻³

2.2.2 Preparation of Samples for Light Scattering

All sample cells for the LS experiment were thoroughly cleaned to remove any dust. The cleaning procedure included sonicating glass sample cells for 20 mins, a rinse in Nano-pure water, and drying in a laboratory oven.

Q9 solutions were prepared in pH 7.8 PBS solution (50 mM with NaCl 50 mM) and then filtered through a sterile Anotop filter (Whatman, 0.1 μm pore size/10 mm diameter). They were

then treated through the extrusion process as described above. The extruded samples were placed in the dust-free sample cells for the LS measurement.

2.2.3 Dynamic Light Scattering

Dynamic light scattering is a technique that measures and correlates the change in scattering light intensity through a liquid sample and is based on the fact that free particles inside the solution undergo a “random walk” based on the theory of Brownian Motion. Thus, the diffusion coefficient value (D) of sample particles can be derived from the change of scattered light intensity in the time frame of a given experiment. The autocorrelation functions recorded in the experiment make the measurement of D possible. If the particles present as a spherical structure, The Stokes-Einstein equation ($R_h = kT/6\pi\eta D$) can be applied in order to calculate the hydrodynamic radius of a given particle.⁴

Dynamic light scattering experiments were conducted using a Zetasizer Nano Instrument (Malvern, Worcestershire). Carefully cleaned glass sample vials were used and were prepared according to the preparation of sample cells referred to the section 2.2.2. Experiment temperature was held constant at 25 °C and was stabilized before the measurement. The buffer viscosity parameter was calculated by the software of the instrument using the concentration of the sodium phosphate present.

2.2.4 Surface Tension Measurement

Surface tension measurements of Q9 in PBS solution were performed using a Sigma 703 tensiometer (KSV Instruments, Monroe, CT) by using the du Nuoy ring method. A platinum ring of 5.99 cm mean circumference (CSC Scientific, Fairfax, VA) was hung on a microbalance. The force applied to this ring was recorded through this microbalance.

A 2.0 mL solution sample of Q9 was placed in a home-made 10 mL glass cup. The platinum ring was cleaned with ethanol and dried under a nitrogen gas flow before the

measurement. Then, the ring was submerged into the solution and raised up slowly until it was no longer in contact with the solution in the glass cup. This operation was repeated three times; each time the maximum force on the ring was recorded as the surface tension. Average values of surface tension and standard deviations were calculated from these sets of runs.

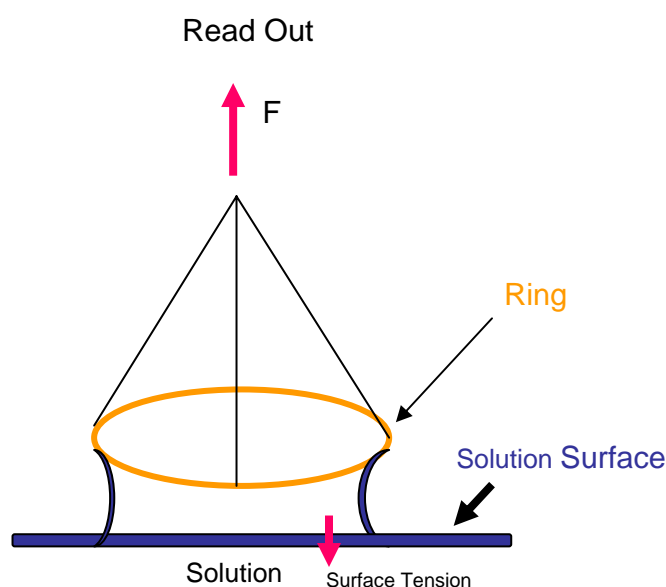


Figure 2.2 Surface tension measurement by du Nuoy ring method.

In order to calculate the CAC of Q9, a series of surface tension measurements were conducted on Q9 samples. Eleven Q9 samples were prepared in PBS solution (50 mM with NaCl 50 mM, pH 7.8) with the concentrations ranging from 0.2 mM to 14 mM. Samples were tested from the highest concentration to the lowest concentration. The surface tension of pure solvent (buffer) was also measured, giving the highest value in this series of experiment results. A surface tension versus concentration curve was plotted and the CAC value was determined from this curve.

2.2.5 Theory of Critical Aggregation Concentration

When surfactant molecules dissolve in water, they are likely to migrate to the air-water interface because of the insolubility of the hydrophobic moiety of the surfactant. The non-polar

group of the molecule is oriented in the air phase. The concentrated hydrophobic structure at the interface results in a decrease of surface tension.

Concentrated surfactant at the air-water interface allows for a increase in the repulsive forces between adjacent molecules. When the concentration is increased to a certain degree, the repulsion force is big enough to prevent more surfactant being taken up at the interface. Thus, aggregation of molecules ensues. The concentration at this moment is called the critical aggregation concentration (CAC). Above the CAC, any further surfactant added into the solution forms aggregates instead of inserting at the water-air interface. The surface tension should stay relatively stable regardless of whether more surfactant is added to the solution.

This surface tension property can be used for the determination of the CAC. Generally a group of water solutions is prepared having different surfactant concentrations. The surface tension of each solution is measured. In the low concentration range, the surface tension decreases as a result of the increasing surfactant concentration due to the migration of the surfactant to the air-water interface. When the surfactant concentration is above the CAC, the surface tension becomes stable due to the formation of aggregates. Thus, the surface tension data can be plotted versus solution concentration; the concentration related to the “turn over” point in this plot will be the CAC.⁵

2.2.6 Mechanism of Asymmetrical Flow Field-Flow Fractionation (AF4)

AF4 systems were developed to separate and characterize particles in solution.⁶⁻⁸ The sample is injected into a channel with a lamellar flow along the channel direction, another flow of the same solvent system is applied orthogonally to the first flow by passing solvent through a membrane on the bottom of the channel. The membrane through which the orthogonal flow passes is designed to have size-exclusion capabilities; the pore size of the membrane is smaller than the sample particles to prevent the injected sample particles from being lost. Thus, particles

inside the sample are pushed closer to the membrane as they move through the channel carried by the lamellar injection flow. Those particles present different distance from the membrane as well as the different flow rate, as they are carried in the lamellar flow, depending on their sizes and the strength of the orthogonal flow. Finally, they will elute out at different times due to flow velocity differences. The mechanism of this technique is shown in Figure 2.3. To achieve the best separation result, both the lamellar and orthogonal field flow is adjusted to optimize particle separation by adopting different programming methods. The programmed field-flow method is called AF4 technology and it was applied to the Q9 system.⁶⁻⁹

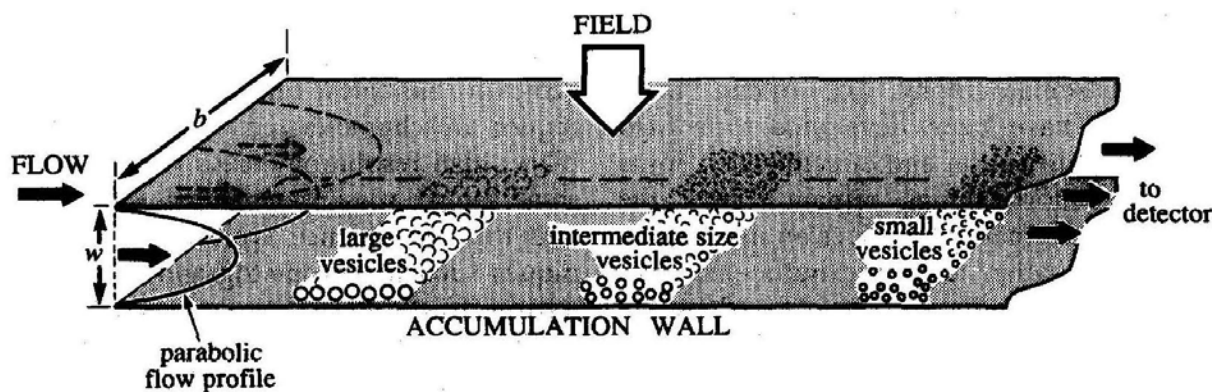


Figure 2.3 The mechanism of AF4 separation based on the particle sizes. Adapted from Reference 7.

2.2.7 AF4 Studies on Extruded Q9 Sample

Q9 aggregates were separated using an Eclipse 2 AF4 system (Wyatt Technology Corp., Santa Barbara, CA). An Agilent 1100 HPLC system (Agilent 1100 isocratic pump, Agilent 1100 autosampler, and Agilent 1100 degasser, Agilent Technologies, Palo Alto, CA) was used for injection of the samples and delivery of solvent through the AF4 system. The AF4 channel was assembled with a 350- μm -thick Mylar spacer; the membrane used was made of regenerated cellulose with a 10 kDa molecular weight cutoff (Wyatt). Three detectors were used for the analysis: a Heleos, multi-angle light scattering (MALS) with a QUELS (DLS) detector (Wyatt Technology Corp., Santa Barbara, CA); an Optilab rEX Differential Refractive Index detector

(Wyatt Technology Corp., Santa Barbara, CA) at 658 nm; and a Waters 484 UV-Vis detector (Waters, Milford MA) at 280nm. Data acquisition of the root mean squared (rms), and hydrodynamic radius (R_h) value were calculated using Astra V software (Wyatt).

For the experiment, PBS solution (3.0 L, 50 mM with NaCl 50 mM, pH 8.0, containing 200 ppm NaN_3) was prepared at 40 mM concentration, then filtered through a 100 nm membrane for use as the mobile phase. Q9 aggregate samples (3.0 mg/mL) and DOPC vesicle samples (1.0 mg/mL) were prepared in the same buffer solution by the extrusion method with a 100 nm membrane. The DOPC sample was used as the reference for the flow control method development.

2.2.8 Preparative Size-Exclusion Chromatography

Size-exclusion chromatography is widely used to separate and characterize particle samples with various particle sizes in polymer and biological studies.¹⁰ In this research it was used to separate Q9 vesicles in solution. Sample solutions having particles with polydisperse size distribution are introduced into a preparative size-exclusion chromatography column that is packed with beads of porous material. Small particles in the solution can go into the pores inside these beads. Thus, they move slowly there until they exit from the pores because of the hydrodynamic shielding effect. Big particles/molecules can not enter the pores; they move rapidly through the void volume between the beads. Thus, different particles elute from the column at different times: big particles move out quickly, small particles come out later.

The preparative size-exclusion column used here is an in-lab prepared column. Sephadex G25 gel (GE Healthcare, Piscataway, NJ) was used for the column packing medium. The sephadex gel (10 g) was hydrated with the same PBS that was used for the eluent (pH 7.8) for 10

hours, then poured slowly into a 100.0 mL titration burette and allowed to settle in order to pack the column.

The particle separation was conducted under air pressure. Q9 vesicle samples that were developed by the extrusion treatment were introduced at the top side of the column via a glass pipette. The volume of PBS solution in the burette was maintained to act as the mobile phase. Particles were separated based on the theory explained above. The effluent was collected at consistent time increments as samples to be analyzed. In accordance with the mechanisms working in the preparative size-exclusion column, Q9 vesicles were contained in the earliest collected effluent samples.

2.2.9 Dye Encapsulation and Release Experiment

Calcein, a water-soluble dye, was explored to study the encapsulation ability of Q9 aggregates. A 50 mM concentration of calcein in pH 7.8 PBS (0.1 M with 0.1 M NaCl) was extruded simultaneously with 3 mg/mL of Q9. Calcein was self-quenching under this concentration. The concentrated calcein was maintained, as well as the self-quenching status, when it was encapsulated inside the Q9 vesicles, because the Q9 vesicle protect it from dilution in the PBS solvent.¹¹ The extruded solution was eluted with pH 7.8 PBS solution (0.1 M with 0.1 M NaCl) through an in-lab prepared size exclusion column (sephadex G25 gel, GE healthcare) to separate the calcein-containing Q9 aggregates from free calcein. After separation by preparative size-exclusion column, the fluorescence intensity of Q9 aggregates containing calcein was monitored with a luminescence spectrometer (PerkinElmer, LS50B, Waltham, MA) in order to observe the impact of adding $\text{Na}_2\text{S}_2\text{O}_4$, a chemical reducing agent.

2.2.10 Preparation of Samples for Transmission Electron Microscopy

Microscope grids and a storage box were purchased from Electron Microscopy Sciences. Grids used for experiments were the 400 mesh carbon-coated Cu type (CF400-Cu-25). For

sample analysis, the grid was carefully placed into a 150 mm x 15 mm polystyrene Petri dish cover (Fisher Scientific) with carbon side facing up. One small drop of sample solution was deposited on the grid with a 2 μ L micropipette. Five minutes later, it was removed by blotting with a small piece of sterile filter paper, being careful not to displace the aggregate sample attaching to the grid while blotting. A negative stain method was used for sample imaging. A small drop of 2% uranyl acetate ($\text{UO}_2(\text{CH}_3\text{COO})_2 \cdot 2\text{H}_2\text{O}$ water solution) was deposited on the sample loaded grid, and allowed to sit for 2 mins before removed by blotting as previously described.^{12, 13}

A JEOL 100 CX transmission electron microscope with an electron acceleration voltage of 80 kV was employed for the experiment (JEOL USA, Inc., Peabody, MA). Tweezers were used to place the grid onto the sample holder inside the TEM microscope. Liquid nitrogen was used as the cooling agent during the experiment process. Kodak electron microscope film (vendor number 1662238) with dimensions of 3.25" x 4" was used for the experiments and was developed and fixed according to the operation menu from Kodak. Negatives were scanned into a computer and edited with Photoshop software (Adobe, San Jose, CA).

2.3 Instrumentation

2.3.1 Nuclear Magnetic Resonance Spectroscopy (NMR)

Proton NMR experiments were performed on several Bruker instruments, including a DPX-250, ARX-300 and DPX-400. ^1H kinetic experiments were performed on Bruker ARX-300 instrument. All these experiments were conducted under at room temperature. For ^1H NMR kinetic studies, 23 ^1H NMR experiments were run for 300 minutes after the addition of 5 equivalents of solid reducing agent, $\text{Na}_2\text{S}_2\text{O}_4$. During each experiment, NMR spectra were recorded at various time points to measure the change in proton signals during the 300 mins experiments. Each ^1H NMR spectrum was integrated to achieve the relative area of the

absorption peaks for each experiment. The change in area of selected peaks was used as the index to monitor the reaction kinetic process.

2.3.2 Gas Chromatography Mass Spectrometry (GC-MS)

GC-MS analysis was performed with a Varian Saturn 2200 GC/MS (Varian, Palo Alto, CA). This instrument was equipped with a CP-3800 GC and the 2000 Series Ion Trap MS with an automatic injection mode. Chloroform was used as the solvent for the sample preparation. The mass range of the instrument is from 10 to 650 m/z . Software utilizes a DB5 control method for all analyses (Injector temperature 250 °C, flow pressure 0.1 psi, column oven temperature 280 °C).

2.3.3 Electrospray Ionization Mass Spectrometry (ESI-MS)

An Applied Biosystems (Foster City, CA) QSTAR XL quadrupole time-of-flight MS with nano LC system was utilized for high-resolution ESI-MS analyses. Samples were measured with a mass accuracy below 4 parts per million (ppm).

2.3.4 Cryogenic Electron Microscopy (CryoEM)

CryoEM experiments were conducted at National Center for Macromolecular Image (Baylor College of Medicine, Houston, TX). The sample was prepared for imaging by means of vitrification of frozen hydrated samples.¹⁴ This method enables the sample to retain its solution properties with the fewest possible artifacts. A Quantifoil (Quantifoil Micro Tools EmbH, Jena Germany) 400 mesh holey carbon copper grid was placed in the Vitrobot (FEI, Hillsboro OR) where temperature and relative humidity were regulated. The 2.5 μL aliquot of sample was applied to one side of the grid, filter paper was used to remove excess liquid on the grid by an automatic blotting process. Then the grid was rapidly plunged into a cup of liquid ethane, thereby freezing the sample almost instantaneously. Vitrification of the sample on the grid was achieved during this process; the resulting “glues” can be examined by the electron microscopy.

The grid was then transferred to a storage holder submerged in a liquid nitrogen tank where it was kept until use (in 7 days). Microscopy was carried out using a JEOL 2010F transmission electron microscope (JEOL, Tokyo Japan) operated at 200 kV under loose dose conditions, and the specimen was maintained at -203 °C by a Gatan Model 626 cryostage (Gatan, Pleasanton CA). Images were recorded with Gatan US4000 4k x 4k charged-coupled device (CCD, Gatan, Pleasanton CA) camera and processed using the EMAN software package.¹⁵

2.3.5 Ultraviolet-visible (UV-vis) Spectroscopy

UV-vis absorption measurements were performed on a Cary 50 Bio UV-vis Spectrometer (Varian, Palo Alto, CA). The emission source in this instrument is a Xenon flash lamp and is able to scan a sample through a range of wavelength from 200 to 1000 nm in 80 seconds. Scan ranges were selected depending on the solvent system used and the purpose of analysis. Medium scan rate was chosen. A quartz cuvette or a polystyrene UV-vis cuvette (Fisher Scientific, Pittsburgh, PA) with 1.0 cm path length were used as the sample cells for the absorbance measurements. Before each sample measurement, a “blank” sample (solvent) was run to allow for background subtraction.

2.3.6 Fluorescence Spectrometry

An LS 50B Fluorescence Spectrometer (Perkin Elmer, LS50B, Waltham, MA) was used for fluorescence measurements. A pulsed Xenon discharge lamp (7.3 W average power at 50 Hz) was utilized as the light source and the operation of the instrument was controlled with FL Winlab software. The software enabled a dynamic process measurement up to 1500 minutes with adjustable interval time scale measurements of the fluorescence intensity change. A 10×10 mm (3.5 mL) quartz cell was used as a cuvette during analysis.

Dynamic fluorescence experiments were conducted on Q9 vesicle samples with calcein encapsulated; the excitation wavelength (495 nm) and the emission wavelength (515 nm) of

calcein were used in the dynamic operation mode to monitor the fluorescence change of the sample. The whole dynamic experiment time was continued for 1500 minutes; the fluorescence intensity was recorded every 5 minutes in the experiment setup. The change of the fluorescence intensity during the dynamic experiment was plotted.

2.4 References

1. Mui, B.; Hope, M. J., *Liposome Technology*. Informa Healthcare USA: London, UK, 2007; Vol. 1, p 55-64.
2. Mui, B.; Chow, L.; Hope, M. J., *Extrusion Technique to Generate Liposomes of Defined Size*. In *Liposomes, Pt A*, 2003; Vol. 367, pp 3-14.
3. Hunter, D. G.; Frisken, B. J., *Effect of Extrusion Pressure and Lipid Properties on the Size and Polydispersity of Lipid Vesicles*. *Biophysical Journal* 1998, 74, (6), 2996-3002.
4. Berry, G. C.; Cotts, P. M., *Modern Techniques for Polymer Characterisation*. John Wiley & Sons: 1999; p 81-105.
5. Evans, D. F.; Wennerstrom, H., *The Colloidal Domain: Where Physics, Chemistry, and Biology Meet*. 2 ed.; wiley-vch: 1999; p 5-10.
6. Janca, J., *Modern Techniques for Polymer Characterisation*. John Wiley & Sons Ltd: 1999; p 57-79.
7. Moon, M. H.; Giddings, J. C., *Size Distribution of Liposomes by Flow Field-Flow Fractionation*. *Journal of Pharmaceutical and Biomedical Analysis* 1993, 11, (10), 911-920.
8. Schauer, T., *Symmetrical and Asymmetrical Flow Field-Flow Fractionation for Particle Size Determination*. *Particle & Particle Systems Characterization* 1995, 12, (6), 284-8.
9. Alasonati, E.; Stolpe, B.; Benincasa, M. A.; Hasselov, M.; Slaveykova, V. I., *Asymmetrical Flow Field Flow Fractionation - Multidetector System as a Tool for Studying Metal-Alginate Interactions*. *Environmental Chemistry* 2006, 3, (3), 192-198.
10. Wu, C., *Handbook of Size Exclusion Chromatography and Related Techniques*. 2 ed.; Marcei Dekker, Inc: New York, 2004; p 1-24.
11. Hamann, S.; Kiilgaard, J. F.; Litman, T.; Alvarez-Leefmans, F. J.; Winther, B. R.; Zeuthen, T., *Measurement of Cell Volume Changes by Fluorescence Self-Quenching*. *Journal of Fluorescence* 2002, 12, (2), 139-145.
12. New, R. R. C., *Liposomes : A Practical Approach*. IRL Press ; Oxford University Press: New York, 1990; p 301.

13. Edwards, K. A.; Baeumner, A. J., Analysis of Liposomes. *Talanta* 2006, 68, (5), 1432-1441.
14. Dubochet, J.; Adrian, M.; Chang, J. J.; Homo, J. C.; Lepault, J.; McDowell, A. W.; Schultz, P., Cryo-Electron Microscopy of Vitrified Specimens. *Quarterly Reviews of Biophysics* 1988, 21, (2), 129-228.
15. Ludtke, S. J.; Baldwin, P. R.; Chiu, W., Eman: Semiautomated Software for High-Resolution Single-Particle Reconstructions. *Journal of Structural Biology* 1999, 128, (1), 82-97.

CHAPTER 3. SYNTHESIS OF A NOVEL SURFACTANT

3.1 Introduction

The first goal of this project is to synthesize a novel, stimuli-responsive surfactant containing a quinone moiety as the redox-active trigger. The reduction of quinone compounds can be easily achieved through multiple methods,¹⁻⁴ and the reaction process can be monitored by kinetic studies.⁵⁻¹⁰ Thus, the redox sensitivity of this new surfactant structure can be characterized.

The first chapter introduced the redox mechanism of tri-methyl lock quinone structures, which readily to conduct cyclization reaction due to the unique high strain energy of the tri-methyl lock structure.^{6, 8, 11, 12} Many researchers have already successfully developed and studied redox-responsive structures based on the tri-methyl lock mechanism; however, most of these systems were designed for pro-drug applications.¹³⁻¹⁵

In this study, the tri-methyl lock quinone structure will be used to build the redox-responsive property into the novel surfactant molecule, while a hydrocarbon chain containing the suitable hydrophobic and hydrophilic parts will be incorporated to promote aggregation.¹⁶ Thus, the quinone will serve as both the redox-sensitive group and as a part of the hydrophobic moiety. The 6-aminohexanoic acid chain will be attached through a carbonyl group and will serve as the hydrophilic head group. This desired novel surfactant will henceforth be referred to as Q9 (Figure 3.1).

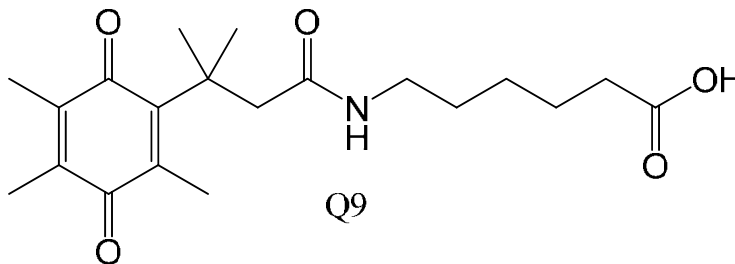


Figure 3.1 Structure of Q9.

The Q9 structure is amphiphilic and should aggregate in aqueous solution. The quinone moiety serves as the redox, stimuli-responsive group in this structure. In the presence of a reducing agent, Q9 is reduced to the corresponding hydroquinone, initiating the tri-methyl lock mechanism to facilitate the intramolecular cyclization/elimination event that breaks the backbone of Q9 and liberates a lactone and 6-aminohexanoic acid (Figure 3.2). Therefore, the disruption and unraveling of these aggregates can be controlled and adjusted through modification of structural elements.

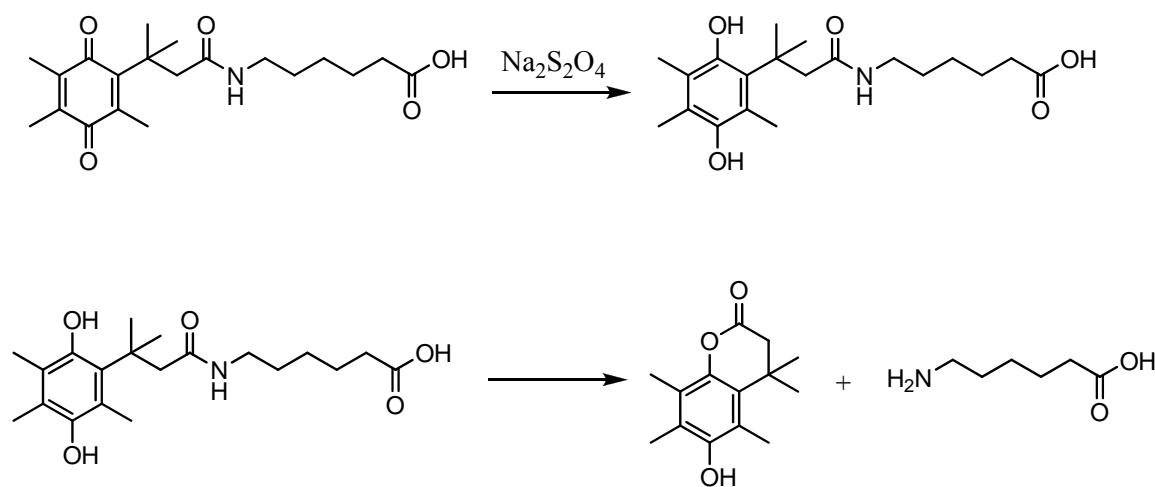
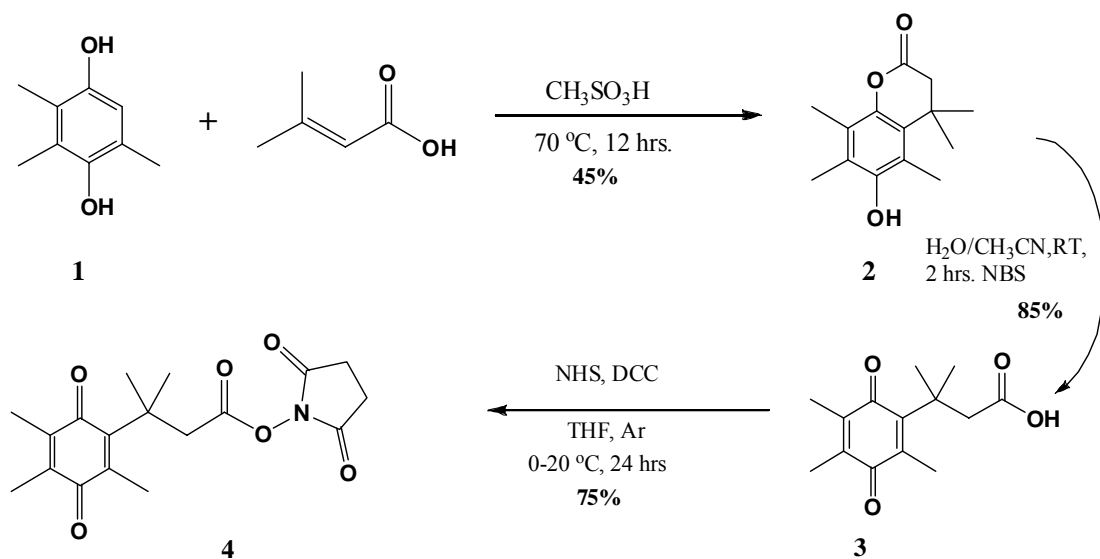


Figure 3.2 Q9 reduction and intramolecular cyclization/elimination event.

3.2 Synthesis Discussion

The first part of this synthesis was to develop the tri-methyl lock quinone moiety, which was based on similar routes as those developed by Cohen and his coworkers.⁶⁻¹¹ Lactone **2** was achieved via a 1,4-Michael addition of 3,3-dimethylacrylic acid to the trimethyl hydroquinone **1**. Hydrolysis and subsequent NBS (*N*-bromosuccinimide) oxidation of lactone **2** lead to the formation of quinone **3**. *N*-hydroxysuccinimide (NHS) was coupled to the carboxylic acid of **3** to form the NHS-substituted quinone **4** in order to later facilitate the linking of the aminohexanoic acid chain onto the quinone molecule (Scheme 3.1).



Scheme 3.1 Synthetic scheme for the NHS-substituted quinone.

The second part of this synthesis was to synthesize the chain structures, because even though several aminocarboxylic acid molecules with varying sized carbon chains are commercially available, they cannot be used due to their low solubility in organic solvent. The following synthetic steps were conducted to develop a *tert*-butyl protected 6-aminohexanoic acid chain structure **7** to be added to the quinone moiety.¹⁷

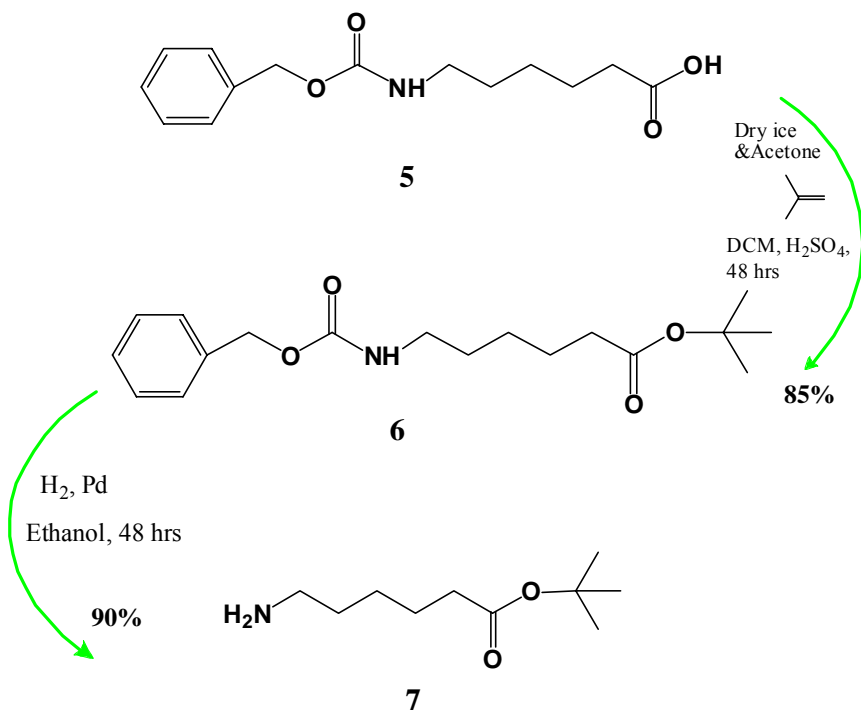
The carboxylic acid group of the starting material CBZ- (carbobenzyloxy) protected 6-aminohexanoic acid **5** was protected with a *tert*-butyl group to yield product **6**. The CBZ moiety was subsequently removed using hydrogen gas and a palladium catalyst to obtain product **7** (Scheme 3.2). This synthetic work was adopted from Lee and coworkers.¹⁷

Because NHS is a good leaving group, the chain structure **7** was easily attached to the synthesized quinone structure **4** to yield product **8**. Finally, the *tert*-butyl protecting group was removed from **8** using formic acid to achieve the final product **9** (Scheme 3.3).

Products in these synthesis steps were characterized by ¹H NMR, GC-MS and ESI-MS. The purity of products were determined by ¹H NMR experiments. Each peak in the ¹H NMR spectra was integrated (solvent peak and TMS peak were not included), and the peaks from the

product were identified by their chemical shift position. Proton peaks not associated with the product were also integrated & totaled to account for impurities. The minimum purity of the product was calculated by the following formula:

Compound minimum purity = $(1 - \text{Total integrated non-product peak area} / \text{Total integrated product peaks area}) \times 100\%$ (See Appendix for each calculation).



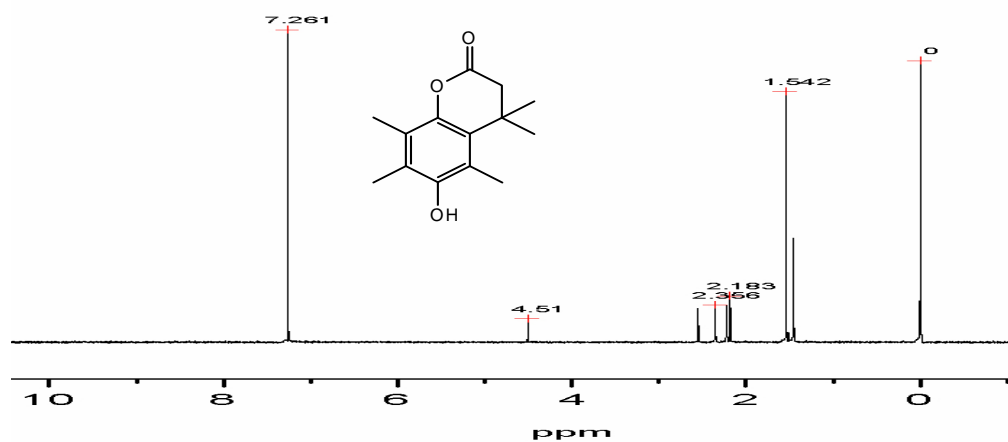
Scheme 3.2 Synthetic route for the *t*-butyl protected 6-aminohexanoic acid (7).

3.2.1 Synthesis of Lactone Product 2

A round bottom flask (RBF) equipped with a stir bar and septum was used for this reaction. Methanesulfonic acid (10 mL) was put into the RBF and heated to 70 °C in a mineral oil bath. Then, 6.6 mmol of the trimethylhydroquinone was added into the RBF, followed by 7.5 mmol of the 3,3-dimethylacrylic acid. After stirring for 2 hours at 70 °C, distilled water (125 mL) was added and the dilute solution was then extracted three times with 50 mL of ethylacetate. The extracts were washed with distilled water, saturated NaHCO₃, and NaCl solution, then dried by MgSO₄. The solvent was removed by rotary evaporation. The product was dissolved into a

CHCl₃:hexane (30:70) solvent for recrystallization, and the solvent was finally removed under a high vacuum. The overall process yielded 45% of the white powder lactone 2. The ¹H NMR spectrum was identical to that reported in literature ⁷ and was 99.1% pure based on the NMR integrated peak intensity calculation (Appendix 1.1). GC-MS showed one dominant peak with a molecule weight of 234 g/mol (Figure 3.3), which corresponds to the lactone product.

¹H NMR (300 MHz, CDCl₃) δ ppm: 7.261 (s, 2H), 2.36 (s, 3H), 2.22(s, 3H), 2.18(s, 3H), 1.54(s, 3H), 1.45 (s, 3H)



Spectrum 3.1 ¹H NMR spectrum of product 2.

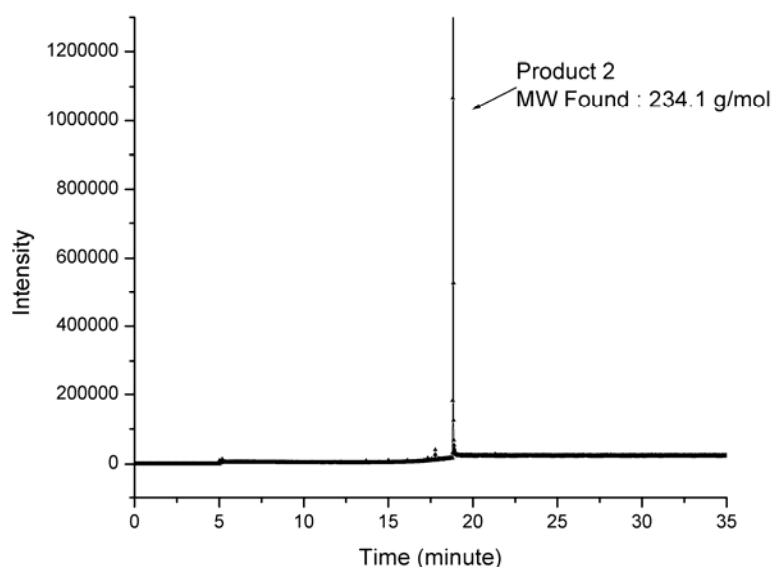
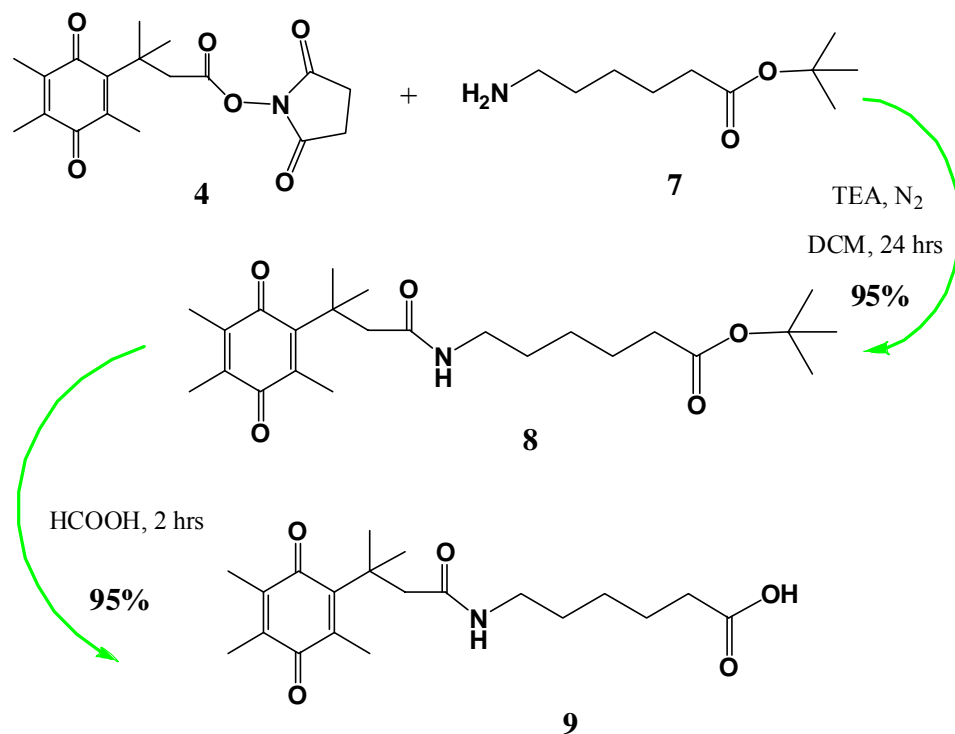


Figure 3.3 GC-MS of product 2.



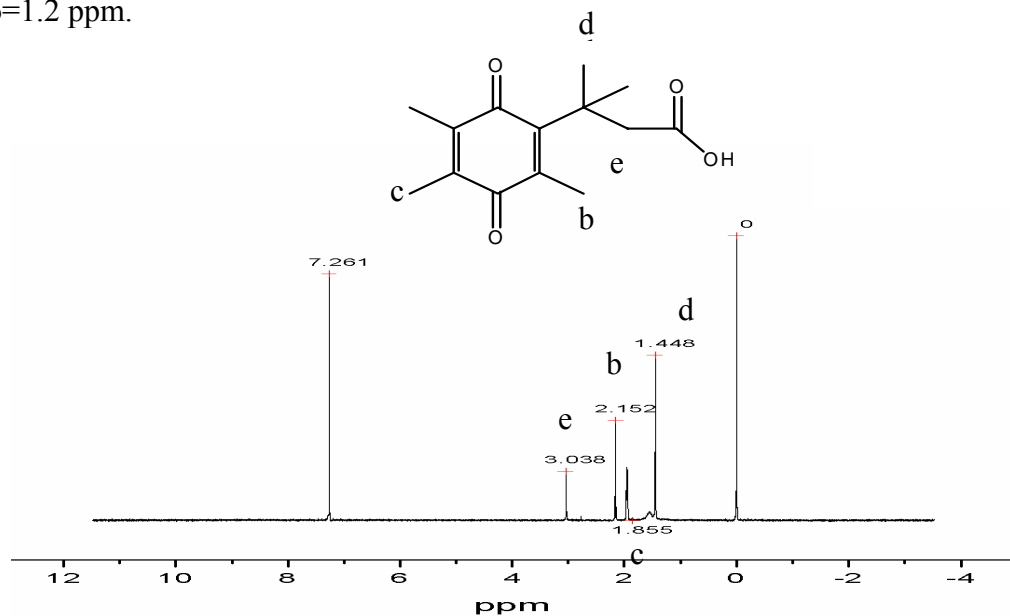
Scheme 3.3 Synthetic route for the amphiphilic molecule Q9 with the quinone stimuli-responsive group.

3.2.2 Synthesis of Quinone Acid 3

NBS was recrystallized three times from water. Lactone **2** (21 mmol) was dissolved in 247 mL of CH₃CN:H₂O (1:9) in a 1.0 L RBF. NBS (22.2 mmol) was dissolved in 49.5 mL acetonitrile and added to the RBF dropwise with constant stirring at room temperature (RT). After two hours, the contents were extracted three times with 150 mL of ether, followed by washing three times with both pure water and NaCl solution. The ether was then removed by rotary evaporation. The product was recrystallized from hexane and acetone. White cube-shaped crystals were obtained in 85% yield. The structure was confirmed by ¹H NMR which agreed with the published data.¹⁸ The purity of product **3** was calculated and found to be 98.8% (Appendix 1.2).

¹H NMR (300 MHz, CDCl₃) δ ppm: 3.03 (s, 3H), 2.15 (s, 2H), 1.95 (s, 3H), 1.93 (s, 3H), 1.44 (s, 6H)

ESI-MS m/z calculated for $C_{14}H_{17}O_4$ $[M-H]^- = 248.1127$. Found 249.1130 $[M-H]^-$ with $\delta=1.2$ ppm.



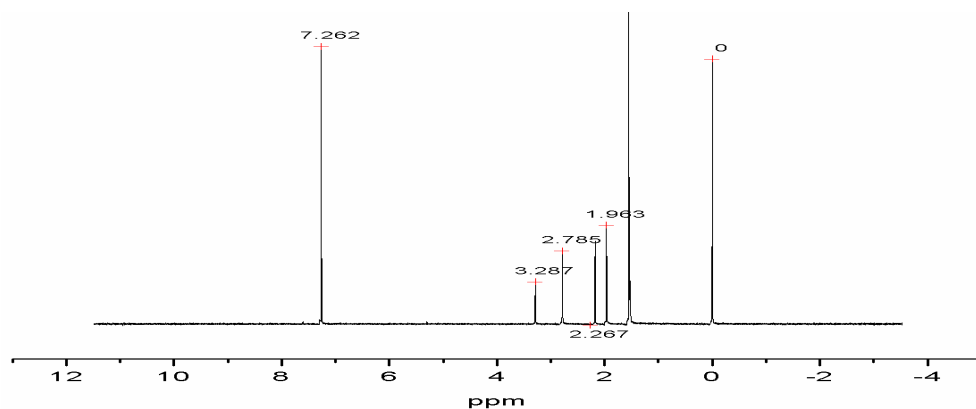
Spectrum 3.2 1H NMR spectrum of quinone acid 3.

3.2.3 Synthesis and Separation of NHS Substitute Quinone 4

Quinone acid **3** (16 mmol) and 17 mmol of *N*-hydroxysuccinimide (NHS) were added to a RBF kept at 0 °C. The mixture was stirred at 0 °C, and 125 mL of THF was added. DCC (19 mmol) was added slowly into the solution to avoid increasing the temperature, and then the RBF was removed from the ice bath and reacted at room temperature for 20 hours. The solution was filtered to remove any solid powder and dried using rotary evaporation to remove THF. DCM (100 mL) was used twice to strip off THF during this process. The product obtained was dissolved in 10 mL DCM, then passed through a silica column, which has been flushed prior with DCM to remove any air bubbles. A mixture of solvent composed of DCM, hexane, and ether acetate was used to flush the column. The product obtained was confirmed by the thin layer chromatography (TLC). The solvent was removed by rotary evaporation and kept under high vacuum overnight. The product **4** was obtained in 75% yield. The chemical shifts of the 1H

NMR spectrum matched the literature values,¹¹ and the purity of product **4** was calculated to be 95.1% (Appendix 1.3).

¹H NMR (300 MHz, CDCl₃) δ ppm: 3.28 (s, 2H), 2.79 (s, 4H), 2.17 (s, 3H), 1.96 (s, 3H), 1.53 (s, 6H)



Spectrum 3.3 ¹H NMR spectrum of the NHS substitute structure **4**.

3.2.4 Synthesis of *tert*-butyl 6-(benzyloxycarbonylamino) Hexanoate **6**

N-benzyloxycarbonyl-6-aminohexanoic acid **5** was purchased from Novabiochem and used without further purification. Ten mmol of **5** was dissolved in 30 mL DCM and introduced into a pressure-resistant bottle, which was cooled in a dry ice and acetone mixture. Isobutylene (40 mmol) was cooled into a liquid state and poured into the bottle. The contents in the bottle were stirred using a stirring bar. To this, 96% sulfuric acid (0.2 mL) was added, and the pressure-resistant bottle was sealed and placed at room temperature for 48 hours. After the reaction was stopped, a NaHCO₃ solution (150 mL) was used to neutralize the reaction and the organic phase was collected and washed with NaCl solution and distilled water three times. MgSO₄ was added to dry the organic phase, it was then filtered, and the solvent was removed under vacuum resulting in an oil-like product in 85% yield. ¹H NMR data confirmed product formation and GC-MS was used to analyze product **6**, which showed a dominant peak whose molecule weight of 321 g/mol corresponded to the product. A comparison of ¹H NMR spectra of

product **6** and reactant **5** showed a *tert*-butyl group attached to the carboxylic acid side (Spectrum 3.4). The purity of product **6** was calculated and found to be 98.6% (Appendix 1.4).

¹H NMR (300 MHz, CDCl₃) δ ppm: 7.40 (m, 5H), 5.13(s, 2H), 3.25 (m, 2H), 2.39 (m, 2H), 1.69 (m, 2H), 1.59 (m, 2H), 1.43 (m, 2H)

3.2.5 Synthesis of *t*-butyl Protected 6-aminohexanoic Acid **7**

Tert-butyl 6-(benzyloxycarbonylamino) hexanoate **6** (6.8 mmol) was dissolved in 10 mL of ethanol, and 10% palladium on carbon catalyst was added to the solution. The solution was stirred under hydrogen atmosphere for 48 hours at ambient pressure. The catalyst was removed by filtration. Ethanol was removed by rotary evaporation and ethyl acetate (10 mL) was added three times to completely remove the solvent. Finally, the product was put under high vacuum overnight to obtain an oily product in 90% yield. GC-MS analysis was used for the characterization of **7**. The molecular weight of compound **7** is 187 g/mol. GC-MS data showed one major peak with an integrated ratio > 90% of this molecular weight. ¹H NMR data also confirmed formation of **7**. The reactant **6** and product **7** ¹H NMR spectra were compared in Spectrum 3.5, which clearly shows that the CBZ group has been removed after H₂/Pd treatment. The product **7** was determined to be 98.3% pure (Appendix 1.5).

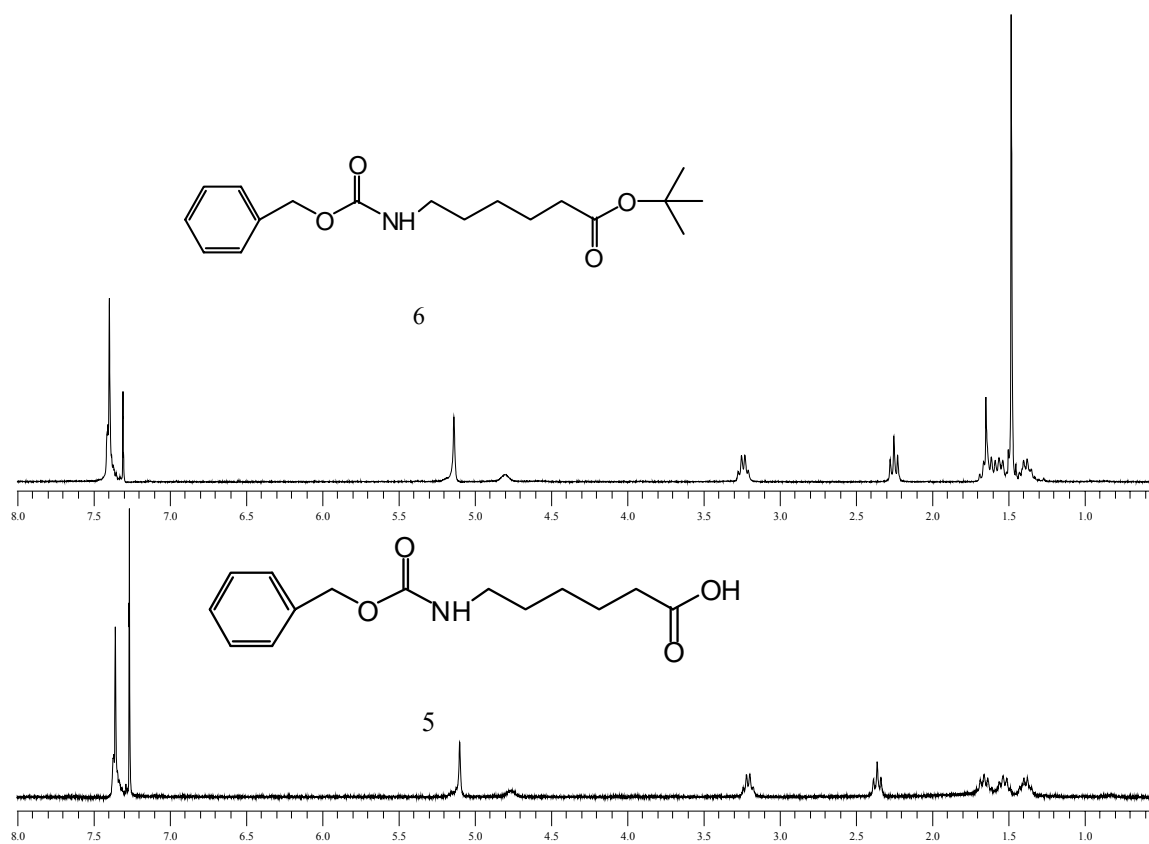
¹H NMR (300 MHz, CDCl₃) δ ppm: 1.36 (m, 2H), 1.44 (s, 9H), 1.4-1.5 (m, 2H), 1.60 (m, 2H), 1.65 (s, 2H), 2.21 (t, 2H), 2.67 (t, 2H)

3.2.6 Synthesis of Molecule **8**

NHS-substituted quinone **4** (1.4 mmol) was dissolved in 20 mL of DCM in a RBF, 1.4 mmol *t*-butyl protected 6-aminohexanoic acid **7** was then added to the above solution with stirring. TEA (1.5 equivalents) was injected into the RBF while purging with nitrogen. The reaction was stirred for 24 hours at room temperature, after which, the solution was washed three times using saturated NaHCO₃ aqueous solution, and followed by nano-pure water two times.

The organic phase was collected and dried using MgSO₄. After filtering, DCM was removed by rotary evaporation. The light yellow cube-like crystals were obtained, and a chromatography column was used to purify the product. Yellow plate-shaped crystals were obtained in 95% yield, and ¹H NMR confirmed the structure. The purity of product **8** was found to be 99.5% (Appendix 1.6). It was shown in Spectrum 3.6 the overlay of **3** and **7** will be similar to **8**.

¹H NMR (300 MHz, CDCl₃) δ ppm: 5.50 (s, 1H), 3.18 (m, 2H), 2.82 (s, 2H), 2.25 (m, 2H), 2.16 (s, 3H), 1.99 (m, 3H), 1.60 (s, 9H), 1.57 (s, 6H), 1.48 (m, 2H), 1.32 (m, 2H)



Spectrum 3.4 Comparison of ¹H NMR spectra of reactant 5 and product 6.

3.2.7 Removal of the Protecting Group in Compound 8 to Achieve the Final Product 9

Compound **8** (50 mg) was dissolved in 20 mL of formic acid in a RBF and the bottle was sealed and magnetically stirred for 2 hours. Upon completion of the reaction, formic acid was

removed by rotary evaporation. Ethyl acetate (10 mL) was used three times to remove the formic acid completely.

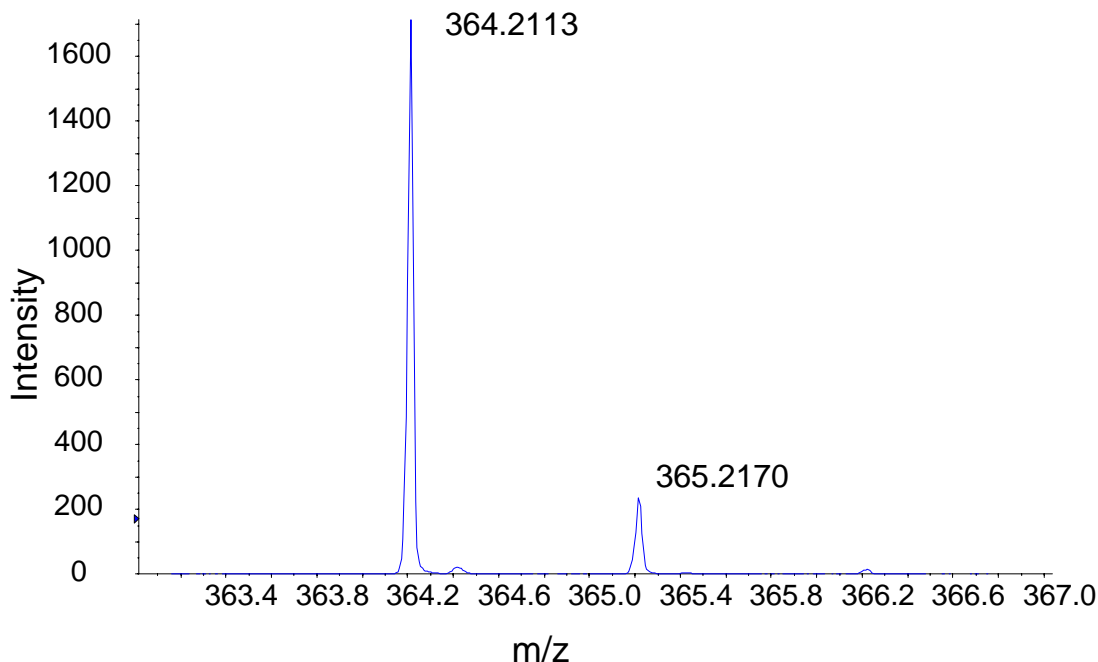
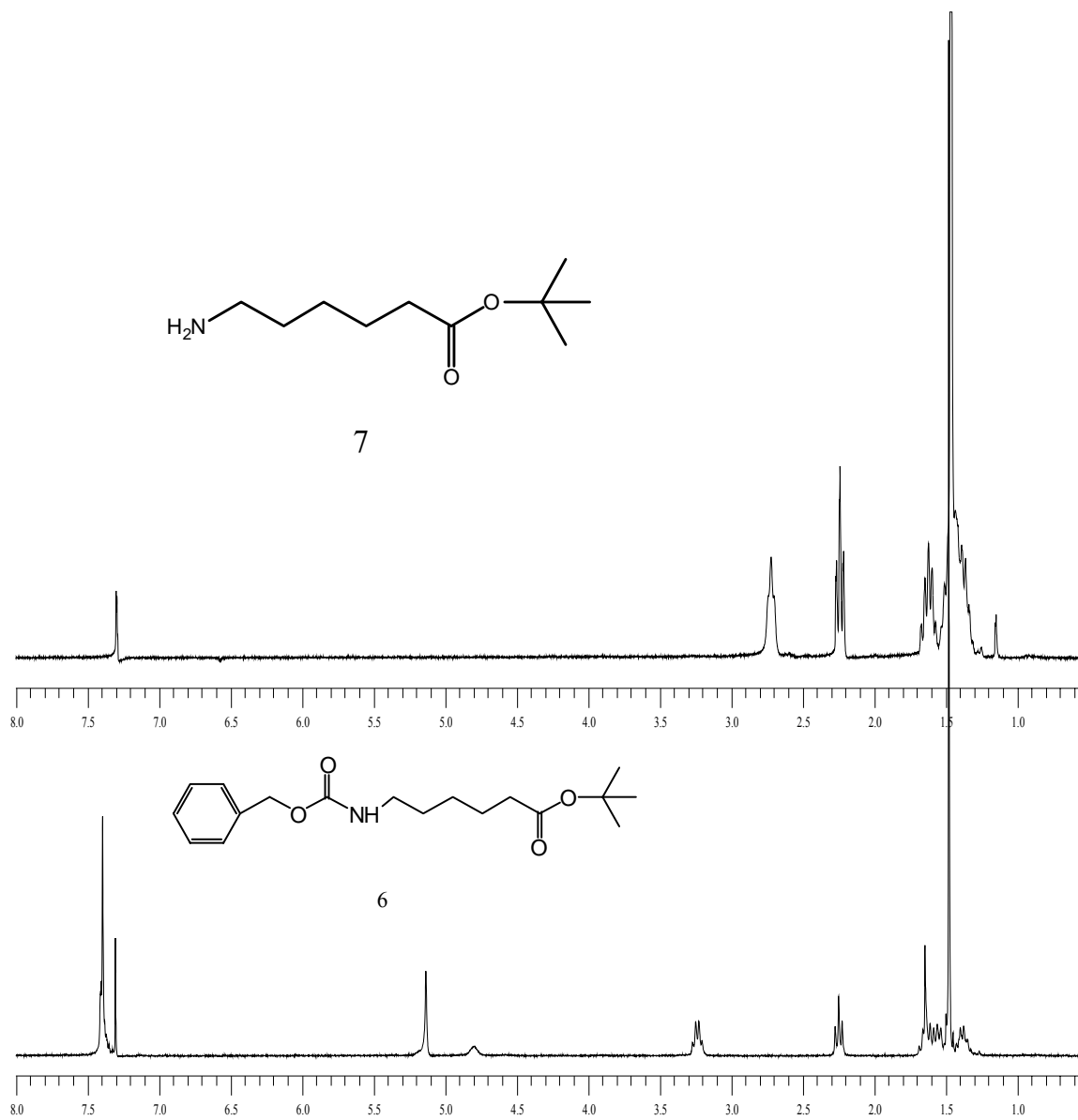


Figure 3.4 High resolution ESI-MS of product 9.

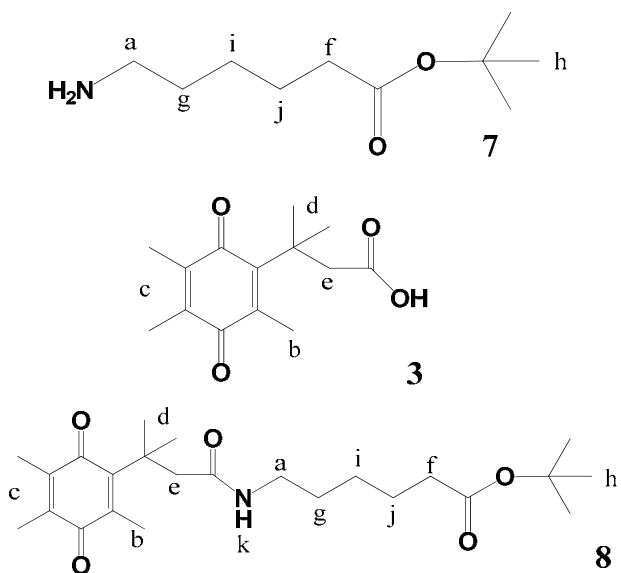
^1H NMR confirmed the formation of compound **9** (Spectrum 3.8). By comparing the ^1H NMR spectrum of the target compound **9** with that of the starting material **8**, it clearly showed that the *t*-butyl group had been removed. The 95% yield was achieved for this reaction. The purity of product **9** was calculated to be 98.9% (Appendix 1.7).

^1H NMR (300 MHz, CDCl_3) δ ppm: 5.50 (s, 1H), 3.18 (m, 2H), 2.82 (s, 2H), 2.25 (m, 2H), 2.16 (s, 3H), 1.99 (m, 3H), 1.57 (s, 6H), 1.48 (m, 2H), 1.32 (m, 2H)

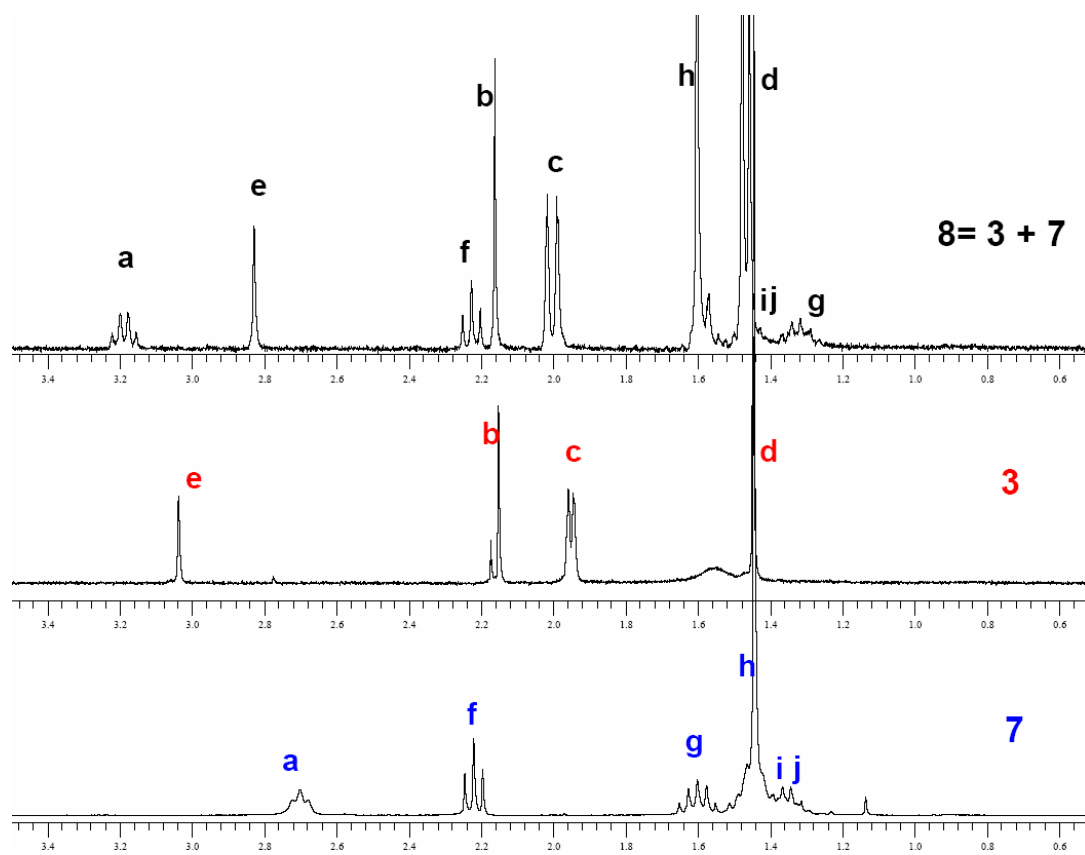
ESI-MS (Figure 3.4): m/z found for **9** is 364.2113, with $\delta=-1.5096$ ppm.



Spectrum 3.5 Comparison of ¹H NMR spectra of *tert*-butyl group protected 6-aminohexanoic acid (7) and (6).

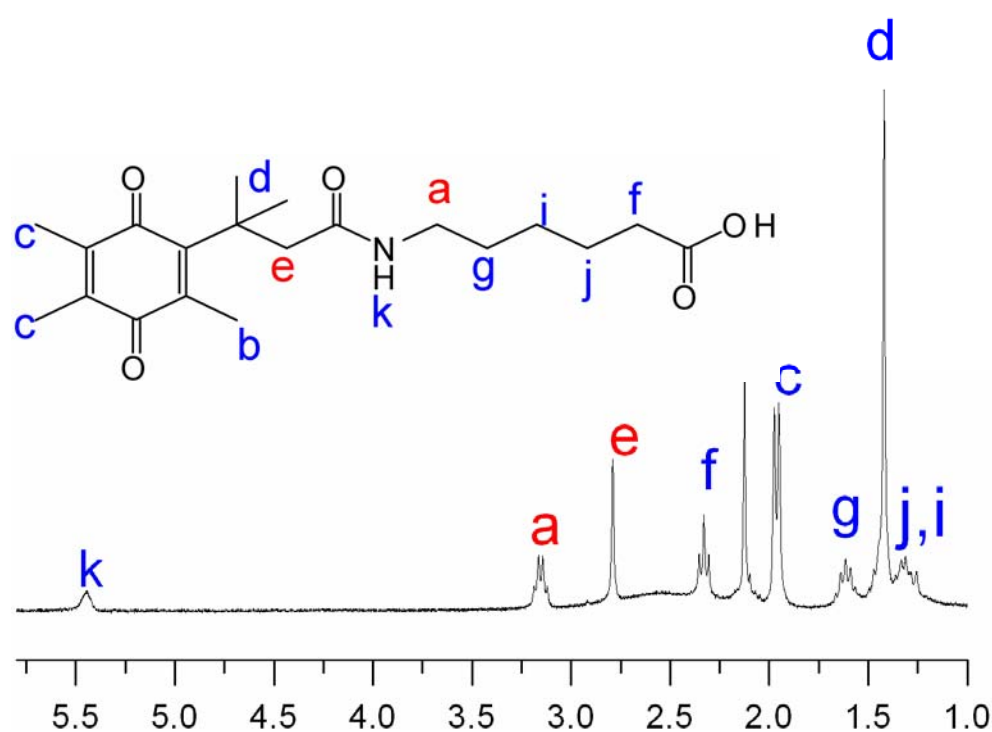


(a)



(b)

Spectrum 3.6 (a) Proton-labeled molecule 7, 3 and 8 (b) Comparison of ^1H NMR spectra of product 8, 3 and 7.



Spectrum 3.7 Labeled ¹H NMR of final product 9.

3.3 References

1. Lenaz, G.; Genova, M. L., Encyclopedia of Biological Chemistry. Elsevier: 2004; p 621-627.
2. Beyer, R. E.; SeguraAguilar, J.; DiBernardo, S.; Cavazzoni, M.; Fato, R.; Fiorentini, D.; Galli, M. C.; Setti, M.; Landi, L.; Lenaz, G., The Role of Dt-Diaphorase in the Maintenance of the Reduced Antioxidant Form of Coenzyme Q in Membrane Systems. Proceedings of the National Academy of Sciences of the United States of America 1996, 93, (6), 2528-2532.
3. Crane, F. L.; Hatefi, Y.; Lester, R. L.; Widmer, C., Isolation of a Quinone from Beef Heart Mitochondria. Biochimica Et Biophysica Acta 1957, 25, (1), 220-221.
4. Mitchell, P., Protonmotive Redox Mechanism of Cytochrome-B-C1 Complex in Respiratory-Chain - Protonmotive Ubiquinone Cycle. Febs Letters 1975, 56, (1), 1-6.
5. Wang, B. H.; Liu, S. M.; Borchardt, R. T., Development of a Novel Redox-Sensitive Protecting Group for Amines Which Utilizes a Facilitated Lactonization Reaction. Journal of Organic Chemistry 1995, 60, (3), 539-543.
6. Borchard, R. T.; Cohen, L. A., Stereopopulation Control .2. Rate Enhancement of Intramolecular Nucleophilic Displacement. Journal of the American Chemical Society 1972, 94, (26), 9166-9174.

7. Borchard, R. T.; Cohen, L. A., Stereopopulation Control .5. Conformational Selection of Alternative Oxidation Pathways. *Journal of the American Chemical Society* 1973, 95, (25), 8319-8326.
8. Borchard, R. T.; Cohen, L. A., Stereopopulation Control .3. Facilitation of Intramolecular Conjugate Addition of Carboxyl Group. *Journal of the American Chemical Society* 1972, 94, (26), 9175-9182.
9. Borchard, R. T.; Cohen, L. A., Stereopopulation Control .4. Facilitation of Intramolecular Conjugate Addition of Hydroxyl Group. *Journal of the American Chemical Society* 1973, 95, (25), 8308-8313.
10. Borchard, R. T.; Cohen, L. A., Stereopopulation Control .5. Facilitation of Intramolecular Conjugate Addition of an Aldehyde Hydrate and Hemiacetal. *Journal of the American Chemical Society* 1973, 95, (25), 8313-8319.
11. Carpino, L. A.; Triolo, S. A.; Berglund, R. A., Reductive Lactonization of Strategically Methylated Quinone Propionic-Acid Esters and Amides. *Journal of Organic Chemistry* 1989, 54, (14), 3303-3310.
12. Milstien, S.; Cohen, L. A., Stereopopulation Control .1. Rate Enhancement in Lactonizations of Ortho-Hydroxyhydrocinnamic Acids. *Journal of the American Chemical Society* 1972, 94, (26), 9158-9165.
13. Amsberry, K. L.; Borchardt, R. T., Amine Prodrugs Which Utilize Hydroxy Amide Lactonization .1. A Potential Redox-Sensitive Amide Prodrug. *Pharmaceutical Research* 1991, 8, (3), 323-330.
14. Amsberry, K. L.; Gerstenberger, A. E.; Borchardt, R. T., Amine Prodrugs Which Utilize Hydroxy Amide Lactonization .2. A Potential Esterase-Sensitive Amide Prodrug. *Pharmaceutical Research* 1991, 8, (4), 455-461.
15. Naylor, M. A.; Thomson, P., Recent Advances in Bioreductive Drug Targeting. *Mini-Reviews in Medicinal Chemistry* 2001, 1, (1), 17-29.
16. Hiemenz, P. C.; Rajagopalan, R., *Principles of Colloid and Surface Chemistry*. 3rd ed.; Marcel Dekker, Inc.: New York, 1997; p 371.
17. Lee, J. K.; Ahn, K. C.; Stoutamire, D. W.; Gee, S. J.; Hammock, B. D., Development of an Enzyme-Linked Immunosorbent Assay for the Detection of the Organophosphorus Insecticide Acephate. *Journal of Agricultural and Food Chemistry* 2003, 51, (13), 3695-3703.
18. Borchard, R. T.; Cohen, L. A., Stereopopulation Control .5. Conformational Selection of Alternative Oxidation Pathways. *Journal of the American Chemical Society* 1973, 95, (25), 8319-8326.

CHAPTER 4. PROPERTIES OF THE NOVEL SURFACTANT Q9

4.1 The pH Sensitivity of Q9 Molecule

Previous studies have confirmed that the formation of fatty acid surfactant vesicles is pH sensitive.¹⁻³ An intermediate pH range was found to be suitable for the development of these types of vesicles, which usually ranged from 7.0 to 9.0. Because of the similarity in the molecular structure of the Q9 surfactant and fatty acids, this pH range was expected to apply for successful Q9 vesicle formation. However, it is important to note that quinones have been shown to be affected by extreme pH values, particularly at high pH ($\text{pH} > 10$).⁴⁻⁶ Thus, it was necessary to explore the stability of Q9 at various pH values.

For the purpose of studying stability, Q9 solutions were prepared in phosphate buffered saline solutions (PBS, 0.1 M) with a pH value that ranged from 7 to 11. The solution color changed from yellow to red when the pH was raised above 10.5, which indicated that the Q9 molecule underwent some changes in the strong base environment. Q9 was stable at pH values between 7.0 and 9.0 for long periods of time (on the order of a week), as noted by the persistent yellow color.

The Q9 samples prepared in vary basic ($\text{pH} = 11$ and 14) and the intermediate pH values were analyzed by UV-vis spectroscopy. The experimental results are displayed in Figure 4.1. There are significant differences in the UV-vis absorbance signals of the samples. The Q9 samples prepared at pH 7.0 and at pH 10.2 in PBS possess one major peak around 267 nm, which is typical of quinone molecule in aqueous solution. However, the Q9 sample prepared in pH 11 PBS has a measurable difference, with a new “broad” peak around 470 nm. This absorbance peak can also be found when strongly basic conditions (pH 14) were used, confirming that high pH values result in appearance of this peak. These differences indicate that some structures changes occur when Q9 was dissolved in a strong base solution. The detail of

the Q9 structural change under the different pH environment is not related to this study, but it is assumed that the quinone moiety is decomposed similarly to other quinones. However, the UV-vis studies showed that the Q9 structure is unaffected under weakly basic environments ($7 < \text{pH} < 10$) for periods of up to seven days.

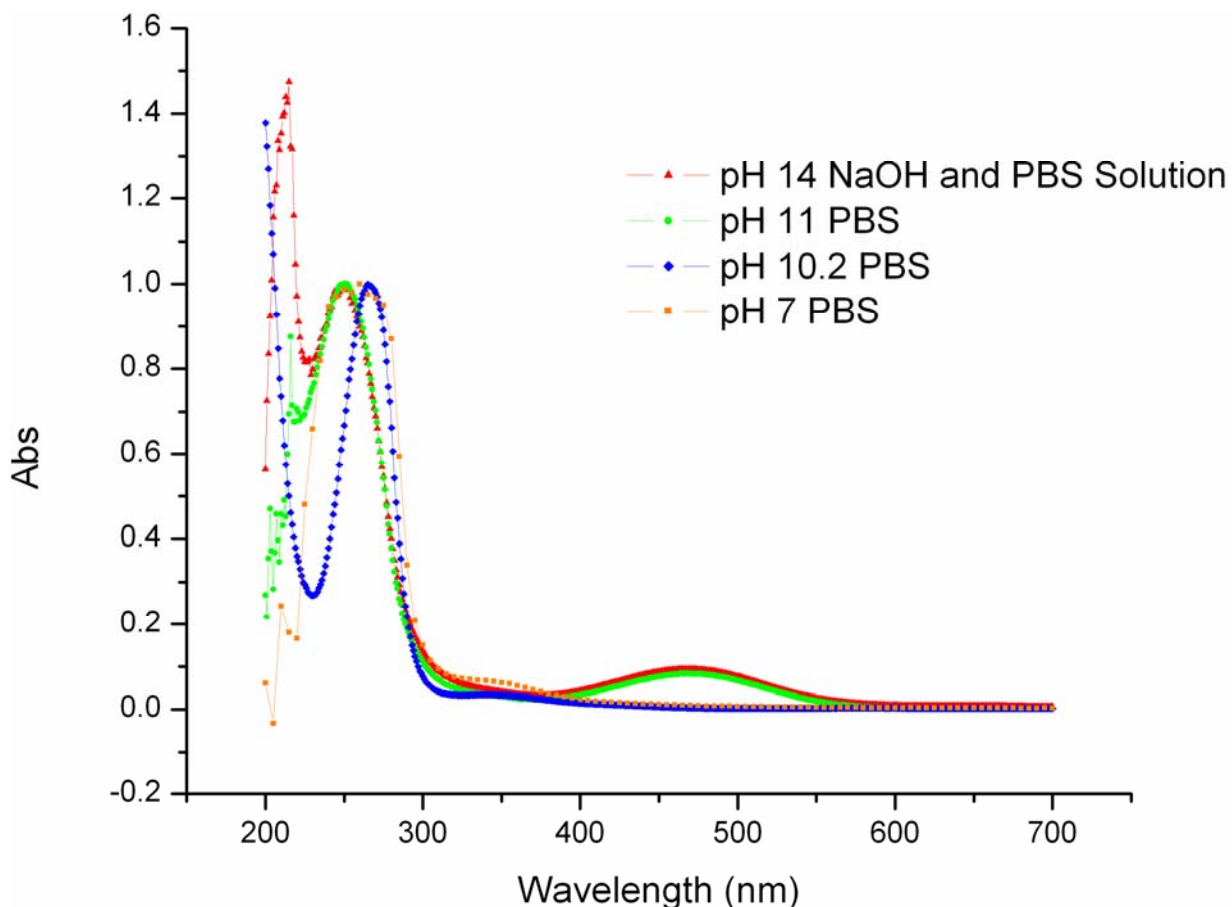
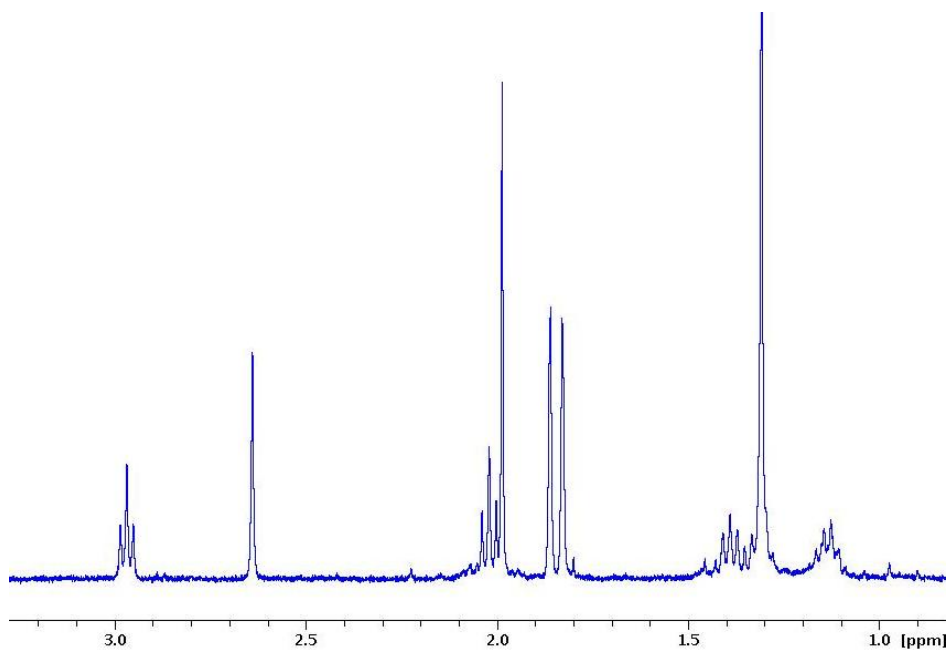
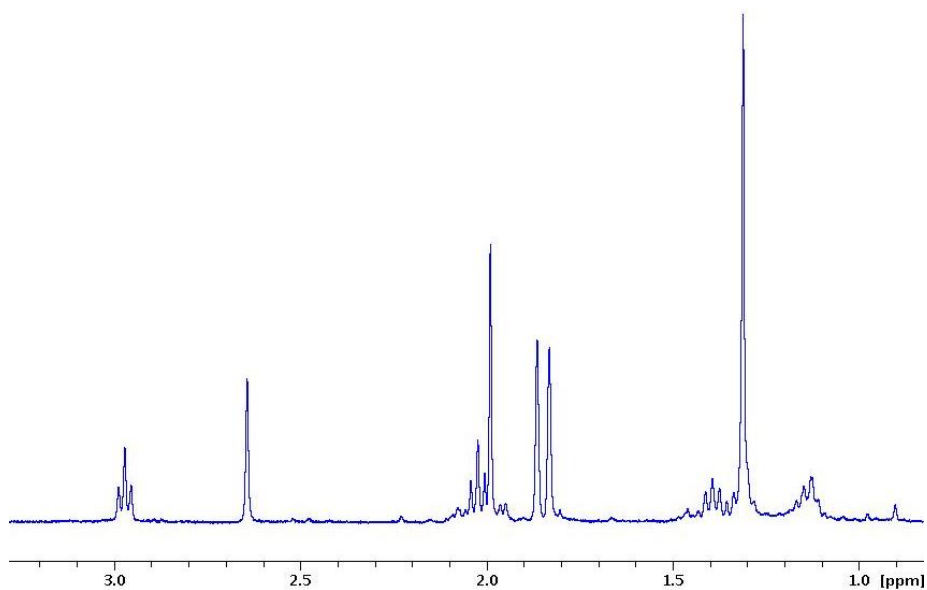


Figure 4.1 UV-vis spectra of Q9 samples prepared in 0.1M pH 7.0 PBS, 0.1M pH 10.2 PBS, 0.1 M pH 11 PBS, 0.1 M pH 14 NaOH and PBS solution.

^1H NMR experiments were conducted on Q9 samples which were prepared at different pH values. It was discovered that the Q9 samples prepared in the pH range of 7.0 to 9.0 retained their characteristic spectra features, as noted by comparing the NMR spectra of Q9 in CDCl_3 with those in Figure 4.2. The stability of Q9 at $\text{pH} \leq 10.5$ was found up to 72 hours after sample preparation.



(a)



(b)

Figure 4.2 ^1H NMR spectra (300 MHz) of 8 mM Q9 in pD 8.0 D_2O (NaD_2PO_4) immediately (a) and 72 hours (b) after sample preparations.

Because of the observed stability of the Q9 structure between $7.0 \leq \text{pH} \leq 10.5$ and the known ability of n-alkanoic acids to form vesicles under such solution conditions, pH 7.8 PBS

was selected as the solution in which Q9 properties were to be examined unless otherwise stated. It was assumed that at pH 7.8 solution conditions would lead to roughly equal amounts of deprotonated and protonated carboxylic acid groups in Q9.^{1,3}

4.2 Redox Stimuli-responsive Property of Q9

The purpose of this project was to use a novel surfactant Q9, which was possible be controlled by redox stimulation, to develop new redox stimuli-responsive vesicles. In previous synthetic steps, Q9 was synthesized successfully with the designed structure (Chapter 3). In the following studies, the potential redox stimuli-responsive mechanism and the surfactant aggregation properties of Q9 will be examined.

4.2.1 Confirmation of the Cleavage of Q9 Structure Upon Redox Stimulation

Q9 possesses a tri-methyl lock quinone moiety, which should be easily reduced by a chemical reducing agent.^{7,8} The reduction product, a hydroquinone, has the potential to undergo a spontaneously intramolecular cyclization/elimination reaction. This lactonization reaction should result in the cleavage elimination of the amino-carboxylic acid backbone of Q9, as well as the loss of its amphiphilic property for aggregation. This is outlined in Figure 4.3.

Sodium dithionite, $\text{Na}_2\text{S}_2\text{O}_4$, has been used as an efficient reducing agent in many redox reaction studies in aqueous environment, including tri-methyl lock molecules similar in structure to Q9.^{9,10} Thus, I have chosen it as the reducing agent to trigger the reduction reaction and drive the cyclization/elimination lactonization of the Q9 molecule.

^1H NMR analysis was used to probe solutions of Q9 exposed to $\text{S}_2\text{O}_4^{2-}$. Upon $\text{S}_2\text{O}_4^{2-}$ addition, the quinone of Q9 should be converted to the hydroquinone to allow for the cyclization/elimination process. Two fragment products should be generated: one being the hydroquinone lactone product, and the other being 6-aminohexanoic acid from the Q9 chain. The lactone is known to be insoluble in water and will form a precipitate. It was found that

proton signal of the lactone was not detected by ^1H NMR upon completion of the reaction, consistent with its insolubility (Figure 4.5). However, the 6-aminohexanoic acid remained soluble, and it was stable in the aqueous phase as noted by the proton signals of 6-aminohexanoic acid after the reduction reaction. Compared to the stable ^1H NMR signal of the 6-aminohexanoic acid chain, the decreasing ^1H NMR signal of the quinone moiety can be used as an index to monitor the cleavage process of the Q9 molecule.

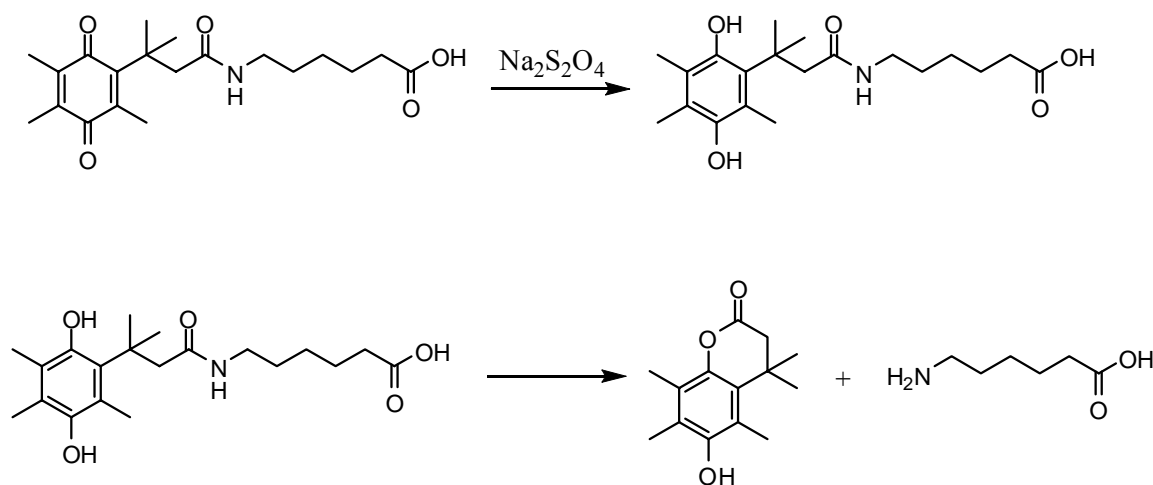


Figure 4.3 Proposed cleavage of Q9 structure triggered by reducing agent.

Two protons, denoted as **e** and **a** (Figure 4.4), were chosen for monitoring the progress of the Q9 destruction process. Proton **e** belongs to the quinone moiety, and due to the insoluble lactone structure, its intensity should decrease with time as is observed in Figure 4.5. Proton **a** belongs to the chain structure and is presented in both the 6-aminohexanoic acid molecule product after the Q9 cleavage and in the original Q9 molecule. The intensity of the ^1H NMR signal of **a** will remain unchanged during the reaction process.

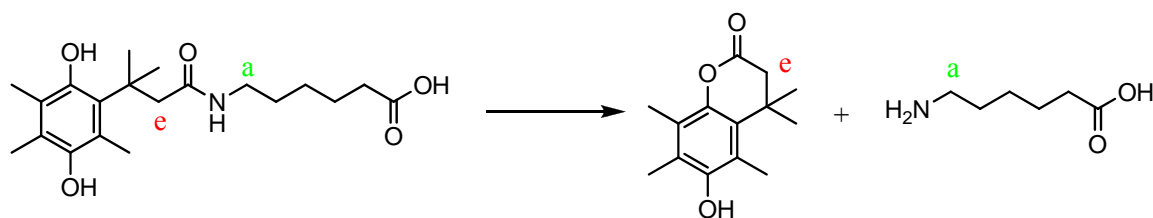


Figure 4.4 Location of proton e and a in the reactant and products.

^1H NMR experiments were set up to observe the intramolecular cyclization/elimination process. Q9 (2 mM) was dissolved at pD 7.8 D_2O and placed in the NMR tube. Five equivalents of $\text{Na}_2\text{S}_2\text{O}_4$ were added to this tube to trigger the reduction reaction and the corresponding lactonization reaction. The first ^1H NMR acquisition was run 3 minutes after addition of $\text{Na}_2\text{S}_2\text{O}_4$. The second one was run 300 minutes later. Experiment results are shown in Figure 4.5.

Signal **a** maintained the same peak intensity after the $\text{Na}_2\text{S}_2\text{O}_4$ addition for the entire time of the experiment (300 mins). Proton signal **e** was observed 3 mins after addition of $\text{Na}_2\text{S}_2\text{O}_4$, but peak **e** is virtually undetectable after 300 minutes. Three minutes later after the addition of $\text{Na}_2\text{S}_2\text{O}_4$, the reduction reaction occurred and the hydroquinone formed from this reduction. At that moment, the intramolecular cyclization/elimination lactonization reaction had not reached completion, and the hydroquinone was still dissolved in solution, proven by the observation of peak **e** in Figure 4.5. During the 300 minute experiment, which was counted from the addition of sodium dithionite, the intramolecular cyclization/elimination lactonization reaction went to completion. The lactone product precipitated from the solution, resulting in the proton **e** signal disappearance from the spectra. These results confirm that the desired Q9 redox response can be achieved in aqueous media with $\text{Na}_2\text{S}_2\text{O}_4$.

There is one thing that needs to be pointed out: not only do proton **e** and **a** experienced these changes, but the intensities of all proton signals from the quinone moiety decreased to almost zero after 300 mins, while all proton signals from the aminohexanoic acid moiety in Q9 remained stable during this time period.

4.2.2 Kinetic Study of Lactonization Reaction

The redox-responsive mechanism was confirmed by using ^1H NMR to monitor the selected proton signals. Using the same strategy, the kinetic process of the lactonization reaction was studied by ^1H NMR experiments.

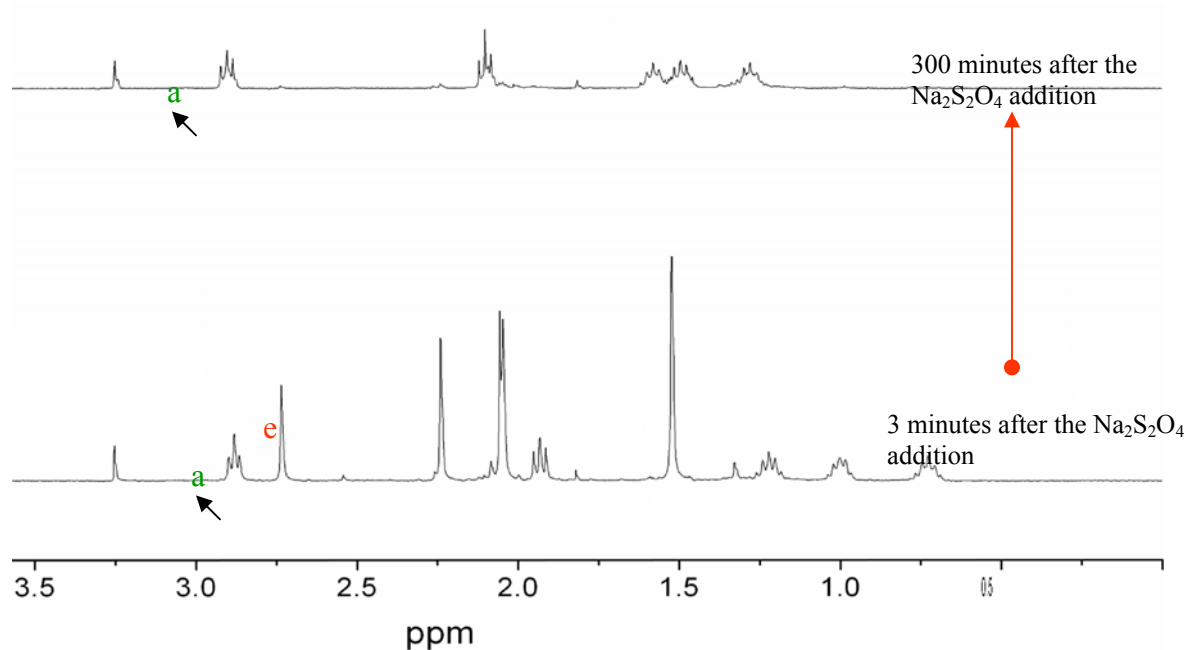


Figure 4.5 ^1H NMR spectra after $\text{Na}_2\text{S}_2\text{O}_4$ addition at 3 and 300 mins.

The intensity changes of proton signals **e** and **a** were selected again as the index for the lactonization reaction (Figure 4.6). As shown in section 4.2.1, when Q9 is reduced to the corresponding hydroquinone structure, the tri-methyl lock mechanism causes the lactonization reaction. The lactone product precipitates from solution, resulting in the decrease of proton **e** intensity, which can be used to determine the rate of the lactonization reaction.

In order to study the kinetic process of the lactonization reaction, twenty three individual ^1H NMR experiments were acquired over a 300 mins time period after the addition of the reducing agent ($\text{Na}_2\text{S}_2\text{O}_4$). Each experiment was undertaken with a time gap scaled from 21 to 32 mins. After the experiments, each of the 23 spectra was integrated to calculate the relative area of peak **e** and **a** (Table 4.1). The relative area of peak **a** (from aminohexanoic acid chain structure) was used as the standard to normalize the corresponding relative area of peak **e** in each spectrum because its intensity is stable. The natural log of the relative area ratio, $\text{I}_{\text{e}(t)}/\text{I}_{\text{e}(t=0)}$, was plotted versus time. The results are shown in Figure 4.7.

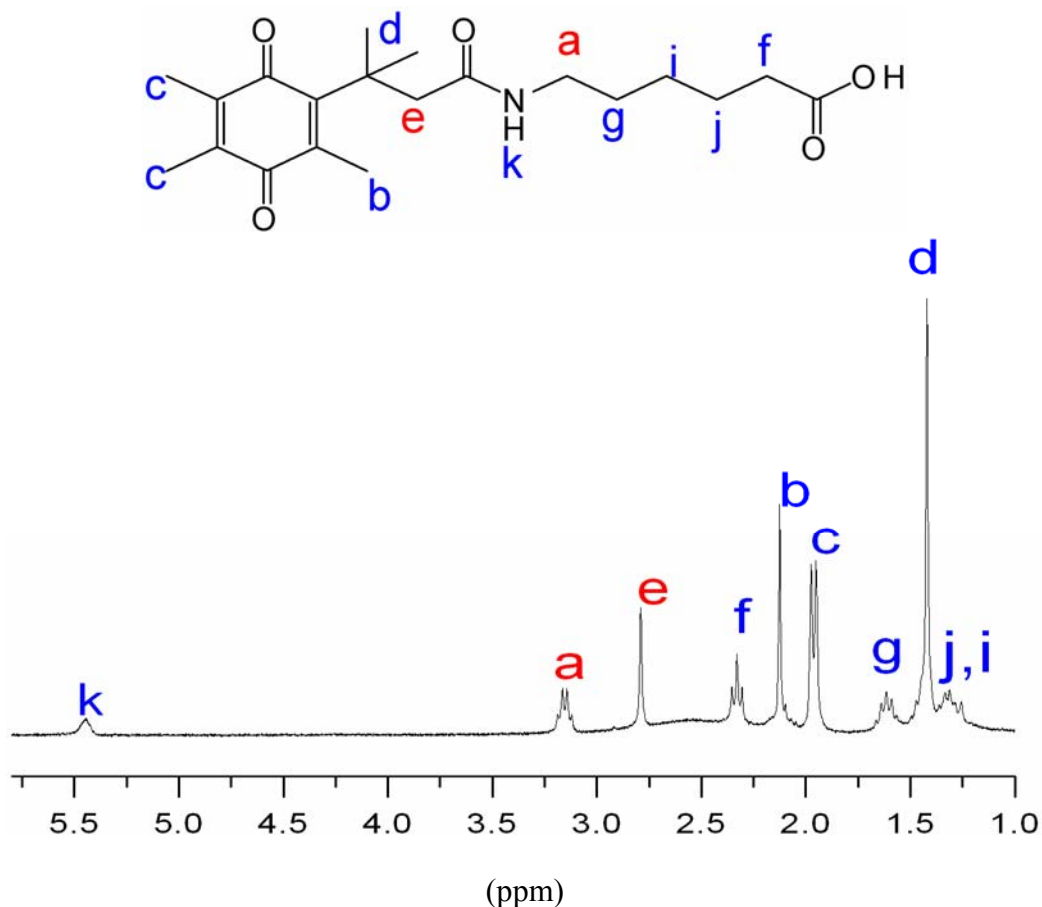


Figure 4.6 Spectrum of Q9 and ^1H NMR assignments.

A linear relationship (correlation coefficient $r=0.997$) was observed between $\ln(I_{e(t)}/I_{(t=0)})$ and the experimental time. This linear relationship can be explained by the mathematical equation:

$$\ln\left(\frac{M_e}{M_0}\right) \sim \ln\left(\frac{I_{e(t)}}{I_{(t=0)}}\right) = -kt$$

with $I_{e(t)}$ being the relative peak area of peak **e** at time t ; $I_{(t=0)}$ being the relative peak area of peak **e** before the redox reaction; M_e the concentration of the product; M_0 the initial concentration of Q9.

The above equation is the integrated rate law for a first-order reaction based on chemical reaction kinetic theory. The rate constant can be calculated from the slope of the line: $k = -0.01$

min⁻¹. From the first-order reaction law, the half-life time of the reaction can be calculated as follows:

$$\ln(0.500) = -kt_{1/2}$$

$$t_{1/2} = \ln(0.500) / -k$$

$$t_{1/2} = 69.3 \text{ min}$$

Table 4.1 Integrated ¹H NMR signals for peak e and peak a of Q9 as a function of time after addition of Na₂S₂O₄ to 5 mM Q9 in pD 7.8 D₂O.

Ia	Ie	Ie(normalized)	I _{e(t)} /I _{e(t=0)}	ln(I _{e(t)} /I _{e(t=0)})	Time(mins)
1.000	0.960	0.960	1.000	0.000	0.000
0.983	0.760	0.773	0.805	-0.217	22.000
0.982	0.604	0.615	0.641	-0.445	43.000
0.968	0.471	0.487	0.507	-0.680	64.000
0.955	0.368	0.385	0.401	-0.913	85.000
0.960	0.281	0.293	0.305	-1.188	111.000
0.972	0.219	0.225	0.235	-1.450	138.000
0.963	0.161	0.167	0.174	-1.748	164.000
0.977	0.127	0.130	0.135	-2.000	195.000
0.971	0.098	0.101	0.105	-2.256	227.000
0.952	0.069	0.073	0.076	-2.584	258.000
0.969	0.059	0.061	0.064	-2.755	290.000

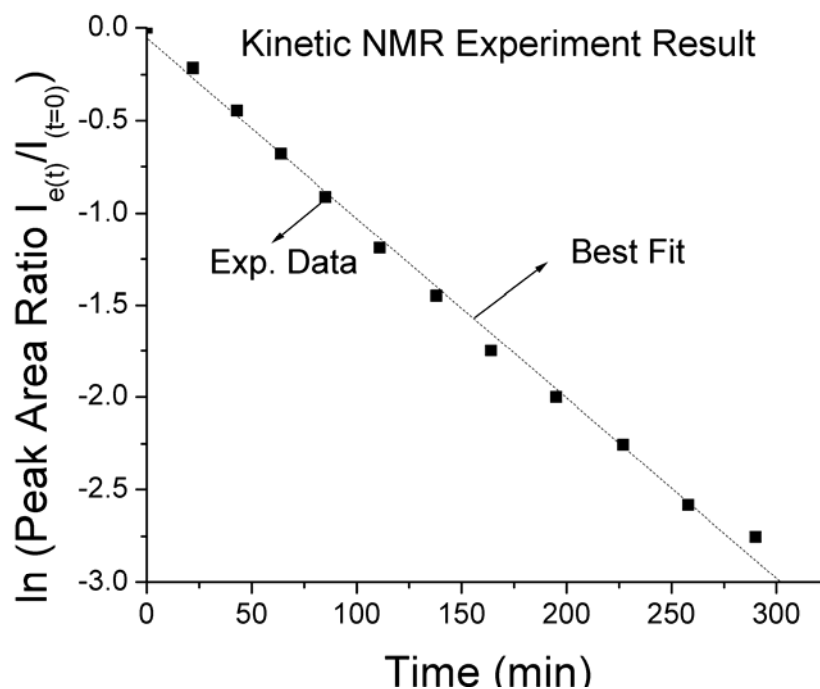


Figure 4.7 NMR kinetic experiments from 5 mM Q9 in pD 7.8 D₂O exposed to solid sodium dithionite.

Compared with other known tri-methyl lock quinone redox systems,⁸ this half-life time is suitable for the application. As shown in Figure 4.2, there are two reactions that occur after the addition of Na₂S₂O₄. The first reaction is the formation of hydroquinone upon the reduction of Q9, which occurs virtually instantaneously as noted from UV-vis experiments on Q9 with added Na₂S₂O₄ in Figure 4.8 (ten seconds were the minimum time for conducting the UV-vis experiment after Na₂S₂O₄ addition). This can also be easily observed by eye, as the quinone form of Q9 is yellow, and the hydroquinone is colorless. The fast speed of this reaction and the virtually identical ¹H NMR spectrum of the hydroquinone of Q9 makes it ignored to follow this reaction by NMR.

4.3 Critical Aggregation Concentration Study

From a structural point-of-view, Q9 should possess the properties of a typical amphiphilic molecule that has the ability to aggregate in aqueous phase if its concentration is high enough. To enable the formation of Q9 vesicles, it is important to find out at what

concentration Q9 begins to form aggregates. There are different methods that can be employed to determine the critical aggregation concentration (CAC) as noted by numerous previous studies. In this study, tensiometry was selected for this purpose.¹¹ The experimental details were described in Chapter 2. In Figure 4.9, the CAC of Q9 was obtained from the surface tension detection method in pH 7.8 PBS (40 mM).

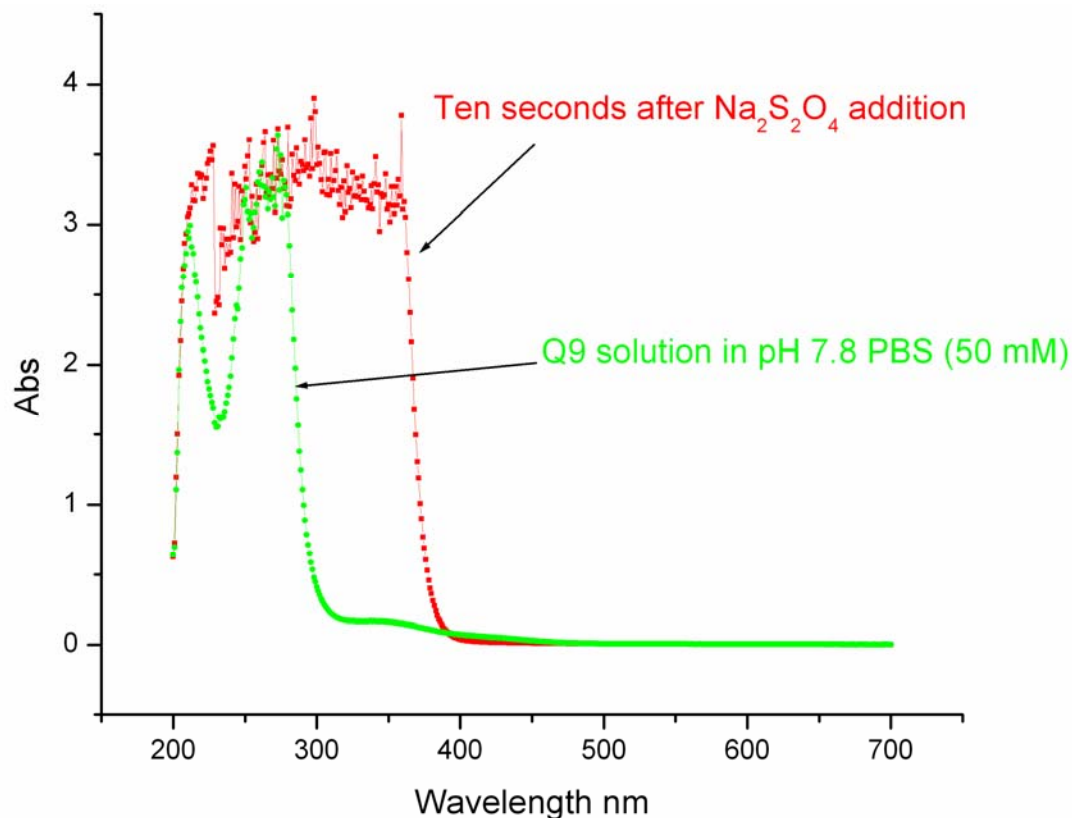


Figure 4.8 UV-vis absorbance change after Na₂S₂O₄ addition of Q9 pH 7.8 PBS solution

To compare these results, surface tension measurements were conducted on 6-aminohexanoic acid, NH₂(CH₂)₅COOH, that under same solution conditions as Q9 in Figure 4.9. Experiment results are plotted in Figure 4.10.

Q9 surface tension experimental results (Figure 4.9) were a good match with surfactant aggregation theory. Two linear relationships were found from the experimental data. In the low concentration range (from 0 to 7 mM), there was a decline that represented the surface tension

was decreasing with increasing Q9 concentration. However, in the high concentration range (> roughly 7mM), another linear relationship was observed. The slope was significantly less, presumably because no more Q9 molecules could insert into the monolayer at the air-water interface. It is unclear at this time why the slope of the line is not zero at Q9 concentration above ~7 mM; however, this is typical of many types of surfactants. The intersection point of these two lines is the turn over point where Q9 aggregates are formed, with the concentration at this point being the CAC of Q9. Thus, the determination of the CAC can be found by setting the two linear equations equal to each other and solving for concentration, yielding a value of 7.1 mM.

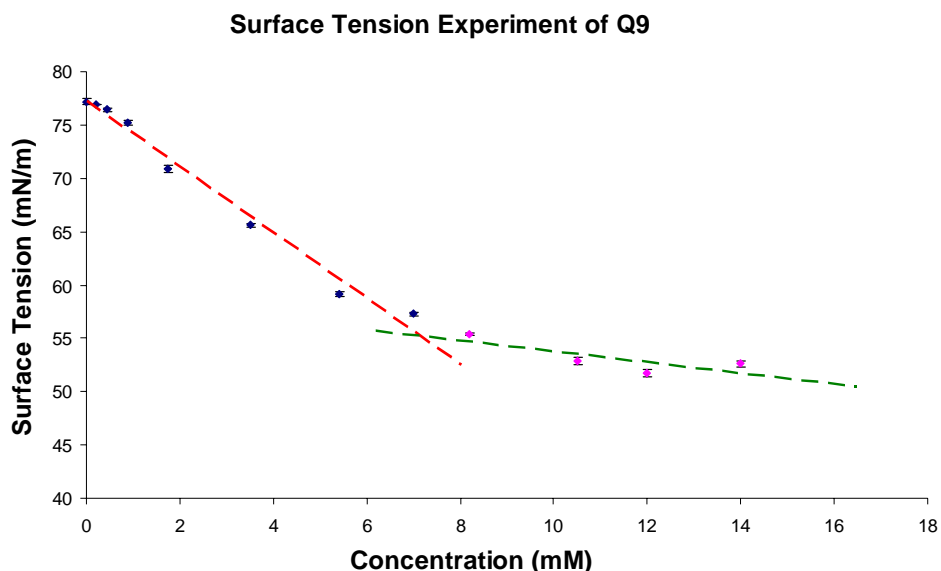


Figure 4.9 Surface tension measurements of Q9 in 40 mM pH 7.8 PBS solution as a function of Q9 concentration.

As we look at the surface tension experiment of the 6-aminohexanoic acid (Figure 4.10), there is no change in the surface tension as its concentration was increased. The surface tension was found to vary between 74 mN/m and 76 mN/m even though the concentration was increased above 50 mM. Based on these results, 6-aminohexanoic acid is not an amphiphilic (surfactant) species, and it can not concentrate at the water-air interface when it is dissolved in aqueous

solution. Thus, the surface tension will not be significantly affected upon the addition of the compound to aqueous solutions.

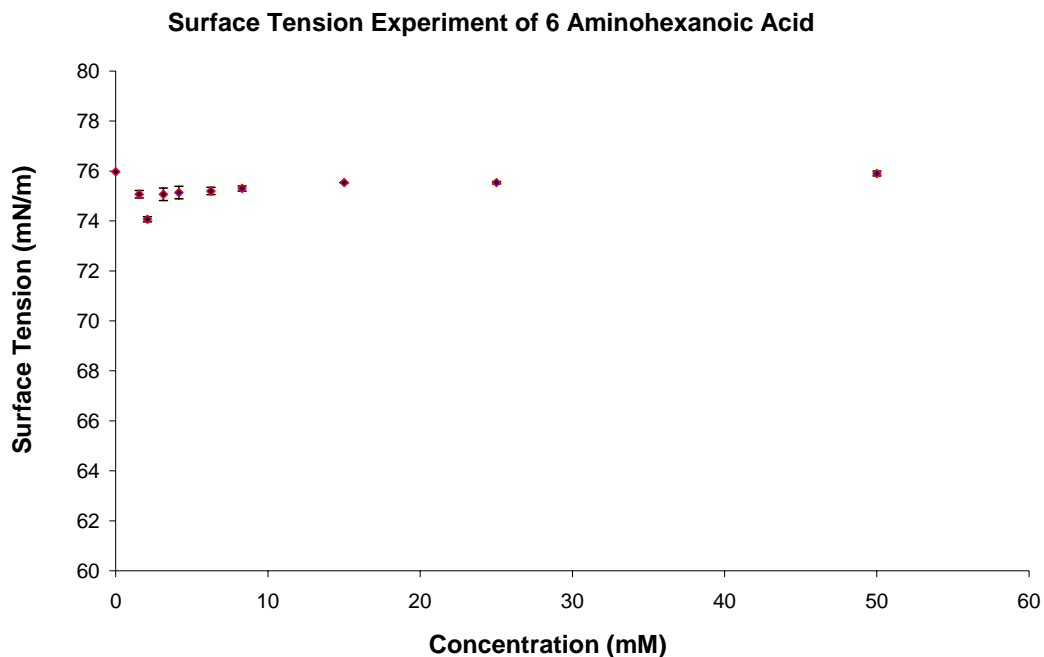


Figure 4.10 Surface tension measurements on 6-amino hexanoic acid in 40 mM pH 7.8 PBS solution.

The different surface tension experimental results between 6-amino hexanoic acid molecule and Q9 confirmed the amphiphilic property of Q9. Meanwhile, based on previous studies, 6-amino hexanoic acid was the only water-soluble structure present after the intramolecular ring cyclization reaction of Q9. The surface tension property of this compound indicated that no aggregates will be formed after the redox reaction has reached completion at its concentration used (maximum concentration of 6-amino hexanoic acid would be ~ 10 mM).

Micelles and planar bilayer aggregates can both be formed in solution from n-alkanoic acid. It is difficult to determine what type of aggregate was formed from Q9 at this point, but previous studies indicated that the single-chain surfactant vesicle formation concentration is

much lower than the critical micelles concentration.^{2,3} Thus, a Q9 solution with a concentration prepared above the CAC concentration should be sufficient for the vesicle formation.

4.4 References

1. Walde, P.; Namani, T.; Morigaki, K.; Hauser, H., Formation and Properties of Fatty Acid Vesicles (Liposomes). *Liposome Technology* (3rd Edition) 2007, 1, 1-19.
2. Namani, T.; Ishikawa, T.; Morigaki, K.; Walde, P., Vesicles from Docosahexaenoic Acid. *Colloids and Surfaces B: Biointerfaces* 2007, 54, 118-123.
3. Namani, T.; Walde, P., From Decanoate Micelles to Decanoic Acid/Dodecylbenzenesulfonate Vesicles. *Langmuir* 2005, 21, (14), 6210-6219.
4. Evans, D. H.; Griffith, D. A., Effect of Ph on the Electrochemical Reduction of Some Heterocyclic Quinones. *Journal of Electroanalytical Chemistry and Interfacial Electrochemistry* 1982, 134, (2), 301-10.
5. Kano, K.; Mori, K.; Uno, B.; Kubota, T.; Ikeda, T.; Senda, M., Voltammetric and Spectroscopic Studies of Pyrroloquinoline Quinone Coenzyme under Neutral and Basic Conditions. *Bioelectrochemistry and Bioenergetics* 1990, 23, (3), 227-38.
6. Saul Patai, Z. R., *The Chemistry of the Quinonoid Compounds*. Chichester: New York, 1988; Vol. 2.
7. Borchard, R. T.; Cohen, L. A., Stereopopulation Control .2. Rate Enhancement of Intramolecular Nucleophilic Displacement. *Journal of the American Chemical Society* 1972, 94, (26), 9166-9174.
8. Carpino, L. A.; Triolo, S. A.; Berglund, R. A., Reductive Lactonization of Strategically Methylated Quinone Propionic-Acid Esters and Amides. *Journal of Organic Chemistry* 1989, 54, (14), 3303-3310.
9. Ong, W.; McCarley, R. L., Chemically and Electrochemically Mediated Release of Dendrimer End Groups. *Macromolecules* 2006, 39, (21), 7295-7301.
10. Baumgarte, U.; Keuser, U., Reducing Agents for Dyeing with Wet Dyes. Ii. Stability in Solutions and Reactivity toward Dyes. *Melliand Textilberichte (1923-1969)* 1966, 47, (10), 1153-60.
11. Evans, D. F.; Wennerstrom, H., *The Colloidal Domain: Where Physics, Chemistry, and Biology Meet*. 2 ed.; Wiley-VCH: 1999; p 5-10.

CHAPTER 5. Q9 VESICLE FORMATION AND CHARACTERIZATION

5.1 Formation of Q9 Vesicles by Extrusion Treatment

Q9 vesicles were formed by the extrusion technique, which has been extensively employed for phospholipid vesicle formation.¹ This operation utilizes a device called an extruder to generate a strong shear force on the surfactant molecule, when they are pushed through a membrane that is located inside the extruder. The shear force has been proposed to help cause surfactants to form vesicles. Although the mechanistic details of vesicle formation during the extrusion event is still under investigation, the practice of this method has confirmed its efficacy for vesicle formation.¹⁻³

Four steps were employed for Q9 vesicle formation using this method: (1) 3 mg of Q9 was dissolved in 5 mL DCM in a round bottom flask and dried by rotatory evaporation to form a thin layer film. Then it was placed under high vacuum for 2 hours to remove any DCM left inside the flask; (2) 0.7 mL PBS solution (pH 7.8, 50 mM with 50 mM NaCl) was added into the flask to hydrate Q9 for 1 hour; (3) After vortexing for 15 minutes, the Q9 solution then underwent a freeze-thaw process 7 cycles by using a dry ice/acetone and a warm-water bath; (4) The liquid was then extruded through a hand-held extrusion device (Avanti Polar Lipids, Alabaster, AL) with 100-nm pore diameter polycarbonate membrane (Whatman, Maidstone, UK). The extrusion process was repeated 20.5 times. Then the solution was transferred into a clean glass container and stored until needed in dark under N₂.

5.2 TEM Experiments on Q9 Vesicles With Stained Materials

TEM experiments were employed to study the formation of Q9 vesicles. The Q9 sample was deposited onto a carbon-coated copper grid. The negative stain method was used to stain the sample with 2% uranyl acetate. This method has been used for the study of phospholipid vesicle formation.^{4,5} The experimental results are shown in Figure 5.1.

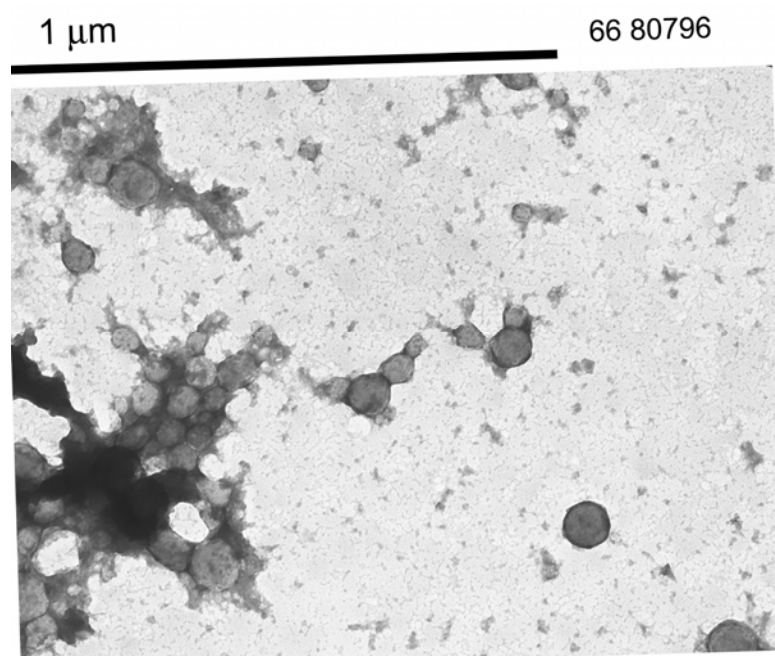
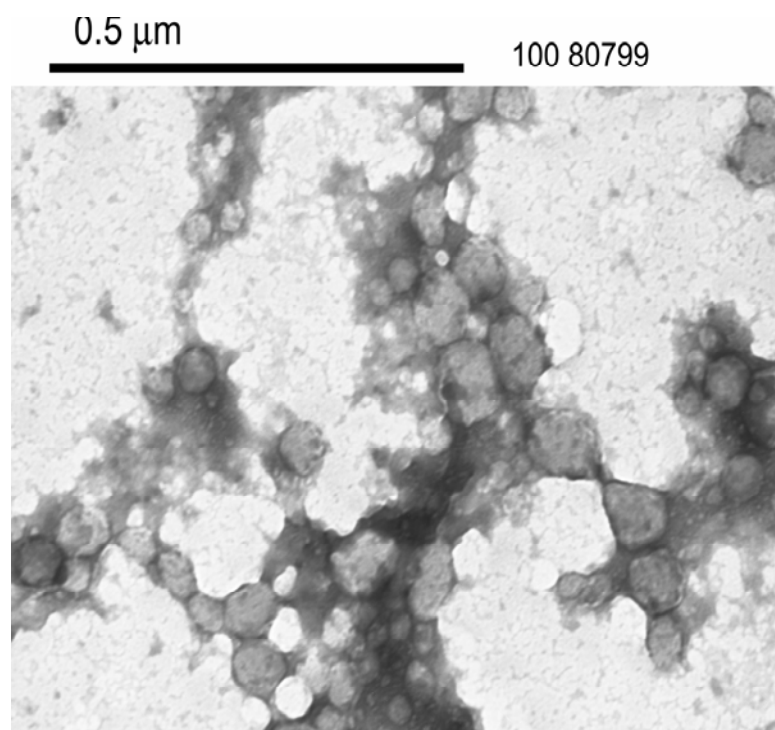


Figure 5.1 Representative TEM experimental results for Q9 vesicles stained with 2% uranyl acetate

These preliminary TEM results indicated that aggregates of Q9 exist in solutions prepared as described here. Vesicles and micelles were two possible aggregates⁶ for these spherical-like structures which were observed in the TEM experiment. The diameter of these

imaged structures ranged from 20 nm to 160 nm in the samples, with an average size distributed around 80 nm. As shown in previous work with n-alkanoic acid, micelles with diameters smaller than 10 nm have been observed for solution pH values of 8.5 to 12.⁷ Larger micelle aggregates have been reported, but generally these structures were resulted from the surfactants that contained high molecular weight polymer chains.^{8,9} The edge area on the captured spherical aggregates in the TEM image was identical to a round spherical structure, which is the typical vesicle aggregate structure. Thus, it is reasonable to conclude the aggregate structures observed in these TEM images are vesicles of Q9.

5.3 Light Scattering Measurement on Q9 Vesicles Sample

Light scattering techniques have been widely used for the characterization of particles in solution.¹⁰ Two different light scattering techniques were used to characterize the Q9 vesicles: static light scattering (SLS) to determine the radius of gyration (R_g), and dynamic light scattering (DLS) to determine the hydrodynamic radius (R_h).

5.3.1 Light Scattering Experiments on a Home-Built Instrument

Q9 vesicle samples prepared in variety PBS solutions (50 mM with 50 mM NaCl) were investigated by both SLS and DLS measurement. The light scattering instrument is a home-built machine in Dr. Russo's lab in the Department of Chemistry at LSU. The experimental results are listed in the following Table 5.1.

Samples 1 and 2 were prepared in pH 8 PBS with different Q9 concentrations. Sample 3 was extruded at pH 10.2 PBS. Sample 4 is Q9 vesicle sample extruded at pH 11.6, then the pH was adjusted to 6.9.

These results revealed some interesting properties about Q9 vesicles. First of all, the light scattering experiments demonstrated the presence of aggregates in solution. Samples and containers had been treated carefully to remove any dust and impurities. Thus, the aggregates

present can only be generated from the Q9 molecule. Sample 1 failed in the observation of R_g because of the low quality decay line recorded during the experiment time. The calculation of R_g is unavailable based on the collected data. This may be caused by the wide distribution of particle sizes that exist in solution for this particular sample.

Table 5.1 Light scattering experiments on Q9 vesicle PBS solutions (50 mM with 50 mM NaCl)

Experiment Number	1	2	3	4
Condition	10 mM Q9, pH 8.0	12 mM Q9, pH 8.0	12 mM Q9, pH 10.2	12 mM Q9, prepared at pH 11.6, then adjust to pH 6.9
R_g (SLS)	N/A	112 ± 1 nm	147 ± 1 nm	119 ± 1 nm
R_h (DLS)	140 nm & 39 nm	132 nm & 24 nm	71.4 nm	61.6 nm

Different R_h sizes are formed at different pH value. Q9 samples prepared at pH 8.0 (samples 1 and 2) possess an R_h value that is obviously larger than the R_h of Q9 samples prepared under a higher pH value (samples 3 and 4). Even for sample 4 where the pH had been decreased to 6.9 after Q9 vesicle formation, the R_h was still much smaller than samples prepared directly at pH 8. The R_g sizes obtained from SLS (112 nm, 147 nm, 119 nm) do not exhibit this significant size change in different pH PBS solution. Based on the LS theory, the R_g vs R_h ratio of the perfect hollow spherical structure equals to 1.0. Except for sample 2 (pH 8), the ratio of R_g vs R_h in sample 3 and sample 4 are much bigger than 1, which indicates the difference of those

aggregates from a hollow spherical structure. One possible reason for these results may come from the different protonation situation of the carboxylic acid group inside the Q9 structures under different pH. The change of ratio between COOH and COO⁻ groups from Q9 structure under high pH value would affect the vesicles' structure.^{11, 12}

Dynamic light scattering has the advantage of measuring smaller sized particles compared with SLS experiments.¹⁰ Each DLS experiment on pH 8.0 samples led to observation of two different size distributions existing in the samples (i.e. samples 1 and 2): one larger size (140 nm or 132 nm) and one small size (39 nm or 24 nm). This observation points to a unique behavior for Q9 in aqueous buffer solutions. Extrusion of phospholipids typically leads to generation of a narrow-sized distribution of vesicles.¹³ The presence of two populations of Q9 vesicles may be contributed by the special quinone group in the molecule, as well as the result of the decreased bilayer stability of Q9 because of its single-chain structure.

5.3.2 Dynamic Light Scattering Experiment on Zetasizer Nano Instrument

The DLS experiments were conducted using a Malvern Zetasizer Nano Instrument (Malvern, Worcestershire, UK). Two different samples were chosen for this experiment. One was a traditional phospholipid vesicle, dioleoylphosphatidylcholine (DOPC), in water solution, which is known to form stable vesicles upon extrusion. The other was Q9 vesicle prepared in pH 7.8 PBS (50 mM) solution under condition identical to sample 2 in Table 5.1. Both samples were developed through the same procedure obtained in Section 5.1.

DOPC was used as a model lipid compound to generate vesicles. DOPC vesicle formation is well documented in previous studies, including those that employ the extrusion technique.^{14, 15} Therefore, it was used as a standard for comparison to Q9 vesicles. The experimental results are shown in Figures 5.2 (DOPC) and 5.3(Q9).

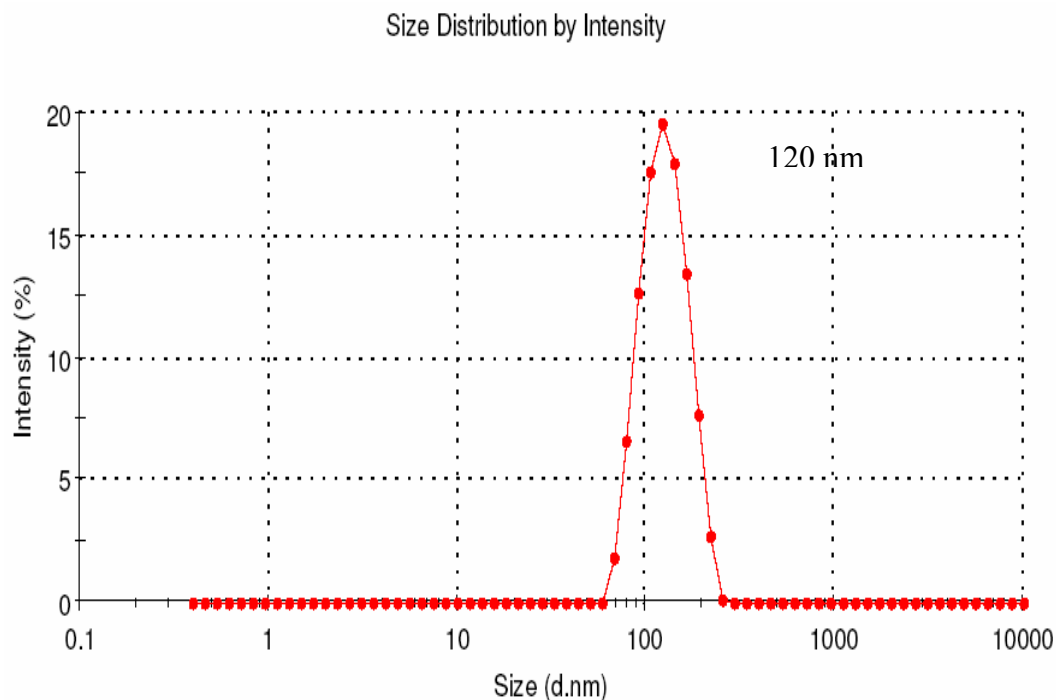


Figure 5.2 DLS experimental results for DOPC vesicle sample (1 mg/mL DOPC in 50 mM pH 7.8 PBS).

Both DOPC and Q9 samples yielded the particle size distribution peaks based on the scattering intensity measurement, confirming the formation of aggregates in these samples. The DOPC data possesses a sharp, narrow peak centered near 120 nm in Figure 5.2. This was in qualitative agreement with previous reports on DOPC vesicles.¹ The Q9 aggregates had a broader distribution range than DOPC (Figure 5.3). Two peaks were observed for this sample. The major peak is located at 160 nm (diameter), and there is also a smaller peak intensity centered at near 40 nm diameter. Because of the overlap of this 40-nm peak with the major peak at 160 nm, the data appears a shoulder style in the Figure 5.3. Compared to the DOPC sample, we can conclude that there were two different size distributions in the Q9 samples.

The mechanism of the extrusion process is still under investigation;¹ however, it is believed the pressure generated inside the membrane hole reorganizes the aggregates and helps form them into spherical vesicles.² For the work here with DOPC, the membrane pores clearly

restricted the size of vesicles when they were formed. Q9 is a single-chain surfactant structure possessing a carboxylic acid group; the stability of the bilayer structures formed from this molecule are evidently more difficult to control compared with the two tailed phospholipid DOPC. Thus, a wide distribution of aggregates was generated during the extrusion process.

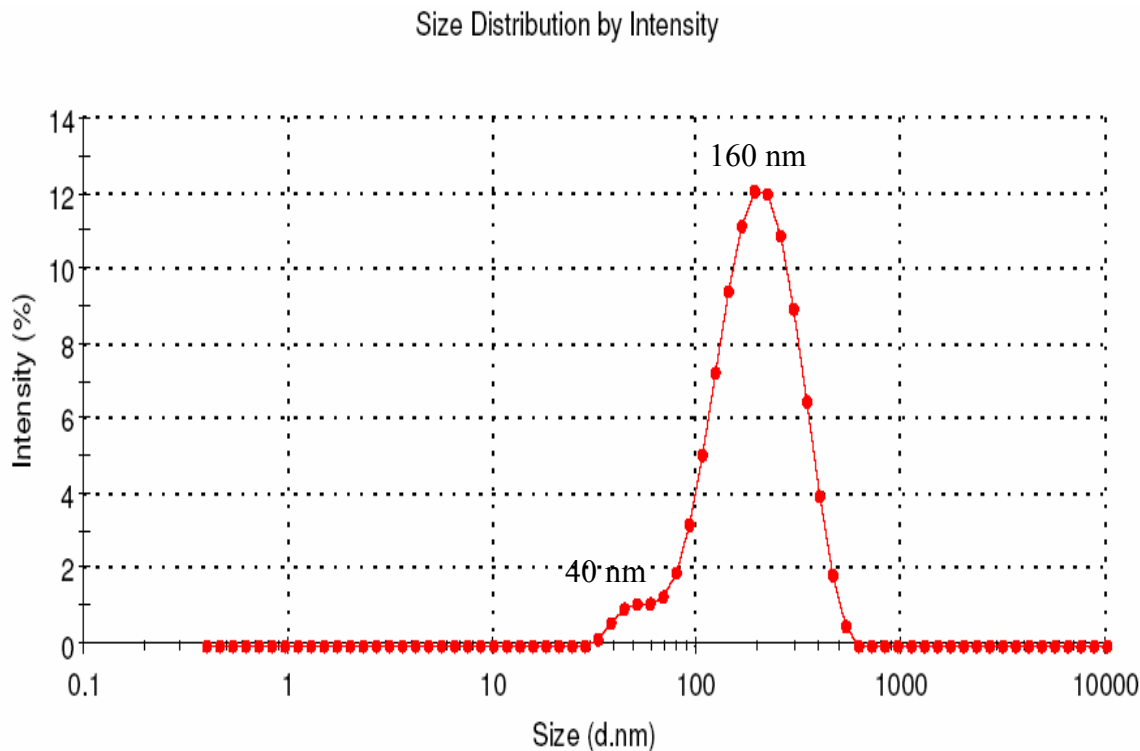


Figure 5.3 DLS experimental results for Q9 vesicle sample (12 mM Q9 in 50 mM pH 7.8 PBS).

5.4 CryoEM Experiment on Q9 Vesicles

CryoEM was used to characterize vesicle size and to obtain possible information on lamellarity of the Q9 structures. As has been previously shown, CryoEM can be used to obtain the closest version of the solution structure of aggregates.¹⁶ The vesicle solution samples were frozen quickly into a thin ice film on TEM grids. The frozen vesicle sample in this process is believed to have the least possible distortion and contain the fewest possible artifacts.¹⁶ Q9 vesicle samples were prepared through the extrusion technique in pH 7.8 PBS (50 mM) solution at 12 mM. Representative results are shown in Figure 5.4.

The CryoEM images not only confirmed the formation of Q9 vesicles upon extrusion of 12 mM Q9 in pH 7.8 PBS, but vesicle' size information can be obtained. From the images, the Q9 vesicles possess widely different sizes, ranging from 20 to 150 nm. The concentration of these vesicle aggregates were not high enough to make them homogeneously observed on the TEM grid. The dynamic fatty acid vesicle formation model can be utilized to describe Q9 vesicle samples¹⁷ (See Figure 1.7 in Chapter 1). The Q9 vesicles may be dynamic balance system constructed by the small number vesicles surrounded by many Q9 single molecules and small Q9 micelles, which has been described by other fatty acid aggregates studies.¹⁷ Based on this theory, it will be difficult to achieve highly concentrated Q9 vesicles in the extruded samples.

5.5 Study of Q9 Vesicle Distribution by Asymmetrical Flow Field-Flow Fractionation (AF4) Technology

AF4 technology was applied to study the size distribution of extruded Q9.¹⁸⁻²⁰ DOPC vesicle samples that were made using the same extrusion technique were used as a standard sample to develop suitable experiment methods for control of the field flow.¹⁸ The light scattering intensity was used to monitor the eluted samples. After the experiment, R_g of the particles was calculated using the instrument software as a function of elution time. Experimental results are shown in Figure 5.5 and Figure 5.6.

Comparing the experiment results of 1 mg/mL DOPC sample and 4.5 mg/mL Q9 sample prepared under the same condition, the recorded light scattering intensity of eluted Q9 aggregates was less than 2% of the light scattering intensity of eluted DOPC vesicle sample, which indicated a much lower concentration of Q9 aggregates in the sample. The high CAC value of 7.1 mM (by surface tension measurement, Chapter 4) would indicate that Q9 does not prefer to exist in the aggregates. Although the Q9 samples were prepared above its CAC, it was difficult to form a high concentration of Q9 aggregates. The effort to increase Q9 aggregate number by increasing Q9 concentration in buffer failed due to reaching the Q9 solubility maximum in the buffer.

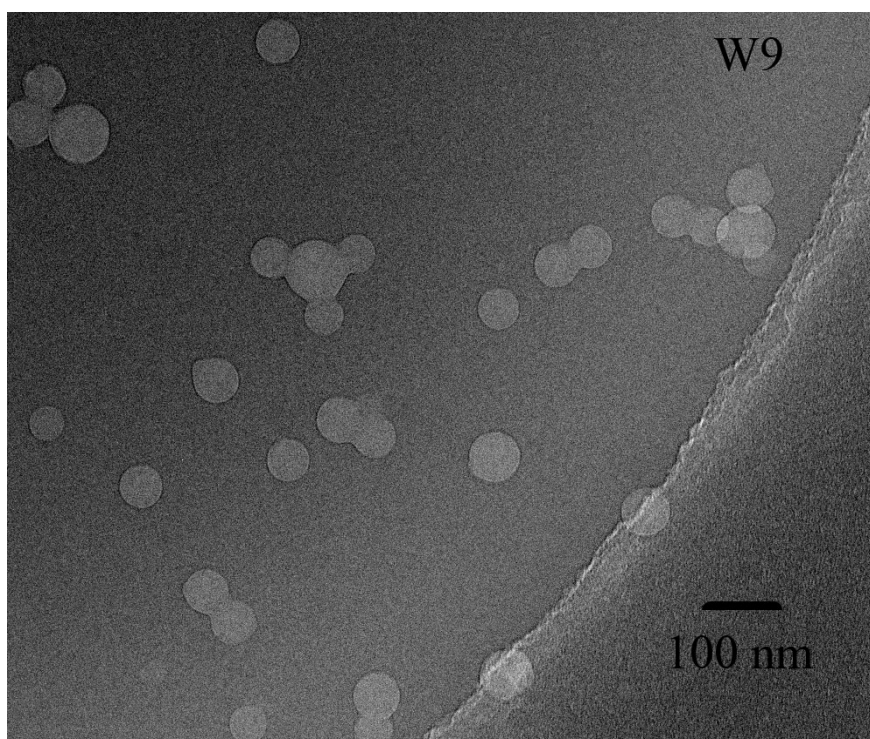
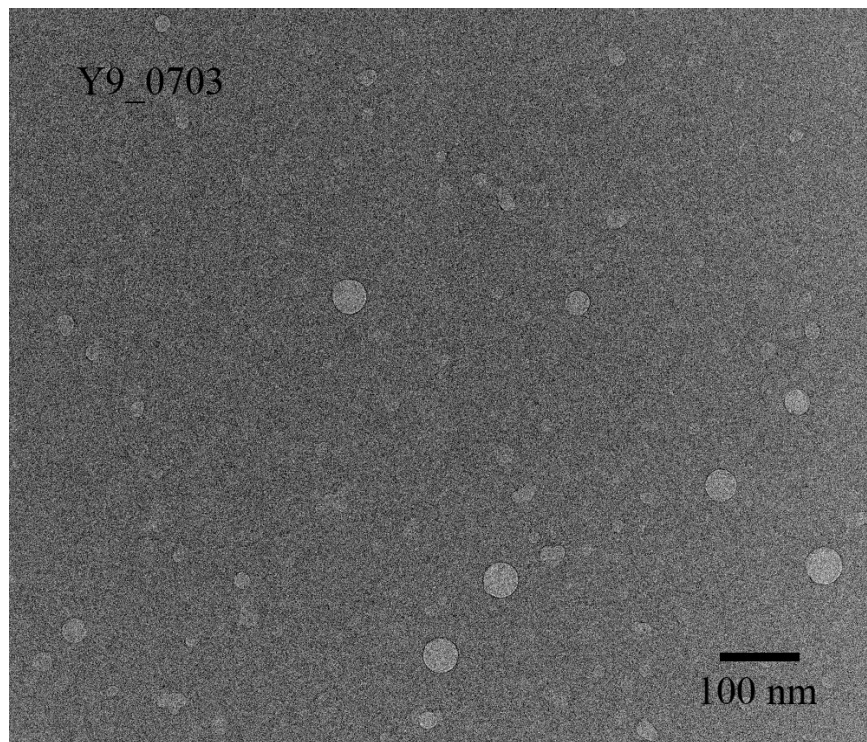


Figure 5.4 Q9 vesicles developed by extrusion treatment with a variety of sizes. Experiments were conducted under conditions described in Section 2.3.4 in Chapter 2.

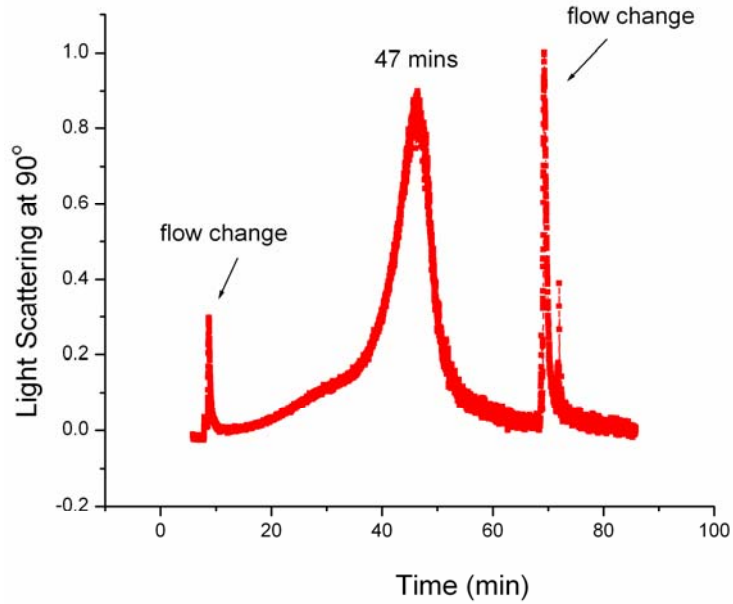


Figure 5.5 Light scattering intensity (recorded at 90°) of 12 mM Q9 sample in pH 7.8 PBS (50 mM) during the AF4 separation process; peak at 9 min and 70 min are generated by the flow condition change.

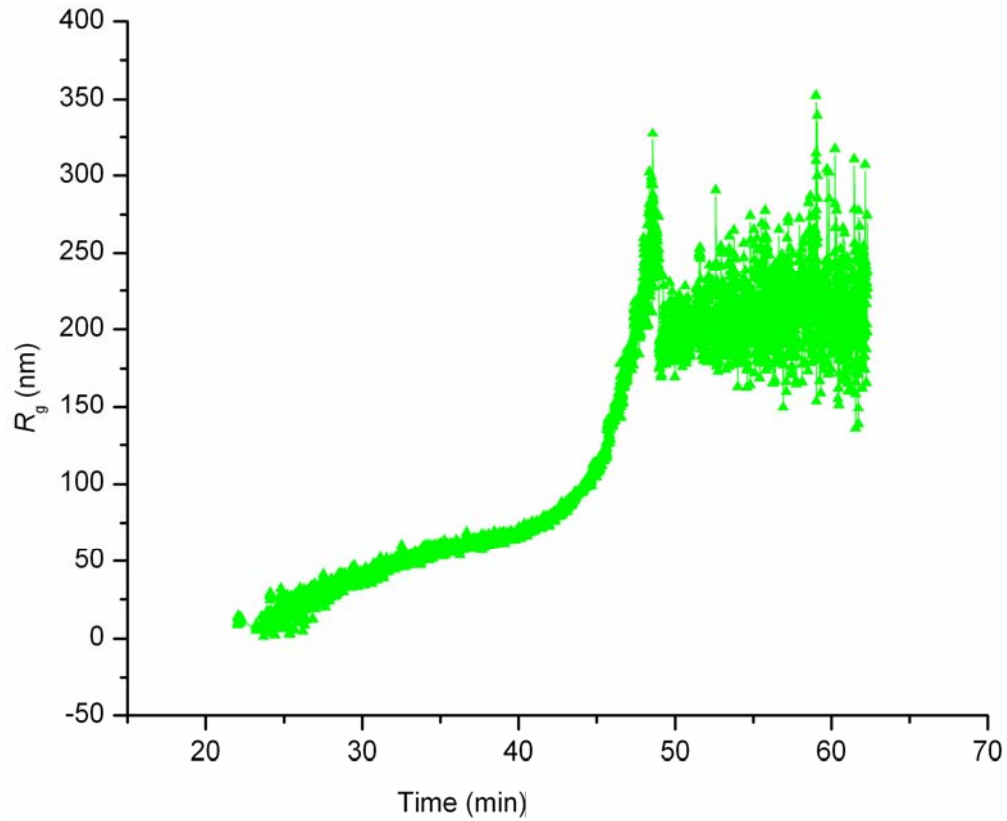


Figure 5.6 R_g size distribution calculated from AF4 experiment on Q9 sample. The data value changed after 50 minutes due to the change of flow condition.

Although the concentration was low, AF4 experiments confirmed the existence of Q9 aggregates with different sizes and provided a size distribution (Figure 5.6). In this experiment, different field-flow conditions were applied to achieve the best separation. Nine minutes after the sample injection the flow condition was maintained to separate the vesicles with different sizes. Fifty minutes later, the flow condition was adjusted to flush the larger particles out. A main elution peak around 47 min can be observed, as well as a small peak around 30 min. The calculated particle sizes (R_g value) for the corresponding peaks were 110 nm (45 min) and 40 nm (30 min). Furthermore, there were different sizes that ranged from 20 nm to 220 nm that eluted at different times. These different-sized aggregates are difficult to be classified as micelles, because one compound usually only forms one uniform micelle structure in a given solvent system.²¹ Vesicle morphology was the suitable model to explain these aggregates type.

5.6 Conclusion from Different Characterization Methods

Through each of the characterization methods, Q9 aggregate formation was confirmed. Light scattering results from the home-built machine (Russo Lab, Chemistry Department, LSU) and Zetasizer Nano Instrument (Malvern, Worcestershire, UK) both point to the existence of Q9 aggregates having different sizes. These particles had a wide size distribution that ranged from 20 nm to 200+ nm. Also, DLS data led to observation of two major sizes for these particles. CryoEM images of Q9 aggregates in buffer solution point to a similar outcome, as different particle sizes were found and spanned the 20-200 nm range. These aggregates are believed to best represent the original structures in buffer solution because of the inherent properties of CryoEM. The typical spherical structure and large size of these Q9 aggregates from these experiment results confirmed them to be vesicles. From the AF4 separation study, the size distribution of Q9 vesicles was observed. These results confirmed the previous DLS and CryoEM results.

Although Q9 vesicle formation was confirmed through these characterization methods, both CryoEM and AF4 separation indicate that the concentration of Q9 vesicles is low in the aqueous buffer solution used here. One reasonable explanation is coming from the structure of the single hydrocarbon chain Q9 molecule, which is difficult to get stabilized as those “double tail” phospholipids, when Q9 vesicles are formed. The whole solution system may be constructed by Q9 vesicles surrounded by many Q9 molecules, which was similar to the other single chain fatty acid vesicle systems.¹⁷

5.7 References

1. Mui, B.; Hope, M. J., *Liposome Technology*. Informa Healthcare USA: London, UK, 2007; Vol. 1, p 55-64.
2. Hunter, D. G.; Frisken, B. J., Effect of Extrusion Pressure and Lipid Properties on the Size and Polydispersity of Lipid Vesicles. *Biophysical Journal* 1998, 74, (6), 2996-3002.
3. Clerc, S. G.; Thompson, T. E., A Possible Mechanism for Vesicle Formation by Extrusion. *Biophysical Journal* 1994, 67, (1), 475-476.
4. New, R. R. C., *Liposomes : A Practical Approach*. IRL Press ; Oxford University Press: New York, 1990; p 301.
5. Edwards, K. A.; Baeumner, A. J., Analysis of Liposomes. *Talanta* 2006, 68, (5), 1432-1441.
6. Evans, D. F.; Wennerstrom, H., *The Colloidal Domain: Where Physics, Chemistry, and Biology Meet*. 2 ed.; wiley-vch: 1999; p 5-10.
7. Stevenson, S. A.; Blanchard, G. J., Investigating Internal Structural Differences between Micelles and Unilamellar Vesicles of Decanoic Acid/Sodium Decanoate. *Journal of Physical Chemistry B* 2006, 110, (26), 13005-13010.
8. Garnier, S.; Laschewsky, A., Synthesis of New Amphiphilic Diblock Copolymers and Their Self-Assembly in Aqueous Solution. *Macromolecules* 2005, 38, (18), 7580-7592.
9. Chen, Y. F.; Zhang, F. B.; Xie, X. M.; Yuan, J. Y., Effects of Micelle Structures Formed in Selective Solvents on Crystallization Behaviors of Poly(Ethylene Glycol)-B-Poly(Styrene) Copolymers. *Polymer* 2007, 48, (9), 2755-2761.
10. Berry, G. C.; Cotts, P. M., *Modern Techniques for Polymer Characterisation*. John Wiley & Sons: 1999; p 81-105.

11. Namani, T.; Walde, P., From Decanoate Micelles to Decanoic Acid/Dodecylbenzenesulfonate Vesicles. *Langmuir* 2005, 21, (14), 6210-6219.
12. Walde, P.; Namani, T.; Morigaki, K.; Hauser, H., Formation and Properties of Fatty Acid Vesicles (Liposomes). *Liposome Technology* (3rd Edition) 2007, 1, 1-19.
13. Mui, B.; Chow, L.; Hope, M. J., Extrusion Technique to Generate Liposomes of Defined Size. In *Liposomes, Pt A*, 2003; Vol. 367, pp 3-14.
14. Reviakine, I.; Brisson, A., Formation of Supported Phospholipid Bilayers from Unilamellar Vesicles Investigated by Atomic Force Microscopy. *Langmuir* 2000, 16, (4), 1806-1815.
15. Hope, M. J.; Bally, M. B.; Mayer, L. D.; Janoff, A. S.; Cullis, P. R., Generation of Multilamellar and Unilamellar Phospholipid-Vesicles. *Chemistry and Physics of Lipids* 1986, 40, (2-4), 89-107.
16. Dubochet, J.; Adrian, M.; Chang, J. J.; Homo, J. C.; Lepault, J.; McDowell, A. W.; Schultz, P., Cryo-Electron Microscopy of Vitrified Specimens. *Quarterly Reviews of Biophysics* 1988, 21, (2), 129-228.
17. Chen, I. A.; Szostak, J. W., A Kinetic Study of the Growth of Fatty Acid Vesicles. *Biophysical Journal* 2004, 87, (2), 988-998.
18. Janca, J., *Modern Techniques for Polymer Characterisation*. John Wiley & Sons Ltd: 1999; p 57-79.
19. Moon, M. H.; Giddings, J. C., Size Distribution of Liposomes by Flow Field-Flow Fractionation. *Journal of Pharmaceutical and Biomedical Analysis* 1993, 11, (10), 911-920.
20. Schauer, T., Symmetrical and Asymmetrical Flow Field-Flow Fractionation for Particle Size Determination. *Particle & Particle Systems Characterization* 1995, 12, (6), 284-8.
21. D. Fennell Evans, H. W., *The Colloidal Domain* Where Physics, Chemistry, Biology, and Technology Meet. 2 ed.; VCH Publishers: p 16.

CHAPTER 6. STUDY OF THE ENCAPSULATION AND CONTROLLABLE RELEASE PROPERTIES OF Q9 VESICLES

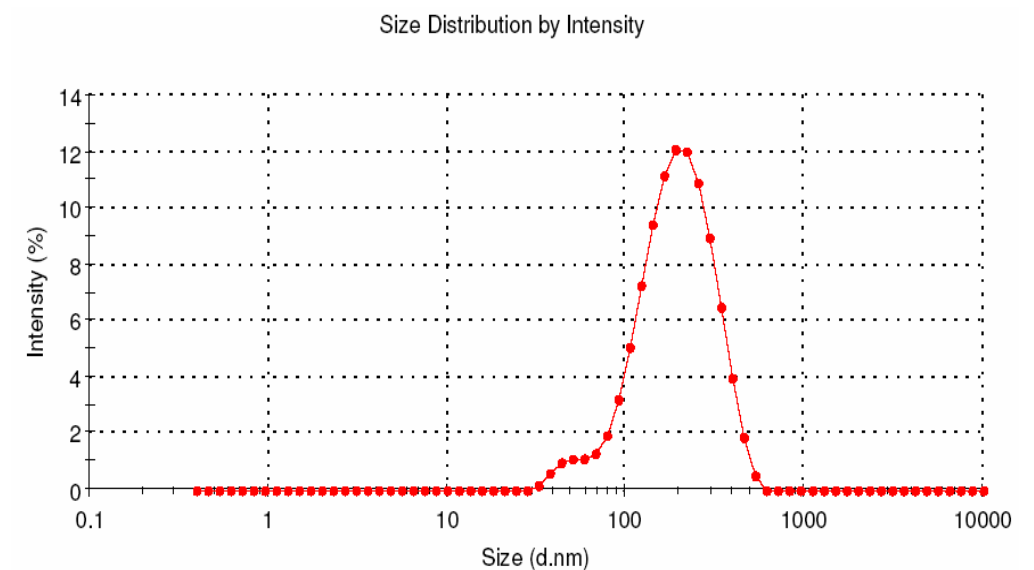
In Chapter 4, sodium dithionite, $\text{Na}_2\text{S}_2\text{O}_4$, was used to successfully trigger the lactonization reaction of Q9, and these experimental outcomes point to the distinct possibility that redox stimulation may allow for control over the confinement of guests within the aqueous interior of Q9 vesicles. Thus, it is anticipated that the ring cyclization lactonization reaction should cause the breaking up of Q9 monomers and disassembly of Q9 aggregates. The encapsulation and possible controllable release properties of Q9 vesicles will be evaluated in this Chapter.

6.1 DLS Experiments on Q9 Vesicles

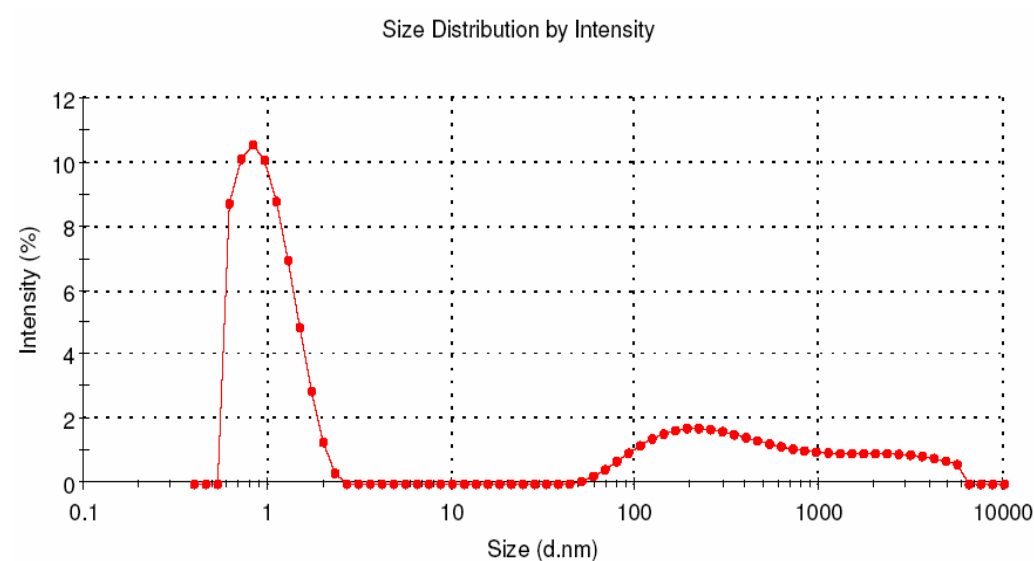
A Nano-Zeta DLS instrument (Malvern, Worcestershire, UK) was utilized for this research. Q9 vesicle samples were prepared via the extrusion technique as outlined in Chapter 5. The Q9 solutions prior to extrusion were made at 12 mM Q9 concentration in 50 mM pH 7.8 PBS solution. Two Q9 vesicle solutions were placed in the DLS sample cells, sample 1 and sample 2. Sample 1 was used as the Q9 vesicle background. Solid $\text{Na}_2\text{S}_2\text{O}_4$ 40 mg (10 equivalents) was added to sample 2 and mixed for 5 minutes. Then DLS was performed on both samples. Results are shown in the Figure 6.1.

Clearly, the addition of $\text{Na}_2\text{S}_2\text{O}_4$ changed the nature of the Q9 vesicles in solution. The original Q9 aggregate peak was diminished after the treatment, leaving a broad peak with low intensity containing some quite large particles (> 200 nm). This indicated that most of the original Q9 vesicles were spontaneously altered (much smaller size) by the reduction reaction. DLS is based on the measurement of particle diffusion coefficient (D), which makes it sensitive for the detection of small particles due to their higher D value.¹ Two products are formed from the Q9 reduction reaction: the hydroquinone lactone and the 6-aminohexanoic acid (Chapter 4).

It would appear that lactone particles formed in the solution precipitated out with a random size distribution, caused a broad DLS peak with low intensity to be observed ($d > 200$ nm).



(a)



(b)

Figure 6.1 DLS experiment on the redox-stimulation results (a) 12 mM Q9 vesicle sample in 50 mM pH 7.8 PBS (b) 12 mM Q9 vesicle sample in 50 mM pH 7.8 PBS after $\text{Na}_2\text{S}_2\text{O}_4$ treatment.

Filtered (membrane pore size 100 nm) 12 mM 6-aminohexanoic acid buffer solutions were examined under the same LS experiment setup, which theoretically should have no

particles present, due to its good solubility in water. However, there were always non-repeatable peaks showing up in the experiment results, which indicated the peaks shown in those results can not represent the real particles inside the solution. Those peaks were similar to the peak around 1 nm in the previously sample 2 experiment (Figure 6.1b) in Q9 vesicle reduction. Based on this control experiment, the small particle peak (around 1 nm) in Figure 6.1b is considered an artifact in the results, and most likely resulted from software limitations.

DLS experiments were also conducted to monitor the change of particle's sizes of 12 mM Q9 vesicle sample after the reduction reaction triggered. Experiment was set up as the same as those described in the first paragraph of 6.1. Each experiment was run every one minute after the addition of 10 equivalents of $\text{Na}_2\text{S}_2\text{O}_4$ (beginning at 3 minute). The results are shown in Figure 6.2.

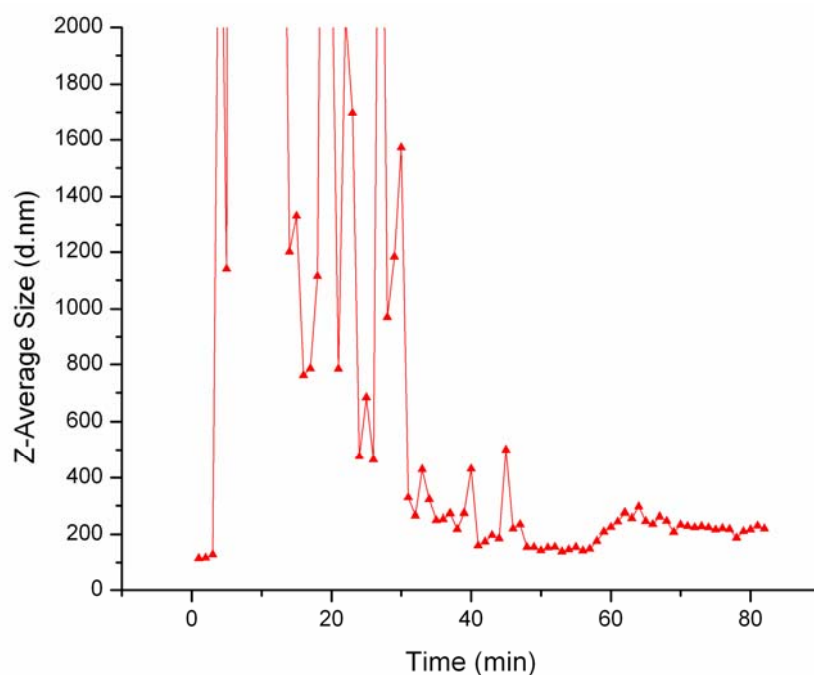


Figure 6.2 Particle's sizes of 12 mM Q9 vesicle sample in 50 mM PBS monitored by DLS after $\text{Na}_2\text{S}_2\text{O}_4$ addition.

The initial Q9 vesicle possesses a diameter of 140 nm in this sample. After the reducing agent addition, the particle size increased dramatically with a random size distribution, which

indicated the formation of lactone solid particles upon the reduction reaction. About thirty minutes later, the particle size began to decrease into the size range below 1000 nm, which can be explained by the precipitation of lactone particles onto the bottom of solution.

6.2 Encapsulation of Water-Soluble Calcein Dye in Q9 Vesicles

The encapsulation characteristics of Q9 vesicles and their reduction induced release properties were investigated using calcein dye, and were followed with fluorescence intensity measurements. Calcein is widely used as an encapsulation agent in vesicle-related studies.²⁻⁴ Upon excitation at 495 nm, a strong emission is monitoring at 510 nm for dilute solution of calcein. The self-quenching property of calcein has been reported in previous work,⁵ with efficient self-quenching occurring when calcein concentrations were higher than 10 mM, leading to a significant loss in fluorescence intensity with increased calcein concentration.⁵ Thus, the difference in fluorescence intensity between quenched and free calcein can be used to monitor its encapsulation and release status in vesicle encapsulation studies. This effect can also be watched by eye, as different colors were observed for different concentrations of calcein, with concentrated self-quenching calcein solutions being red in color, low concentration non-quenching samples being green. This color difference was utilized to facilitate the collection of size-exclusion separation of vesicles.

Based on self-quenching property of calcein, highly concentrated calcein (50 mM) solution were prepared in PBS solution (100 mM with 100 mM NaCl, pH 7.8). Q9 (12 mM) was dissolved in this concentrated calcein solution, then the solution was extruded as the same Q9 vesicles preparation method as those described in Chapter 5. Thus, calcein was encapsulated during the Q9 vesicle formation. Free calcein molecules left in solution were removed by size-exclusion chromatography as described below.

The characteristic of preparative size-exclusion chromatography were described in Chapter 2.⁶ When calcein was encapsulated inside the vesicles, the initial concentration of 50 mM will be well maintained upon vesicle dilution/separation due to the protective of the vesicles nature. Thus, the calcein inside the vesicle will stay self-quenched during the chromatography process and will be red in color. However, free calcein in solution will be diluted to be lower than the self-quenching concentration during the separation process and will be green in color. Red Q9 vesicles containing calcein will move faster in the column based on the principle of size-exclusion chromatography. Thus, different colors should be observed in different parts of the column, as schematically shown in Figure 6.3, if the calcein has been encapsulated successfully.

Experimental results were identical to that predicted above. The observed red color at the leading edge of the separation can be explained only by the presence of encapsulated, self-quenching calcein in the Q9 vesicles. This result confirmed Q9 vesicles can be used to encapsulate water-soluble agents over the time scale of the separation process (60 min). The red band was collected and the green aliquot was discarded. The calcein containing vesicles were passed through another column to ensure all the free dye was removed. Finally a UV-vis experiment was carried out on this sample to measure the absorbance intensity. The UV-vis experiment result was compared with the UV-vis experiment of the Q9 molecule absorbance intensity in the same buffer solution in the Figure 6.4.

The recorded UV-vis absorbance peak for the column separated sample was located around 490 nm, which was identical to the calcein absorbance wavelength (Figure 6.4). The pure Q9 molecule UV-vis absorbance intensity measurement in the same buffer solution shows no peak at 490 nm (Figure 6.4). The sample was collected to exclude free dye, therefore, only big particles should be present in the sample. The presence of small calcein molecule in this sample indicated that calcein was encapsulated inside the Q9 vesicles.

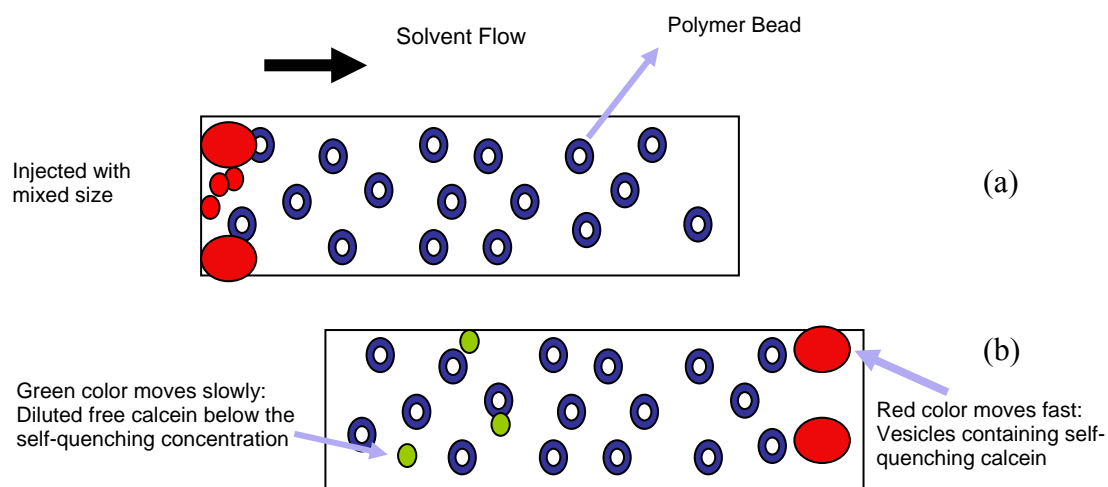


Figure 6.3 Illustration of the color change during the preparative size-exclusion chromatography separation. (a) mixed free calcein and vesicle samples with self-quenching concentration; (b) particles separated based on size. Q9 vesicles (large) containing calcein move faster through the column and diluted free calcein (small) moves slower.

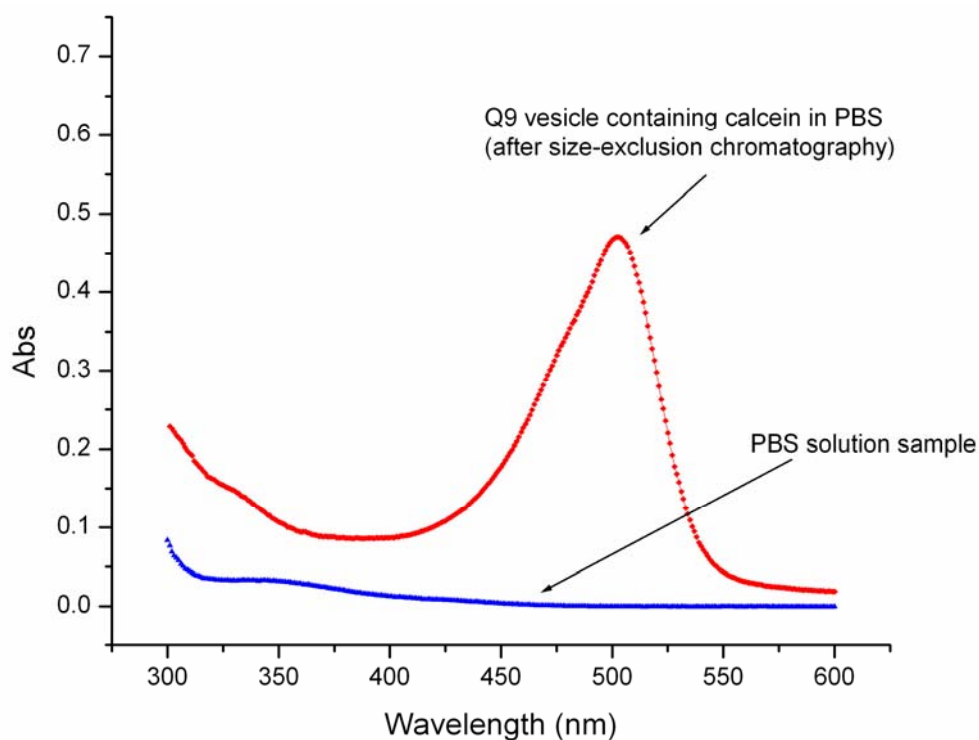


Figure 6.4 UV-vis absorbance experiment on the preparative size-exclusion chromatography separated Q9 vesicle sample with calcein encapsulated; and UV-vis absorbance experiment on 1 mM Q9 molecule in 100 mM pH 7.8 PBS.

6.3 Study of the Controllable Release Property of Q9 Vesicles

Q9 vesicles containing calcein from Section 6.2 were separated and collected in the buffer solution. This sample was used to study the controlled release of dye from Q9 vesicles triggered by $\text{Na}_2\text{S}_2\text{O}_4$ reducing agent.

pH 7.8 PBS solution (100 mM with 100 mM NaCl,) was used to dilute the separated vesicle sample until the UV-vis absorbance intensity was within the range of 0.05 – 0.1. This intensity range will allow the fluorescence study to be conducted within the instrument detection limits.

The diluted Q9 sample was placed in the fluorescence sample cuvette and then put into the luminescence spectrometer (Perkin Elmer, LS50B, Waltham, MA). A kinetic fluorescence mode was applied for this study. Every 5 minutes a fluorescence intensity measurement was obtained on the sample using an excitation wavelength of 495 nm and an emission wavelength of 510 nm. After a stable background was achieved, $\text{Na}_2\text{S}_2\text{O}_4$ was added into the sample, and intensity measurements were recorded every 5 min. The experiment results are shown in Figure 6.5.

The fluorescence signal of column-purified Q9 sample increased after the reducing agent was added. The intensity changed immediately (47% intensity increase) and kept increasing (110% intensity increase) in the next 20 hours. This result indicated the encapsulated calcein was released after the redox-stimulation occurred. The fluorescence signal increased due to loss of the previous self-quenching state after calcein was released into the buffer solution. This result confirmed the controllable release of calcein from Q9 vesicles can be achieved by the redox stimulation.

The increase in calcein intensity was not as large as that found in previous work with encapsulation of calcein.^{5, 7, 8} In AF4 experiments, we found the concentration of these

aggregates (light scattering relative intensity) is obviously smaller than the traditional phospholipid based liposome vesicles formed under the same conditions. This was also confirmed by observations from the CryoEM experiments. The decrease in number of aggregates will dramatically reduce the total volume available for calcein and result in lower fluorescence intensity than expected. Meanwhile, AF4 experiment results showed small Q9 aggregates are counted more than big ones. The decrease in radius of a spherical structure will decrease its packing volume on a large scale ($V \sim R^3$). The more small vesicles present in the solution, the less the fluorescence intensity would change.

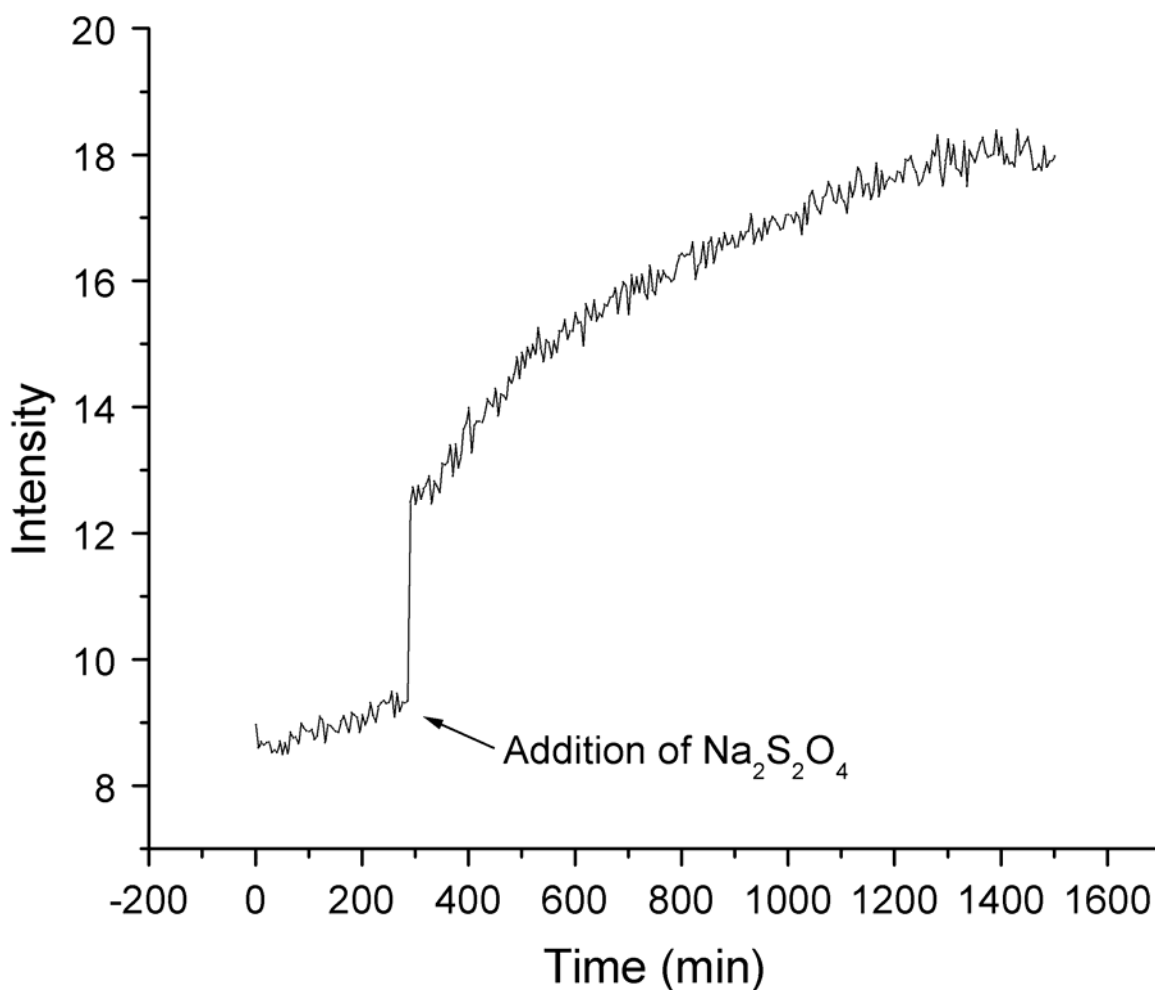


Figure 6.5 Fluorescence intensity increases upon the addition of $\text{Na}_2\text{S}_2\text{O}_4$ to Q9 vesicle sample containing calcein.

6.4 References

1. Berry, G. C.; Cotts, P. M., *Modern Techniques for Polymer Characterisation*. John Wiley & Sons: 1999; p 81-105.
2. Were, L. M.; Bruce, B. D.; Davidson, P. M.; Weiss, J., *Size, Stability, and Entrapment Efficiency of Phospholipid Nanocapsules Containing Polypeptide Antimicrobials*. *Journal of Agricultural and Food Chemistry* 2003, 51, (27), 8073-8079.
3. Paasonen, L.; Romberg, B.; Storm, G.; Yliperttula, M.; Urtti, A.; Hennink, W. E., *Temperature-Sensitive Poly(N-(2-Hydroxypropyl)Methacrylamide Mono/Dilactate)-Coated Liposomes for Triggered Contents Release*. *Bioconjugate Chemistry* 2007, 18, (6), 2131-2136.
4. Yoshino, K.; Kadowaki, A.; Takagishi, T.; Kono, K., *Temperature Sensitization of Liposomes by Use of N-Isopropylacrylamide Copolymers with Varying Transition Endotherms*. *Bioconjugate Chemistry* 2004, 15, (5), 1102-1109.
5. Hamann, S.; Kiilgaard, J. F.; Litman, T.; Alvarez-Leefmans, F. J.; Winther, B. R.; Zeuthen, T., *Measurement of Cell Volume Changes by Fluorescence Self-Quenching*. *Journal of Fluorescence* 2002, 12, (2), 139-145.
6. Wu, C., *Handbook of Size Exclusion Chromatography and Related Techniques*. 2 ed.; Marcei Dekker, Inc: New York, 2004; p 1-24.
7. Benachir, T.; Monette, M.; Grenier, J.; Lafleur, M., *Melittin-Induced Leakage from Phosphatidylcholine Vesicles Is Modulated by Cholesterol: A Property Used for Membrane Targeting*. *European Biophysics Journal* 1997, 25, (3), 201.
8. Roberts, K. E.; O'Keeffe, A. K.; Lloyd, C. J.; Clarke, D. J., *Selective Dequenching by Photobleaching Increases Fluorescence Probe Visibility*. *Journal of Fluorescence* 2003, 13, (6), 513-517.

CHAPTER 7. SUMMARY OF CONCLUSIONS AND FUTURE STUDIES

7.1 Summary of Conclusions

Novel redox stimuli-responsive surfactant structure was synthesized successfully in seven steps. ^1H NMR and MS were used to characterize the products. The final product, Q9, was confirmed by ESI-MS and ^1H NMR. A “trimethyl-lock” quinone moiety was utilized in the Q9 to enable the redox-stimuli responsive property. Once the quinone moiety was reduced to the hydroquinone, a spontaneous intramolecular cyclization/elimination reaction occurred that broke the Q9 backbone. This redox stimuli-responsive mechanism was confirmed by the ^1H NMR kinetic study by monitoring the protons intensity change on the Q9 structure.

Q9 is a typical amphiphile that can aggregate in an aqueous solution. A critical aggregation concentration (CAC) of 7.1 mM for Q9 was obtained using surface tension measurement at room temperature. Q9 structure is sensitive to the pH of the solution. A UV-vis study on the Q9 solution samples prepared in different pH buffers found that a new absorbance peak near 470 nm appeared among the Q9 samples prepared in high pH PBS (pH>11). ^1H NMR was applied to observe the stability of the Q9 structure while the pH was varied. Experimental results confirmed that the structure stability of the Q9 was maintained in the intermediate pH range from 7.0 to 9.0. Previous work found that a roughly equal amounts of protonated and deprotonated fatty acid group in fatty acid molecules was achieved in this pH range, which was suggested to be important for the formation of the fatty acid vesicle aggregates. Thus, a pH 7.8 PBS was used as the solvent system to prepare the Q9 vesicles.

The Q9 vesicle formation process was conducted by extrusion, which was used widely to develop phospholipids vesicles. Q9 PBS solution (12 mM) above the CAC was chosen for the extrusion to ensure aggregation would occur. After extrusion, CryoEM and Light Scattering (LS) experiments were used to check the vesicle formation. Both Static Light Scattering (SLS) and

Dynamic Light Scattering (DLS) confirmed the Q9 vesicle formation in the extruded sample. DLS also detected that the sample was polydisperse with sizes ranging from 20 nm to 200+ nm. CryoEM experiments captured the direct image of these spherical Q9 vesicles. The concentration of Q9 vesicle was small based on the observation of these CryoEM images.

Asymmetrical flow field-flow fractionation (AF4) was used to study the Q9 aggregates size distribution. A variety of sizes of Q9 aggregates can be separated from the sample, which matched with the DLS and CryoEM results. A lower intensity was observed from the scattering light of Q9 vesicle sample than DOPC vesicle sample. Because AF4 separated the different sizes of particles, the size effect on the light scattering intensity should be eliminated. Thus, the observed low intensity of light scattering signal can be inferred that there are less Q9 vesicles present than the DOPC vesicle sample prepared under same conditions.

Sodium dithionite ($\text{Na}_2\text{S}_2\text{O}_4$) was used as the reducing agent to trigger the intramolecular cyclization/elimination reaction, which can break the Q9 monomer. Disassembly of Q9 vesicles was monitored by DLS. After the addition of 10 equivalents of sodium dithionite, Q9 vesicles were destroyed based on the DLS experiment observation. This result confirmed Q9 vesicles can be controlled by the designed redox stimuli-responsive mechanism.

To study the encapsulation and controllable release properties of the Q9 vesicles, concentrated water soluble dye, calcein (50 mM), was chosen to be entrapped within the Q9 vesicles. The encapsulation was conducted by the mixing of calcein and Q9 molecule together before extrusion. After extrusion, vesicles containing calcein were separated from the free calcein by a preparative size-exclusion chromatography. A fluorescence study was conducted on the Q9 vesicle/calcein sample without the interference from the free calcein molecule. Sodium dithionite was added into this solution to trigger the release of calcein from the vesicle. The fluorescence intensity increased after the $\text{Na}_2\text{S}_2\text{O}_4$ addition, which indicated that the calcein

molecule was released after the redox-stimulation occurred. The fluorescence signal increased due to loss of the previous self-quenching state after calcein was released into the buffer solution. This result confirmed that the Q9 molecules possess the ability to encapsulate a water soluble agent and to release it under the controllable redox stimulation.

The fluorescence intensity increased in the controllable release experiment was not as large as that found in previous work with encapsulation of calcein. This could be contributed by the low concentration of Q9 vesicles which generated by the extrusion method. More studies were needed to be conducted in the future to improve the capacity ability of Q9 vesicles. However, the achievements in this study have confirmed Q9 vesicle system can be made by extrusion, and possesses the ability to encapsulate water soluble compound and release them under redox stimulation method.

7.2 Future Work

Q9 vesicles possess unique properties. The work presented in this study demonstrated they can be controlled by the reducing chemical agent, sodium dithionite. To adopt the Q9 vesicles into a variety of applications, a more comprehensive study is needed to explore the properties of Q9 under different environment. Other methods can be utilized to manipulate Q9, depending on the types of application desired.

One potential application of Q9 vesicles is for the drug delivery system. The toxicology studies of this molecule should be evaluated. Q9 has low toxicity to human based on the previous quinone based prodrug research.¹⁻⁴ It is predicted the Q9 vesicle would meet the clinical standard when it is applied *in vivo* environment.

The study in this dissertation exhibited the encapsulation and protecting mechanism of Q9 vesicles for the water soluble compound, which is crucial for the drug delivery system.

However, the reduction of the chemical compound sodium dithionite is difficult to apply in this kind of application. Thus, a new stimuli-responsive mechanism should be used.

It has been confirmed that some reductase enzymes have abnormal strong activities in the mutated cells.⁵ For example, DT-diaphorase (NADH:quinone) is an oxidoreductase enzyme widely exists in the cell membrane that can reduce quinone molecules. Recent study on cancer cells found DT-diaphorase presented a super high activity compared with other enzymes in variety of cancer cells. Although the mechanism of this strong enzyme activity is still under investigation, this property can be used to design the new stimuli-responsive mechanism for the Q9 vesicle delivery system.

It was proven that the redox reaction of “trimethyl lock” quinone moiety in Q9 structure will cause the deterioration of Q9 molecule. DT-diaphorase possesses a strong reduction ability that reduces the quinone molecule in the cell membrane. This strong activity in the mutated cell will lead to the similar reduction of the Q9 structure. It is reasonable to adopt this ability onto the Q9 molecule to develop a new controllable release mechanism.

Q9 vesicles containing water-soluble drug (developed by the extrusion technique) should be mixed with DT-diaphorase *in vitro* to study the drug release process. The UV-vis detection method can be applied to monitor the change of the specific UV-vis adsorption peak of drug molecules during this process. These changes indicate the drug compound can be released upon the breakage of the Q9 vesicles. Different DT-diaphorase samples with a variety of activities can be achieved by adjusting the concentration and should be tested to find out the different response of the Q9 vesicles. Due to the complex environment for the *in vivo* application, the enzyme activity will be different from their *in vitro* behavior. Thus, more studies are needed with a clinical and pharmaceutical resource.

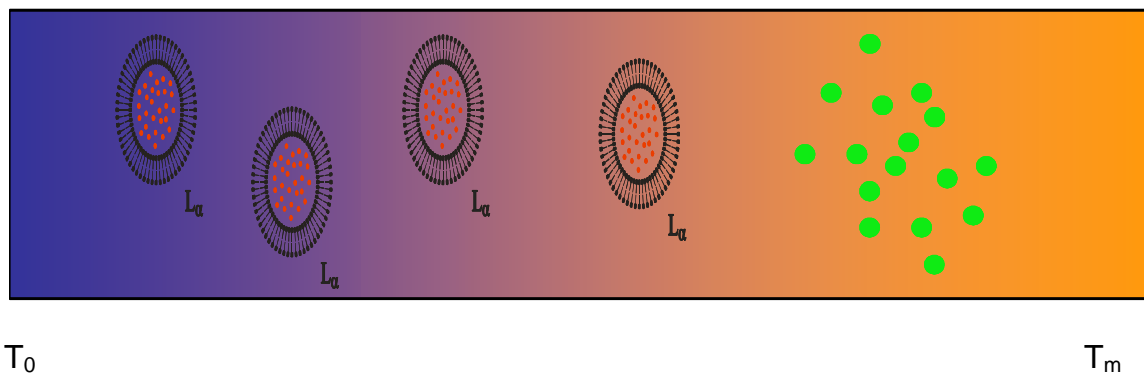


Figure 7.1 Microfluidic channel with temperature gradient.

Another application of the Q9 vesicle is to use them as the efficient containment and delivery system in the microfluidic analysis device, which can enable advances in “lab-on-a-chip” technology. The microdiameter channels inside these microfluidic devices cause the reagent to flow slowly and mix sluggishly compared to the regular flow condition. Locascio and Vreeland, who specialize in this area at the National Institute of Standards and Technology (NIST), suggest that high efficiency mixing and reagent delivery is “fundamental important for the successful development and application of lab-on-a-chip devices”.⁶ Phospholipids vesicle aggregates have been employed for this kind of delivery application in microfluidic devices (Figure 7.1). The release of the agent from these vesicles has been accomplished by a temperature gradient that is prebuilt in the channel.⁶ Results in this study showed that vesicles containing a small molecule can achieve high efficiency mixing and reagent delivery. However, the temperature gradient vesicle breaking mechanism used in this system limited its application in many areas. The increased temperature could not be applied to many samples including biological and chemical agents. Furthermore, change of internal channel temperature will cause a different reaction kinetic process, which is difficult to monitor.

The sizes of the developed Q9 vesicles ranged from 20 to 200+ nm. They can move effortlessly inside these microsized channels. The protective nature of these vesicles will help

transport agents in the channel safely. Thus, both a target sample and an analysis agent can be contained and delivered with Q9 vesicles.

The packing efficiency of the Q9 vesicles needs to be enhanced for these applications to be successful. Two strategies can be adopted for this purpose. One is to increase the Q9 vesicles number (vesicle concentration), and the other is to increase the size (diameter) of the Q9 vesicles. Either can enhance the encapsulation ability of Q9 vesicles.

It has been pointed out, in this dissertation, that it was difficult to produce a large number of Q9 vesicles through the extrusion treatment compared with the phospholipids vesicles prepared under the same conditions. This indicated the difficulties on the stabilization of the Q9 vesicles. It has been reported that the addition of the fatty alcohol compounds inside the fatty acid vesicle solution would help to stabilize the vesicle aggregates.⁷ This method can be applied to increase the lifetime of Q9 vesicles. Also, the size of Q9 vesicle would hopefully increase as the spherical structure became more stable. The fatty alcohol that could be adopted for this purpose should possess a similar carbon chain length as the Q9 structure. However, fatty alcohols with carbon chains greater than 11 are insoluble in aqueous solution, which make them very difficult to be applied directly.

To adopt the fatty alcohol stabilization method, chemical modification should be applied on the fatty alcohol structure. A hydrophilic moiety should be attached on the fatty alcohols (C>11), to increase their water solubility at room temperature. The new synthesized structures are hoped to be soluble in PBS solution and mix with Q9.

The vesicles formation should be checked through CryoEM and AF4 experiment. The impact of the chain length and the adding ratio of the new developed water soluble additives should be evaluated. The controllable release property of this new vesicle should be monitored by water soluble dye encapsulation and release experiment. The vesicle composed of two

components could perform differently from the pure Q9 vesicles in encapsulation ability. The kinetic process of the breaking of this vesicle could be studied by NMR kinetic experiments and fluorescence method.

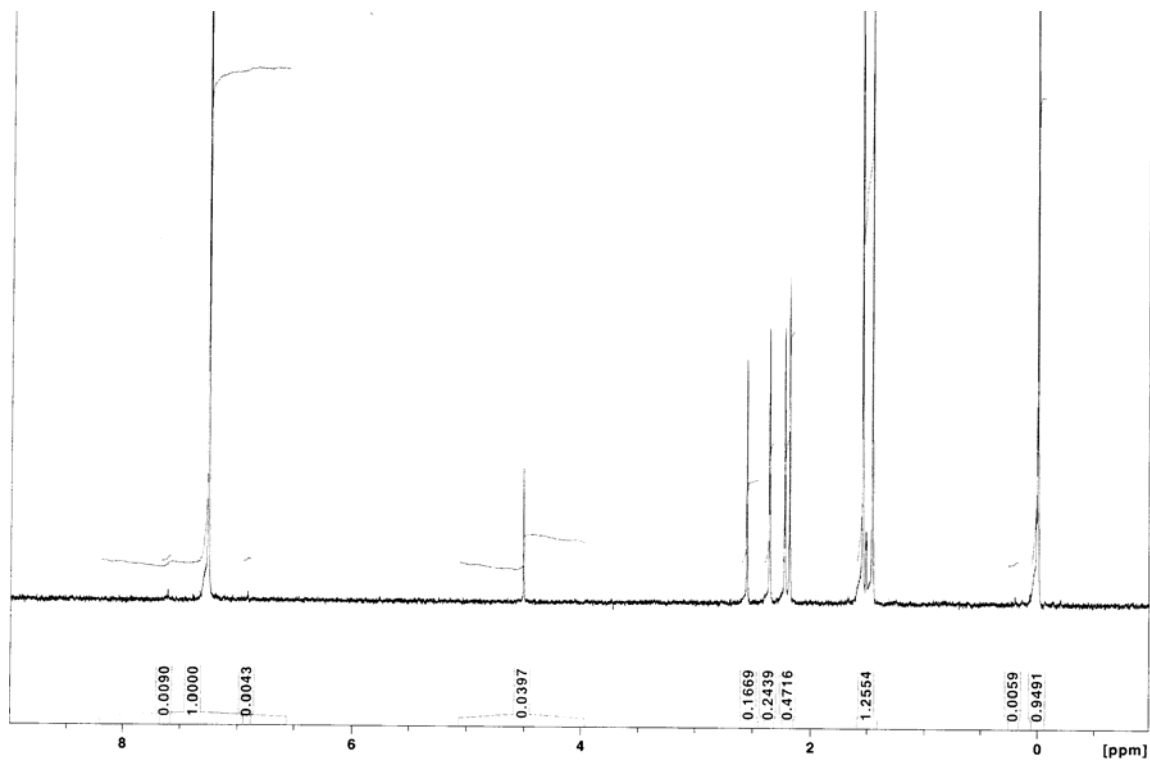
After this work, it is predicted a suitable additive system can be selected. Large quantities of vesicles will be produced with added stability due to this new water soluble additive, and bigger size vesicles are expected. Thus, the enhanced packing capacity will finally allow these vesicles for more applications.

7.3 References

1. Ross, D.; Beall, H. D.; Siegel, D.; Traver, R. D.; Gustafson, D. L., Enzymology of Bioreductive Drug Activation. *British Journal of Cancer* 1996, 74, S1-S8.
2. Silva, A. T. D.; Chung, M. C.; Castro, L. F.; Guido, R. V. C.; Ferreira, E. I., Advances in Prodrug Design. *Mini-Reviews in Medicinal Chemistry* 2005, 5, (10), 893-914.
3. Amsberry, K. L.; Gerstenberger, A. E.; Borchardt, R. T., Amine Prodrugs Which Utilize Hydroxy Amide Lactonization .2. A Potential Esterase-Sensitive Amide Prodrug. *Pharmaceutical Research* 1991, 8, (4), 455-461.
4. Amsberry, K. L.; Borchardt, R. T., Amine Prodrugs Which Utilize Hydroxy Amide Lactonization .1. A Potential Redox-Sensitive Amide Prodrug. *Pharmaceutical Research* 1991, 8, (3), 323-330.
5. Fitzsimmons, S. A.; Workman, P.; Grever, M.; Paull, K.; Camalier, R.; Lewis, A. D., Reductase Enzyme Expression across the National Cancer Institute Tumor Cell Line Panel: Correlation with Sensitivity to Mitomycin C and Eo9. *Journal of the National Cancer Institute* 1996, 88, (5), 259-269.
6. Vreeland, W. N.; Locascio, L. E., Using Bioinspired Thermally Triggered Liposomes for High-Efficiency Mixing and Reagent Delivery in Microfluidic Devices. *Analytical Chemistry* 2003, 75, (24), 6906-6911.
7. Monnard, P.-A.; Deamer, D. W., *Methods in Enzymology*. Elsevier Inc: 2003; p 136-137.

APPENDIX 1. PRODUCTS MINIMUM PURITY CALCULATION

Appendix 1.1 Product 2



Non-product peaks intensity: 0.0090, 0.0043, 0.0059, 0.0192;

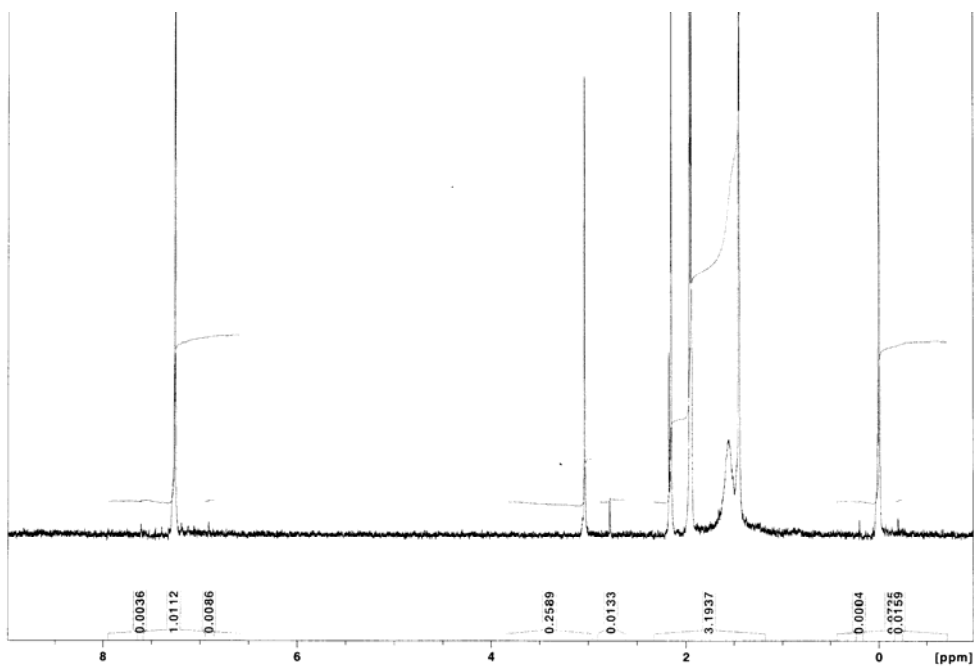
Product 2 peaks intensity: 0.0397, 0.1669, 0.2439, 0.4716, 1.2554;

Product 2 purity =

$$1 - \frac{\sum(0.0090,0.0043,0.0059,0.0192)}{\sum(0.0397,0.1669,0.2439,0.4716,1.2554) + \sum(0.0090,0.0043,0.0059,0.0192)}$$

= 99.12%

Appendix 1.2 Product 3



Non-product peaks intensity: 0.0036, 0.0086, 0.0133, 0.0004, 0.0159, 0.0408;

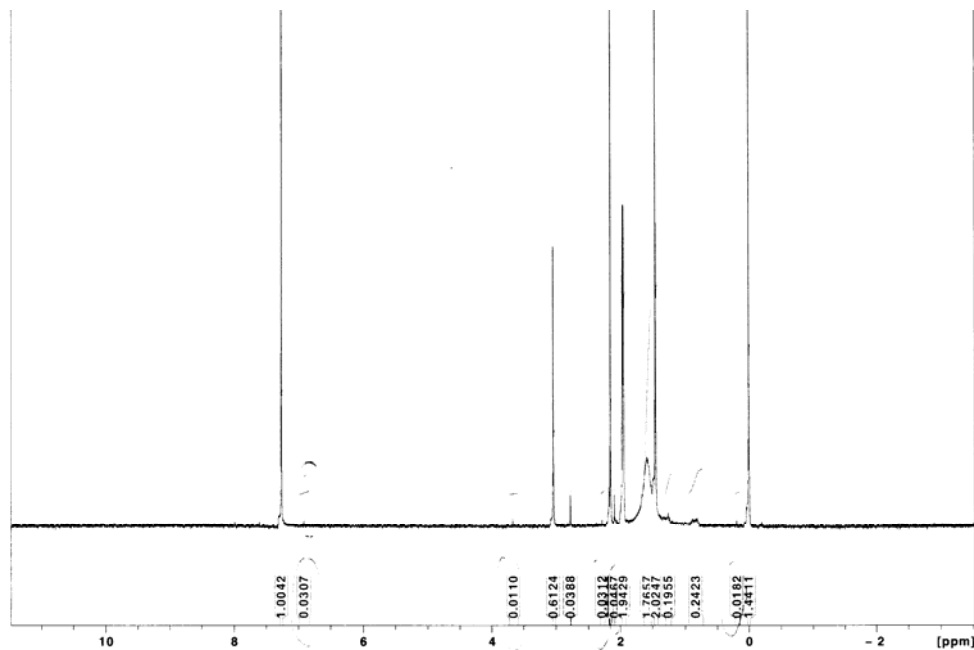
Product 3 peaks intensity: 0.2589, 3.1937;

Product 3 purity =

$$1 - \frac{\sum(0.0036, 0.0086, 0.0133, 0.0004, 0.0159, 0.0408)}{\sum(0.2589, 3.1937) + \sum(0.0036, 0.0086, 0.0133, 0.0004, 0.0159, 0.0408)}$$

= 98.8%

Appendix 1.3 Product 4



Non-product peaks intensity: 0.0307, 0.011, 0.0312, 0.0467, 0.195, 0.0182, 0.0388, 0.3716;

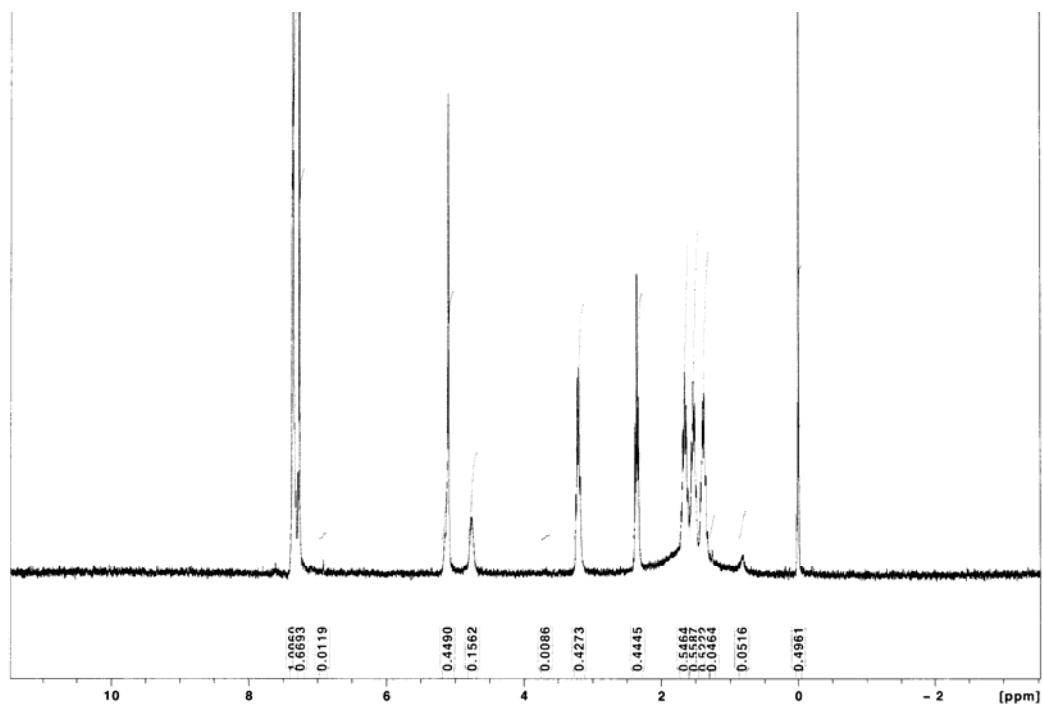
Product 4 peaks intensity: 0.6124, 1.9429, 1.7657, 2.0247, 0.9186, 7.2643;

Product 4 purity = 1 -

$$\frac{\sum(0.0307, 0.011, 0.0312, 0.0467, 0.195, 0.0182, 0.0388, 0.3716)}{\sum(0.6124, 1.9429, 1.7657, 2.0247, 0.9186, 7.2643) + \sum(0.0307, 0.011, 0.0312, 0.0467, 0.195, 0.0182, 0.0388, 0.3716)}$$

= 95.1%

Appendix 1.4 Product 6



Non-product peaks intensity: 0.0119, 0.0086, 0.0464, 0.0516, 0.1185;

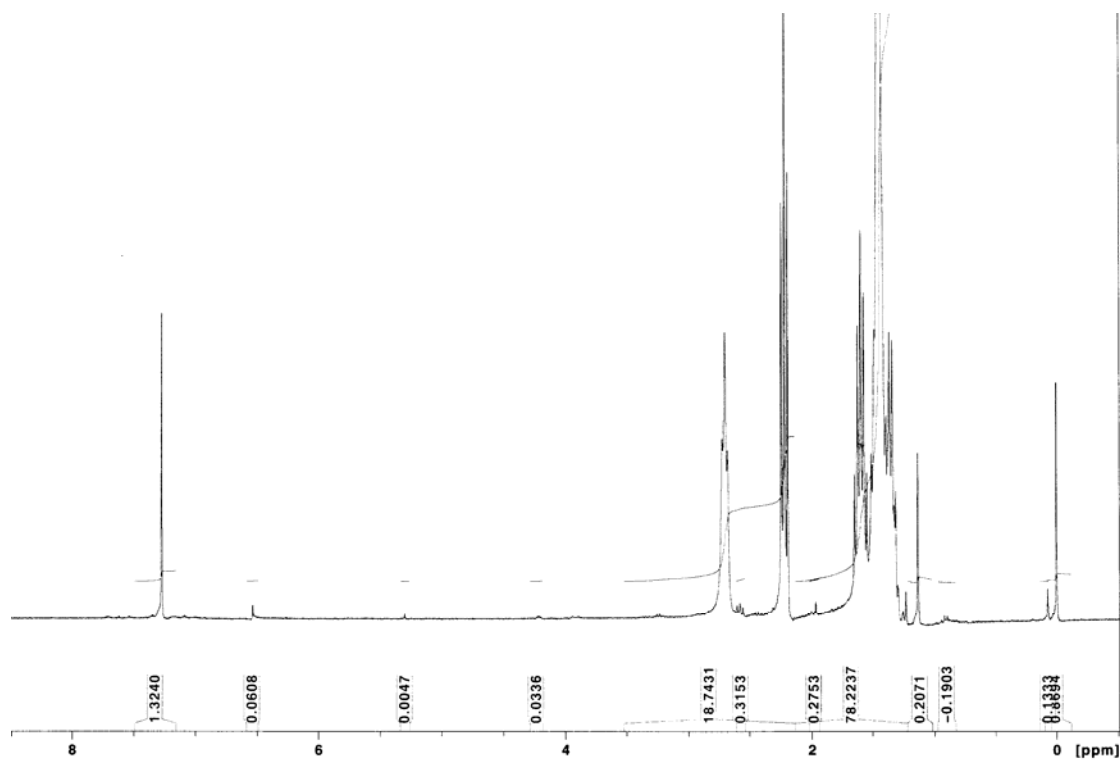
Product **6** peaks intensity: 0.6693, 0.4489, 0.1562, 0.4273, 0.4445, 0.5464, 0.5587, 0.5225;

Product **6** purity = 1 –

$$\frac{\sum(0.0119, 0.0086, 0.0464, 0.0516, 0.1185)}{\sum(0.0119, 0.0086, 0.0464, 0.0516, 0.1185) + \sum(0.6693, 0.4489, 0.1562, 0.4273, 0.4445, 0.5464, 0.5587, 0.5225)}$$

= 98.6%

Appendix 1.5 Product 7



Non-product peaks intensity: 0.0608, 0.0047, 0.0336, 0.3153, 0.2753, 0.2071, 0.7715, 1.6683;

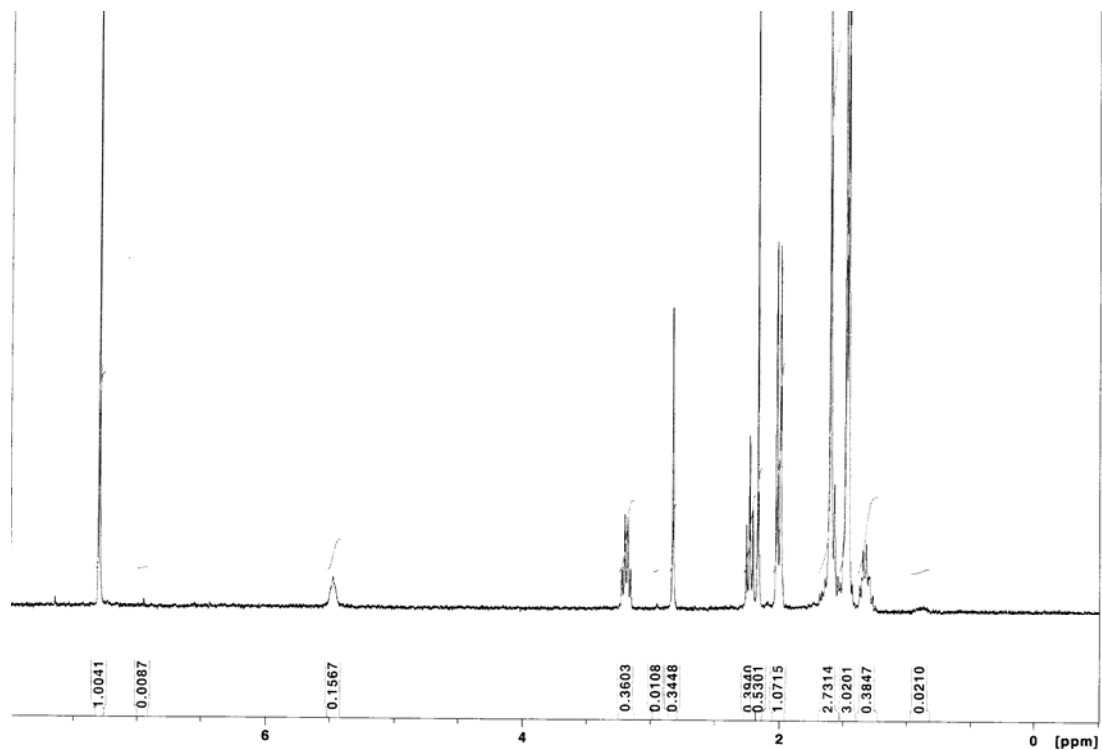
Product **7** peaks intensity: 18.4234, 78.5656;

Product **7** purity = 1 -

$$\frac{\sum(0.0608, 0.0047, 0.0336, 0.3153, 0.2753, 0.2071, 0.7715, 1.6683)}{\sum(18.4234, 78.5656) + \sum(0.0608, 0.0047, 0.0336, 0.3153, 0.2753, 0.2071, 0.7715, 1.6683)}$$

= 98.3%

Appendix 1.6 Product 8



Non-product peaks intensity: 0.0087, 0.0108, 0.021, 0.0405;

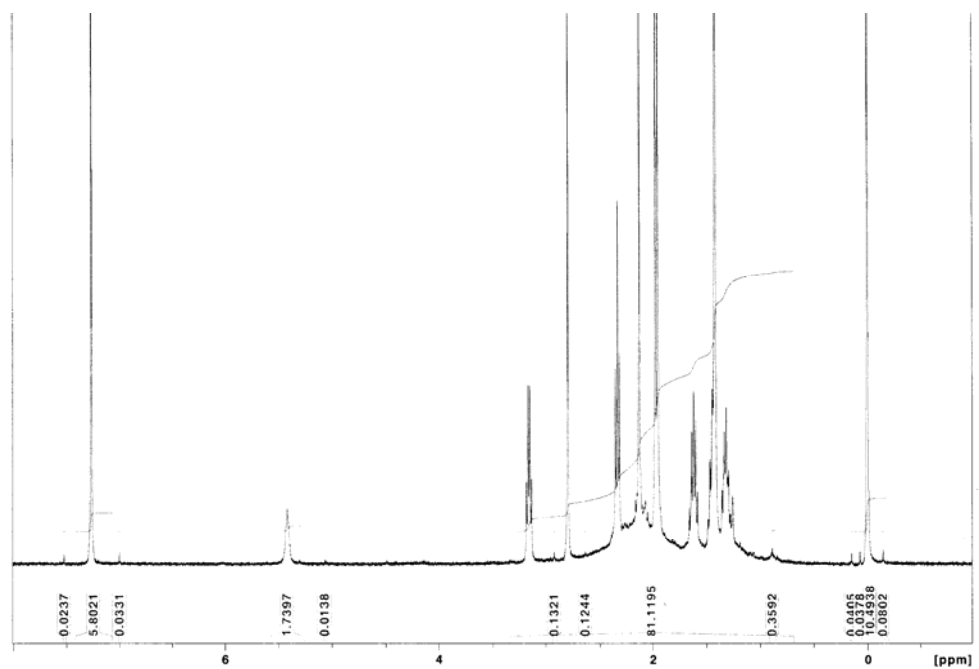
Product **8** peaks intensity: 0.1567, 0.3603, 0.3448, 0.394, 0.5301, 1.07146, 2. 7314, 3.0201, 0.3847;

Product **8** purity = 1 -

$$\frac{\sum(0.0087, 0.0108, 0.021, 0.0405)}{\sum(0.1567, 0.3603, 0.3448, 0.394, 0.5301, 1.07146, 2. 7314, 3.0201, 0.3847) + \sum(0.0087, 0.0108, 0.021, 0.0405)}$$

= 99.5%

Appendix 1.7 Product 9



Non-product peaks intensity: 0.0237, 0.0331, 0.0318, 0.1321, 0.1244, 0.3592, 0.0405, 0.0378, 0.0802;

Product **9** peaks intensity: 1.7397, 81.1195;

Product **9** purity = 1 -

$$\frac{\sum (0.0237, 0.0331, 0.0318, 0.1321, 0.1244, 0.3592, 0.0405, 0.0378, 0.0802)}{\sum (0.0237, 0.0331, 0.0318, 0.1321, 0.1244, 0.3592, 0.0405, 0.0378, 0.0802) + \sum (1.7397, 81.1195)}$$

= 98.9%

APPENDIX 2. PERMISSION OF REPRINT

Appendix 2.1 ACS Permission of Reprint

02/28/2008 17:26 FAX 2027768112

001/001

PERMISSION REQUEST FORM

Date: 02/27/2008

FROM: Copyright Office
Publications Division
American Chemical Society
1155 Sixteenth Street, N.W.
Washington, DC 20036

FAX: 202-776-8112

TO: Yuming Yang
FROM: Louisiana State University
232 Chopin Hall
Baton Rouge LA 70803

Your Phone No. (225) 578-6950
Your Fax No. (225) 578-3458

I am preparing a paper entitled:

Development of New Stimuli-responsive Vesicles Using a Novel Surfactant
to appear in a (circle one) book, magazine, journal, proceedings, other dissertation
entitled: _____

to be published by: Louisiana State University

I would appreciate your permission to use the following ACS material in print and other formats with the understanding that the required ACS copyright credit line will appear with each item and that this permission is for only the requested work listed above:

From ACS journals or magazines (for ACS magazines, also include issue no.):

ACS Publication Title	Issue Date	Vol. No.	Page(s)	Material to be used*
<u>Langmuir</u>	<u>2005</u>	<u>21</u>	<u>14</u>	<u>Figure 4</u>
<u>Journal of Physical Chemistry B</u>	<u>2006</u>	<u>110</u>	<u>26</u>	<u>Figure 2</u>

From ACS books: include ACS book title, series name and number, year, page(s), book editor=s name(s), chapter author's name(s), and material to be used, such as Figs. 2 & 3, full text, etc.*

* If you use more than three figures/tables from any article and/or chapter, the author's permission

**PERMISSION TO REPRINT IS GRANTED BY
THE AMERICAN CHEMICAL SOCIETY**

368 or use the FAX number above.

ACS CREDIT LINE REQUIRED. Please follow this sample:
Reprinted with permission from (reference citation). Copyright
(year) American Chemical Society.

APPROVED BY: C. Arleen Courtney 2/28/08
ACS Copyright Office

If box is checked, author permission is also required. See original article for address.

RECEIVED

FEB 27 2008

ACS COPYRIGHT OFFICE

LSU CHEMISTRY

2255793458 10:25 02/27/2008

Appendix 2.2 Elsevier Limited Permission of Reprint

ELSEVIER LIMITED LICENSE TERMS AND CONDITIONS

Feb 06, 2008

This is a License Agreement between yuming yang ("You") and Elsevier Limited ("Elsevier Limited"). The license consists of your order details, the terms and conditions provided by Elsevier Limited, and the payment terms and conditions.

License Number	1883381301355
License date	Feb 06, 2008
Licensed content publisher	Elsevier Limited
Licensed content publication	Journal of Pharmaceutical and Biomedical Analysis
Licensed content title	Size distribution of liposomes by flow field-flow fractionation
Licensed content author	Moon Myeong Hee and Giddings J. Calvin
Licensed content date	October 1993
Volume number	11
Issue number	10
Pages	10
Type of Use	Thesis / Dissertation
Portion	Figures/table/illustration/abstracts
Quantity	1
Format	Print
You are an author of the Elsevier article	No
Are you translating?	No
Purchase order number	
Expected publication date	May 2008
Elsevier VAT number	GB 494 6272 12
Permissions price	0.00 USD
Value added tax 0.0%	0.00 USD
Total	0.00 USD
Terms and Conditions	

INTRODUCTION

The publisher for this copyrighted material is Elsevier. By clicking "accept" in connection with completing this licensing transaction, you agree that the following terms and conditions apply to this transaction (along with the Billing and Payment terms and conditions established by Copyright Clearance Center, Inc. ("CCC"), at the time that you opened your Rightslink account and that are available at any time at <http://myaccount.copyright.com>).

VITA

Yuming Yang was born in Sichuan, China, to Guowei Yang and Cheng He. Yuming obtained his bachelor of engineering degree in industrial chemistry from Southwest Petroleum Institute in July 1994. From 1994 to 2001, Yuming worked as a research engineer in the National Engineering Research Center for Silicone in Chengdu, China. In August 2001, he attended Louisiana Tech University in the chemistry graduate program (Master). In August 2003, Yuming graduated from Louisiana Tech University with a Master of Science degree in chemistry. Upon his graduation, Yuming attend the doctoral program in the Department of Chemistry in Louisiana State University. He joined the group of Dr. Robin McCarley and is currently completing the requirements for the degree of Doctor of Philosophy in chemistry.